THE CREEP BEHAVIOUR OF THREE ALLOY STEELS FOR STEAM TURBINE APPLICATIONS

A Thesis Submitted to the College of Graduate Studies and Research
in Partial Fulfillment of the Requirements
for the Degree of Master of Science
in the Department of Mechanical Engineering
University of Saskatchewan
Saskatoon, Saskatchewan

By
Shane H. Griffin
January 2001

PERMISSION TO USE

Whereas this thesis is submitted in partial fulfillment of the requirements for the degree of Master of Science from the University of Saskatchewan, the author has agreed that the Libraries of this University may make it freely available for inspection. Further, the author has agreed that permission for copying of this thesis for scholarly purposes may be granted by the professor who supervised the thesis work reported herein or, in his absence, by the Head of the Department or the Dean of the College in which the thesis work was carried out. It is understood that any copying or publication or use of this thesis or parts thereof for financial gain shall not be allowed without the author's written permission. Furthermore, it is understood that due recognition shall be given to the author and to the University of Saskatchewan in any scholarly use which may be made of any material in this thesis.

Requests for permission to copy or make other use of material in this thesis in whole or part should be addressed to:

Head of the Department of Mechanical Engineering
University of Saskatchewan
Saskatoon, Saskatchewan, Canada
S7N 0W0

ABSTRACT

University of Saskatchewan
Mechanical Engineering Abstract

The Creep Behaviour of Three Alloy Steels
for Steam Turbine Applications

Student: S. Griffin Supervisor: S. Yannacopoulos

M.Sc. Thesis Submitted to the
College of Graduate Studies and Research
January 2001

ABSTRACT

Understanding the elevated temperature behaviour of materials is extremely important for the efficient selection of materials for use in steam turbines, which require high operating temperatures to achieve maximum efficiency.

In this study, an attempt to characterize the creep behaviour of three ASTM grade high alloy steels to determine their suitability for use in various steam turbine applications was made. The steels of interest were ferritic in nature and include a 12%CrMoV stainless steel, a 1%CrMoV steel, and a steel suitable for nitriding. The testing consisted mainly of creep tensile tests to determine the creep behaviour of these materials at temperatures near the service temperature, which is approximately 538°C. Other tests such as tensile and hardness tests were also performed to determine or verify other material properties. Scanning and transmission electron microscopy and X-ray analysis work were performed on as-received materials and ruptured creep specimens.

The results of the creep testing showed that the creep strength and oxidation resistance of the 12%CrMoV steel was significantly greater than that of the two low alloy steels, although the rupture ductility was significantly lower. The shape of the creep curve for each steel was also well established. The rupture data was used to create a master curve for each steel using time-temperature parameters. The Goldhoff-Sherby parameter was used for the two low alloy steels, while the Larson-Miller parameter proved to fit the stainless steel best.

Many particles were observable in the microstructure of these steels, which are most likely carbide and nitride particles. The largest of these particles were examined using EDX analysis and large amounts of chromium were found to be present, suggesting that they are likely chromium carbides. Many smaller particles were also observable which are likely vanadium nitrides, although they were too small for reliable EDX analysis.

The creep behaviour of these steels under service conditions is not easily characterized using data obtained from short term creep tests performed at much higher stresses than would be seen in service.

ACKNOWLEDGEMENTS

I would like to thank my supervisor Dr. S. Yannacopoulos for his direction and assistance in this project. I would also like to thank Tom Kishchuk and Curtis Yuskiw of Hitachi Canadian Industries Ltd. for assistance and technical discussions. I am also very grateful for technical assistance received from Phil Siminoff, Dave Deutscher, Doug Bitner, H.J. Steinmetz and the staff of Engineering Shops.

I would like to thank my colleagues, Ray Taheri, George Quainoo, Jared Miner, and Darryl McCullough for many useful discussions.

Dad and Mom, thanks for everything you taught me.

Priscilla, thanks for just always being there.

I would also like to acknowledge the God who created me, and my Lord and Saviour, Jesus Christ.

But God forbid that I should glory, save in the cross of our Lord Jesus Christ, by whom the world is crucified unto me, and I unto the world. Galatians 6:14

TABLE OF CONTENTS

LIST OF TABLES

LIST OF FIGURES

LIST OF SYMBOLS

T_m	melting point temperature
ε	engineering strain
$\dot{\varepsilon}$	strain rate, or change in strain with respect to time
σ	engineering stress
A	multiplier constant of power law relationship
n	exponent of power law relationship
Q	activation energy
R	universal gas constant
T	absolute temperature
E	elastic modulus
t	time
α,m,K	experimentally determined fitting parameters
$\dot{\varepsilon}_s$	steady state strain rate
k_s	fraction of grain boundaries with observable grain boundary sliding
P	time-temperature parameter
C	constant of Larson-Miller parameter
T_A	temperature constant of Manson-Haferd or Goldhoff-Sherby parameters
t_A	time constant of Manson-Haferd or Goldhoff-Sherby parameters
θ	uniaxial parameter of θ-projection model
t_f	creep fracture life
HV	Vickers hardness number
F	test load for Vickers microhardness test
d	arithmetic mean of the two diagonals of Vickers microhardness indentation

1. INTRODUCTION

1.1. Background

The development of materials to meet the specific needs of mankind has been an ongoing process for thousands of years. The development of steel alloys for high temperature applications in power generation plants is just a continuation of this tradition.

Alloy steels have seen widespread application in power generation plants for many years due to their relatively low cost and inherent strength. A whole genre of alloy steels labelled heat-resisting steels has been developed for their ability to resist the effects of high temperature, including oxidation and creep.

Creep is a term that describes the time-dependent plastic flow of materials under a constant load. Creep is a very complex phenomenon that is controlled by a number of mechanisms and is not fully understood. Although creep does not really affect most metallic materials at room temperature, it is an important factor in high temperature processes.

The creep behaviour of steels used for steam turbine applications is of great importance due to the high operating temperatures to which these steels are subjected. Without a good understanding of the mechanisms that are controlling the process of creep, the selection of suitable materials is difficult.

In recent years, the desire of industry to improve the efficiency of power generation plants has led to attempts to increase the operating temperature of the processes involved. This has spurred the development of many new heat-resisting steels with improved creep resistance, giving them the ability to be used at higher operating temperatures.

1.2. Research Outline

1.2.1. Problem Definition

The creep behaviour of steels used for steam turbine applications is of great importance due to the high operating temperatures to which these steels are subjected. Without a good understanding of the mechanisms that are controlling the process of creep, the selection of suitable materials is difficult.

Many heat-resisting steels have been developed for high temperature applications, and the development of these steels has been focused on specific needs within the power generation industry. One such specific niche is bolting steels, which are used for bolting large flanges together as well as various other applications. The materials used for bolting are of extreme importance as their failure can present a serious safety issue due to high pressure steam leakage. Another small family of steels that have been developed are the nitriding steels, intended for applications such as valve stems in which an extremely hard surface is required.

Hitachi Canadian Industries Ltd. (HCI) currently utilizes several proprietary grade steels developed by steam turbine manufacturers for bolting and nitriding purposes. These steels are expensive and difficult to source. Major benefits would accrue from using ASTM grade steels in place of these proprietary grade materials including:

1) material cost reduction, and
2) manufacturing cycle time reduction due to wider material availability.

However, the lack of high temperature creep data for ASTM grade steels has limited their application.

Hitachi Canadian Industries is interested in the creep behaviour of three ASTM steels in particular: A193 Grade B16, A355 Class A, and A437 Grade B4B. A193 Grade B16, which is a 1%CrMoV low alloy steel, and A437 Grade B4B, which is a 12%CrMoW martensitic stainless steel, are intended for high temperature bolting materials. A355 Class A is a low alloy CrMo steel with a 1% Al content developed for nitriding applications.

A study of the creep characteristics of these steels was necessary, including a review of literature to determine what creep test data were already available and to obtain an understanding of the creep behaviour of steels in general. Based on the results of the

literature search, a test program would also be implemented to complement the test data currently available.

1.2.2. Research Objectives

A literature review was conducted to determine the creep data available for these specific steels and for chromium molybdenum alloy steels in general. Little information was found on the specific ASTM grades under consideration although a significant amount of data on the creep behaviour of related steels was uncovered. The three ASTM grade steels under consideration were all developed for specific applications and as a result have not seen widespread use.

A significant test program was needed to more thoroughly examine the creep behaviour of the three ASTM grade steels of interest. Therefore, the objectives of this project are mainly threefold:

1) To determine the high temperature creep characteristics of three ASTM grade steels for the purpose of utilizing these materials for high temperature steam turbine applications.

2) To identify the mechanisms which are controlling the creep behaviour of these steels through analysis of creep strain data and observations of microstructural characteristics prior to and after creep testing.

3) To identify materials that may have better high temperature creep characteristics than those materials tested. Required characteristics for a new material are superior creep performance, low cost, wide availability and high machinability.

The possibility of finding materials that are more suited to the particular applications than the three ASTM grade steels being studied should not be overlooked, and perhaps such materials could be the subject of future testing.

1.2.3. Thesis Outline

This thesis contains five chapters pertaining to the research subject previously outlined. The present chapter is an introduction to the thesis topic. A critical survey of the existing theoretical and experimental works pertaining to the substance of the present topic is presented in the second chapter. The third chapter contains a detailed description of the experimental methods used in this investigation, while a discussion of the

experimental results is presented in the fourth chapter. In the final section, the findings from the study are summarized and recommendations for future work are advanced.

2. LITERATURE REVIEW

2.1. Creep

2.1.1. Background

Under the application of a load, most materials will instantaneously deform a certain amount depending on their mechanical properties. At room temperature, many materials will maintain the same amount of strain until the applied load is changed, at which time the strain will instantaneously change proportional to the load. The strain level will change very little even if the load is applied for a long period of time. However, at higher temperatures, the material will continue to deform with time even though the applied load is unchanged. This phenomenon is called creep and is demonstrated in Figure 1, which displays curves of stress versus strain after various time intervals.

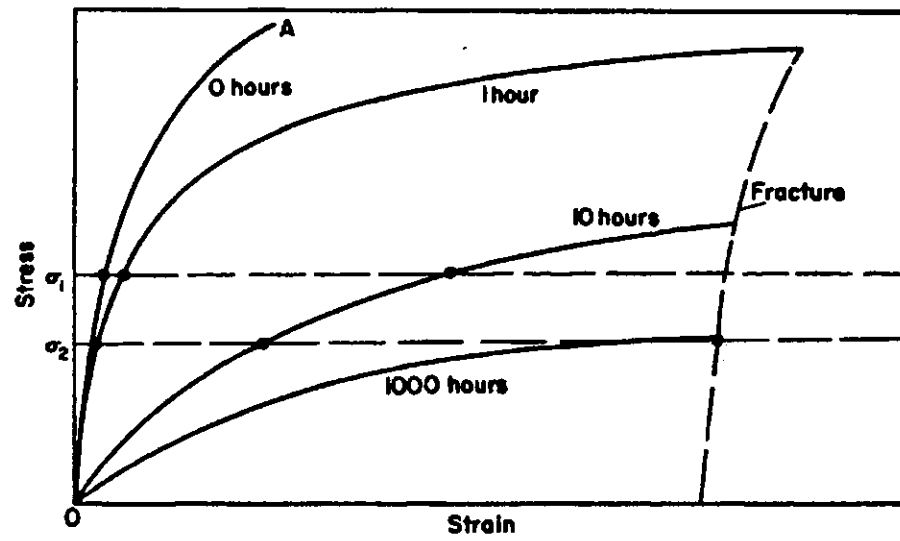

Figure 1: The effect of stress and time on strain.[1]

The curve for 0 hours is a normal stress-strain curve. However, as can be seen in Figure 1, at a given level of stress the strain would continue to increase with time until fracture occurs. The rate of strain increases with increasing stress.

Creep is greatly dependent on temperature and only becomes of any practical significance at higher temperatures. However, the term "high temperature" is relative to the material in question. Usually the melting point, T_m, is used as a reference temperature and it is generally assumed that creep does not greatly affect mechanical behaviour at temperatures below about 0.3 T_m on an absolute scale. Therefore, many materials such as plastics, ice and even lead experience creep at room temperature. However, the melting point of most metals is significantly higher and thus most metals are not influenced by creep until the temperature reaches a value considerably above room temperature.

There are many factors besides temperature that influence the creep behaviour of a material. As a result, the melting point of a material only provides a rough estimate of the effect of creep at a given temperature. Some materials do not experience creep until the temperature rises well above 0.5 T_m.

2.1.2. Stages of Creep

Creep tests are usually performed by measuring the strain as a function of time at a given temperature and under a condition of constant load or stress. Under the condition of constant load, three distinct stages of creep are often observed as shown in Figure 2.

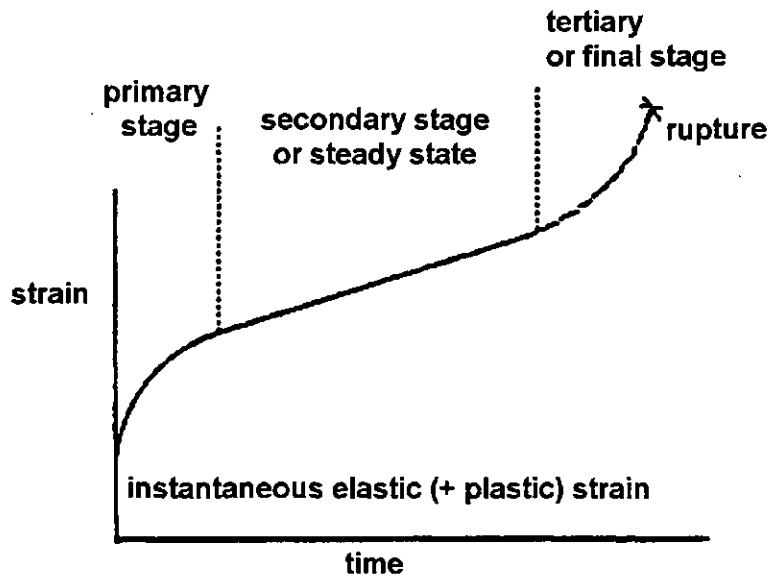

Figure 2: The three stages of creep.

The instantaneous strain is simply the sum of the elastic and plastic yielding that would normally occur on the application of stress. The rate of strain does not remain constant with time. The first stage is usually labeled primary or transient creep and is characterized by a decreasing strain rate with time. The decrease in the strain rate is caused by work hardening in the material. Secondary or steady state creep is characterized by a constant strain rate, which results from a balance between work hardening and recovery processes. Secondary creep is often of the most interest for industrial applications as it usually lasts for a longer period of time than the other stages of creep and the constant rate of strain allows for more accurate design assumptions. The third and final stage is labeled tertiary creep and is terminated by rupture. Tertiary creep involves an increasing strain rate caused by the growth of microcracks in the material. It is important to note that all three stages are not observed in all cases.

In most practical applications, in which the service temperatures and stresses are relatively low, the amount of time required for metals to suffer significant deformation as a result of creep is very large and can be measured in terms of years. The steady state portion of the creep curve is of interest as it allows for the prediction of the life span of a part based on the maximum permissible deformation. However, small changes in stress and temperature can result in large changes in the steady state strain rate if the mechanism controlling creep changes.

2.1.3. Effect of Stress and Temperature

In general, the strain rate due to creep increases with increasing temperature and stress. Creep deformation during the steady state regime is often described using the Norton – Bailey relation

$$\dot{\varepsilon} = A\sigma^{n} \exp\left(-\frac{Q}{RT}\right) \qquad (1)$$

where $\dot{\varepsilon}$ = the steady state strain rate,

σ = the stress,

Q = the activation energy for creep,

R = the universal gas constant, and

T = the absolute temperature.

A and n are coefficients which are used to describe the power law relationship of the strain rate to stress. The second portion of the above expression is the Arrhenius equation, which describes many thermally activated processes.

The activation energy of creep can be determined relatively easily by abruptly changing the test conditions of a creep test from temperature T_1 to temperature T_2 while at a constant stress. It has been observed that in many cases for pure metals the activation energy of creep is similar to the activation energy of atomic self-diffusion as shown in Figure 3.

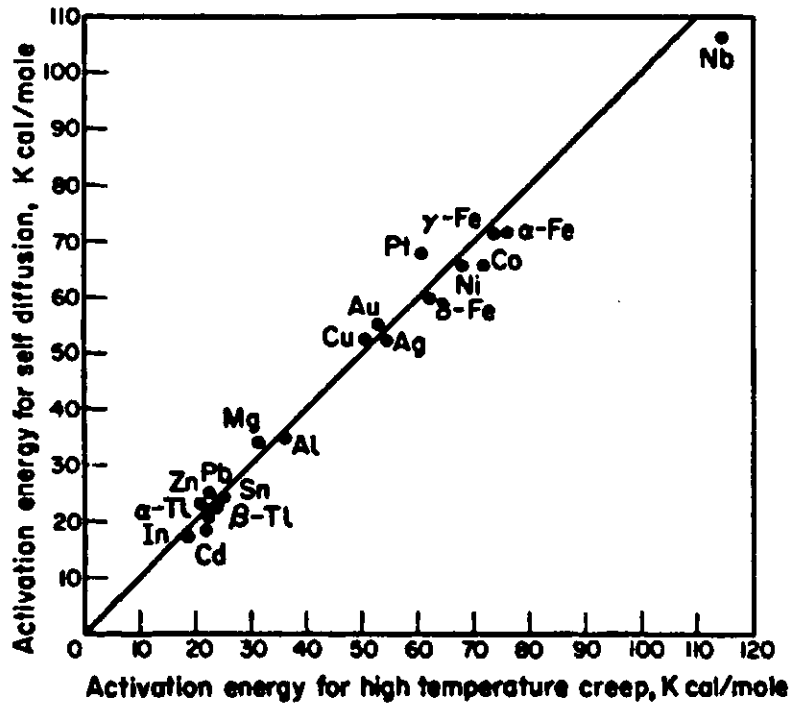

Figure 3: Activation energies of creep and atomic diffusion.[2]

For alloys, the activation energy for creep is often the same as the activation energy for atomic self-diffusion of one of the principal elements. From this relationship it can be inferred that some of the mechanisms controlling creep are dependent on atomic self-diffusion.

As can be seen from equation 1, the creep rate for a specific material at a constant stress will increase as the temperature increases. This behaviour would be expected in a process controlled by atomic diffusion. It should be noted that there are exceptions to this rule such as in dispersion hardened materials.

If the temperature is held constant, in the majority of cases the steady state strain rate will increase exponentially with increasing stress as described by the power law in equation 1. The coefficient n varies between 3 and 8 for most pure metals and many alloys although it is dependent on temperature as well. As the temperature approaches the melting point, metals begin to act as a viscous liquid and n approaches 1.

At very high or very low stresses the power law relationship no longer applies. The expression given above is quite limited as it only applies to secondary creep and the power law coefficients must be determined for specific materials at specific temperatures.

Many other expressions have been developed which attempt to describe the strain during creep. These expressions usually apply to a specific stage of creep or are only suitable for a specific set of conditions. An example is the expression

$$\varepsilon = \frac{\sigma}{E} + \frac{\sigma}{\alpha m + K}\left(1 - e^{-(K/m)t}\right) + \frac{\sigma}{\alpha m + K}\left(e^{\alpha t} - 1\right) \qquad (2)$$

where ε = the strain,

E = the elastic modulus,

t = time, and

α, m, and K = experimentally determined fitting parameters.[3]

This expression is very general and is applicable to all three stages of creep. However, it does not distinguish metallic materials strongly hardened with second-phase particles such as those due to precipitation or dispersion hardening.

2.1.4. Creep Mechanisms

Creep is a complex process that is the result of the interaction of a number of mechanisms. The exact contribution of each of these mechanisms is not fully understood and thus the creep behaviour of materials is not easily described by a single equation.

However, there are two major mechanisms by which creep occurs – dislocation creep and grain boundary sliding. These mechanisms become the important controlling factor at different ranges of temperature and stress. The diagram shown in Figure 4 displays how the controlling mechanism changes as temperature and stress changes.

At lower temperatures the controlling mechanism is dislocation creep. Dislocation creep is a process that occurs at the rate of atomic diffusion. Metals deform by the passage of imperfections called dislocations through the material. When these dislocations hit barriers or pile up, the deformation stops. At temperatures where creep occurs, these dislocations will overcome these barriers through thermally assisted mechanisms such as dislocation climb. As temperature increases and thus the rate of atomic self-diffusion, the resistance to these transgranular failure mechanisms decreases. As a result the creep strength of the material decreases as shown in Figure 4, thus increasing the creep rate. The creep strength of a material is simply a general term used throughout this thesis to describe the relative resistance of a material to the effect of creep.

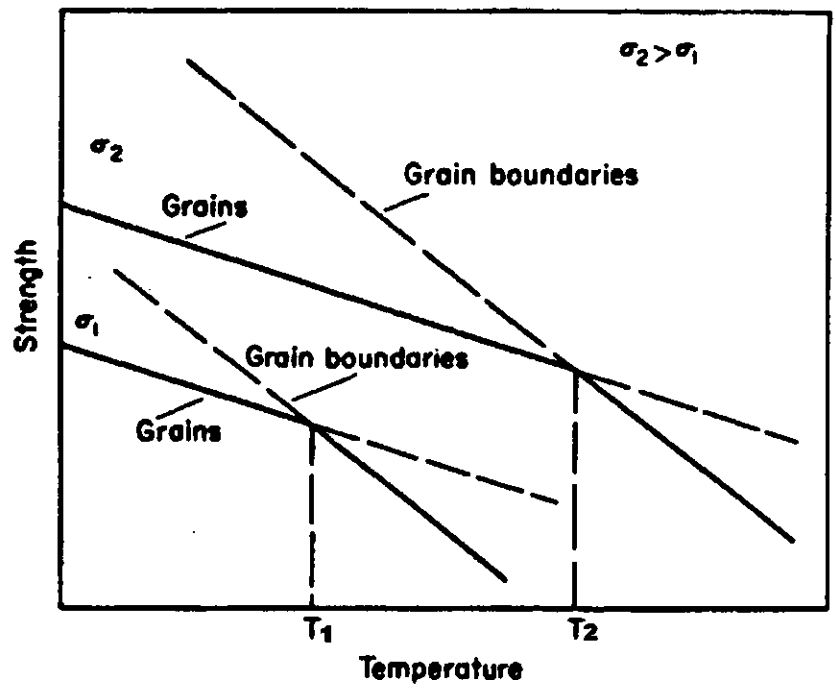

Figure 4: Relative importance of creep mechanisms.[1]

However, as the temperature continues to increase, grain boundary sliding begins to have a more dominant effect on creep. As can be seen in Figure 4, the resistance to grain boundary sliding decreases at a greater rate than the resistance to dislocation creep and the curves eventually intersect at some temperature. At low temperatures, grain boundaries are a source of strength as they block the spread of dislocations. However, at high temperatures grain boundaries may become a source of weakness.

Grain boundary sliding tends to have a greater effect on creep at higher temperatures and lower strain rates, whereas dislocation creep is of more importance at lower temperatures and greater strain rates. This can also be seen in Figure 4 by comparing two stress levels, σ_1 and σ_2. As the stress is increased, the temperature at which the mechanism changes tends to increase, which suggests that grain boundary sliding is less likely to be a factor.

2.1.5. Creep Resistance

The ability of a material to withstand creep at high temperatures is affected by a number of factors. One of the most obvious is the melting point of the material. A material with a higher melting point will generally have greater creep resistance at any given temperature.

The main metallurgical features that influence the creep resistance of a material are:

1) solid solution strengthening,
2) grain size,
3) crystal structure,
4) precipitation strengthening, and
5) dispersion hardening.

Work hardening will also increase the creep resistance in the initial stages of creep especially at low temperatures. However, in the long term it may be detrimental to the creep strength of a material due to the increase in the number of dislocations caused by work hardening.

Solid solution strengthening is simply the addition of elements that form a single phase with the parent material in the original crystal structure. The strengthening effect is a result of the lattice strains caused by the introduction of atoms of different size into the lattice structure.

The effect of grain size on the creep resistance is not fully understood and is somewhat dependent on the creep mechanism at work. In a single-phase alloy, increasing the grain size usually increases the creep resistance due to the smaller grain boundary area, which is a point of weakness at higher temperatures. However, testing has not conclusively shown that creep resistance is affected by grain size.

The crystal structure affects the rate of atomic self-diffusion and thus has an influence on creep resistance. In an otherwise identical material, a close packed structure such as face centered cubic will have a much lower rate of diffusion than a body centered cubic structure.

Precipitation strengthening and dispersion hardening are similar in that they both involve the production of a fine matrix of particles of a different phase than the parent material. This is often the most effective method of increasing creep strength.

Other factors may have an effect on the creep behaviour of a material as well although the net change in creep resistance is likely to be small.

Figure 5 shows the relative creep resistance of a number of alloys for comparison. It can be seen that the 12%CrMoV steels have significantly better creep resistance than the 1%CrMoV steels. This is a result of the solid solution strengthening and precipitation strengthening effects of the additional alloying elements. Figure 5 also shows that the nickel alloys display resistance to creep at much higher temperatures than the steel alloys. However, they are much more expensive to produce and thus their usefulness has been limited.

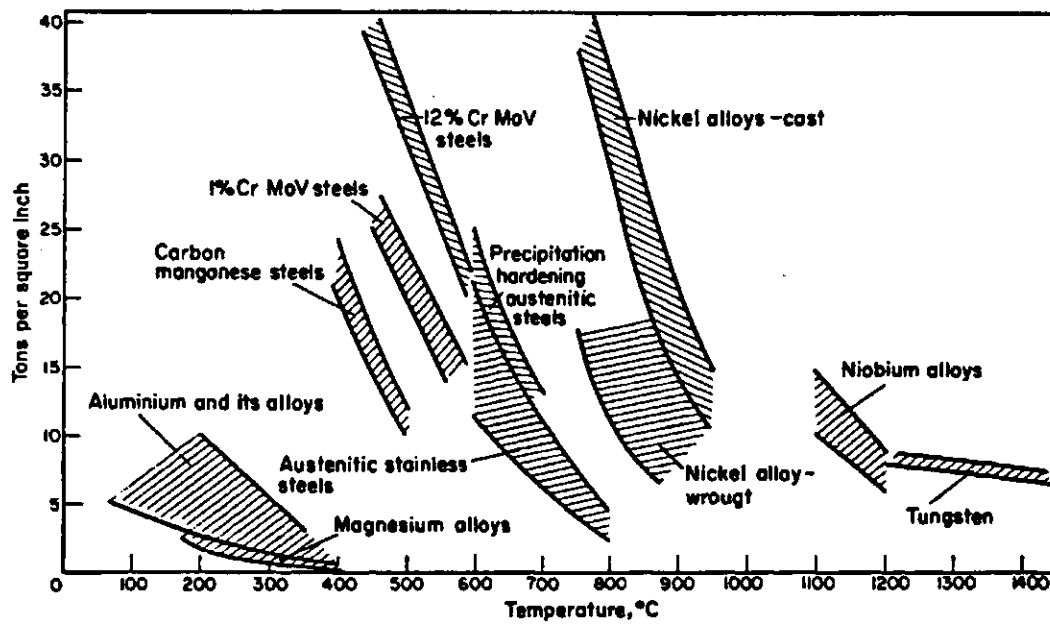

Figure 5: Stress required to produce rupture in 100 hours.[1]

2.2. Low Alloy Steels

As discussed in the previous section, the addition of alloying elements that provide solid solution strengthening or precipitation strengthening is an important method for improving the creep resistance of a material. Many different alloy steels have been developed using these principles. Some of the most common are low alloy steels containing chromium and molybdenum, which includes both the ASTM A193 Grade B16 and ASTM A355 Class A steels. These steels have been used extensively in the power generating and chemical industries for high temperature applications such as boiler tubes, pressure vessels, piping, and bolting materials.[4,5] These steels demonstrate considerably better creep and oxidation resistance than plain carbon steels. The 2.25%Cr-1%Mo and 1%Cr-0.5%Mo steels are among the most common of these alloys. Vanadium has also been added to some of these low alloy steels in small amounts generally between 0.2-0.3%. The effect of these elements on the creep behaviour of steel is discussed in the following section.

2.2.1. Major Alloying Additions

Although the creep resistance of plain carbon steels is relatively good, it can be improved considerably by the addition of certain alloying elements. The main alloying elements used in low alloy steels are chromium, molybdenum, and vanadium.

2.2.1.1. Chromium

Chromium is typically added to steel to improve corrosion resistance, although it also provides a strengthening effect. By itself, chromium provides some increase in creep resistance through solid solution strengthening. However, it has been observed that when used in conjunction with molybdenum, chromium tends to reduce the creep resistance compared to an alloy containing only molybdenum.[6,7] An example of the effect of chromium on the creep behaviour of a 0.5%Mo steel is shown in Figure 6.

As can be seen in Figure 6, the addition of chromium caused an increase in the strain rate or a decrease in the creep resistance. This is a due to a reduction in the initial interstitial solute level and succeeding level of precipitate particles. Chromium tends to precipitate more rapidly than the molybdenum compounds thus limiting the nucleation of Mo_2C and Mo_2N particles which tend to reduce the creep rate. However, chromium is often added to increase the rupture ductility compared to that of steel containing only molybdenum.

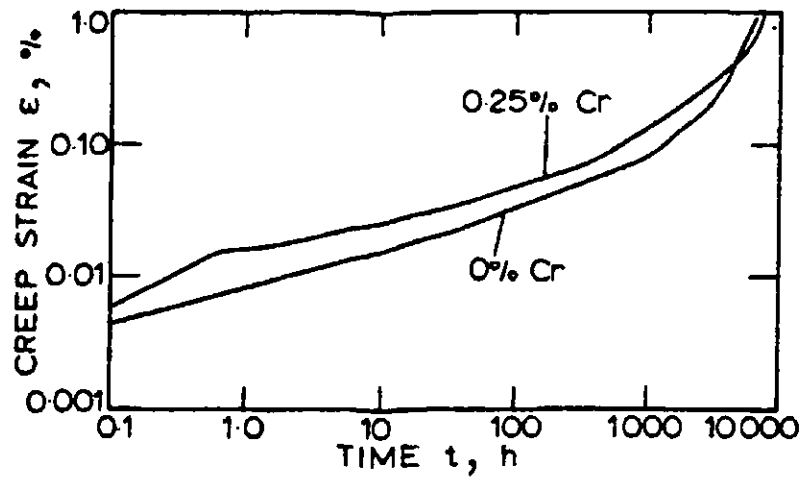

Figure 6: Effect of chromium content on creep of 0.5%Mo steel.[6]

There appears to be an optimum chromium content beyond which no significant increase in creep resistance will occur.[5] This point is a function of the amount of molybdenum in the steel. For steel containing 1%Mo, the optimum chromium content is about 2.25%, which explains the evolution of the 2.25%Cr-1%Mo steel mentioned earlier. For steel with a 0.5%Mo content, a chromium content beyond about 2% may result in a loss of creep resistance.

2.2.1.2. Molybdenum

The addition of molybdenum to steel can produce a material with excellent creep resistance but the rupture ductility may be affected. Molybdenum increases the creep strength initially through solid solution strengthening. However, as aging occurs, molybdenum carbides and nitrides precipitate along grain boundaries and within the grains themselves. These precipitates block the movement of dislocations thus providing a strengthening effect. Precipitation strengthening then becomes the principal strengthening mechanism.[7]

2.2.1.3. Vanadium

Vanadium is added in very small amounts (less than 0.1%) to steels to control grain size. However, in larger concentrations it also has a significant effect on creep resistance. Vanadium increases creep resistance predominantly through precipitation hardening. The vanadium compounds take significantly longer to precipitate and show

significantly more resistance to overageing than the molybdenum compounds.[6,8] In the tertiary creep stage, the molybdenum precipitate particles tend to become coarser, or overage, eventually negating their strengthening ability. Vanadium is important for long-term creep strength, as it is not as susceptible to overaging. The addition of vanadium to a 2.25%Cr-1%Mo steel has also been shown to result in a material with improved resistance to hydrogen attack, hydrogen embrittlement, and temper embrittlement, which are other elevated temperature phenomena related to creep.[9]

2.2.2. Minor Alloying Additions

Many other elements are present in small amounts in alloy steels that can influence their creep resistance.

2.2.2.1. Nitrogen

Nitrogen is an important element as it results in the formation of molybdenum nitride and vanadium nitride compounds, which help to precipitation strengthen low alloy steels thereby increasing their creep strength. Nitrogen is also a significant contributor to solid solution strengthening initially, but obviously this effect diminishes as precipitation occurs. As would be expected, studies have shown that increasing the amount of nitrogen reduces the creep rate as seen in Figure 7.

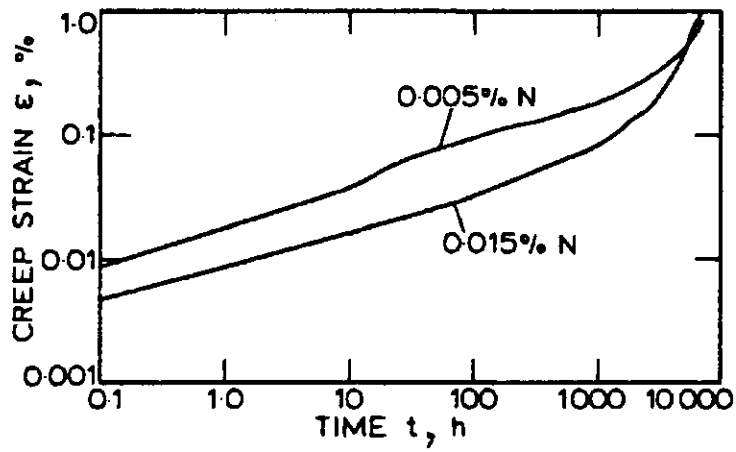

Figure 7: Effect of nitrogen content on creep of 0.5%Mo steel.[6]

2.2.2.2. Carbon

The influence of carbon content on the creep resistance is obviously of interest as carbon is always present in steels in various amounts. Increasing the carbon content actually results in an increase in the creep rate as shown in Figure 8. This is partially

due to the fact that the initial levels of interstitial solutes decrease as the carbon content increases although this difference disappears by the end of primary creep.[6] The reason for the decrease in secondary creep strength with increasing carbon content is not fully understood.

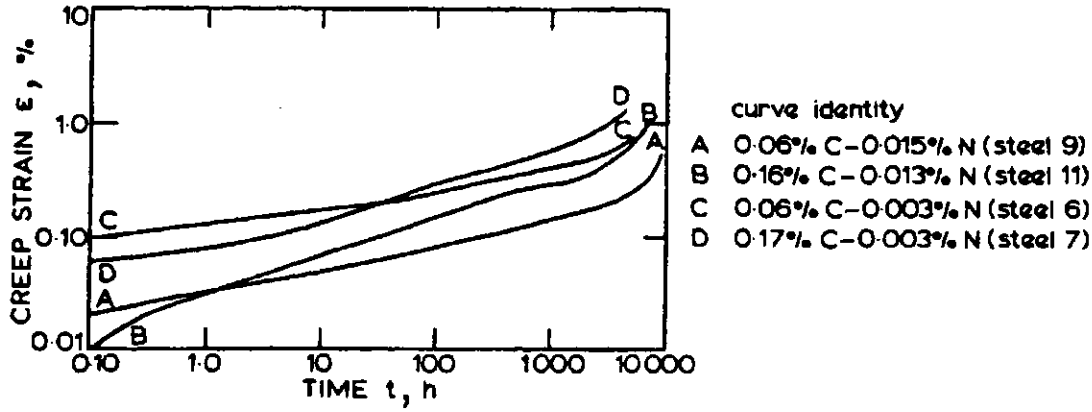

Figure 8: Effect of carbon content on creep of 1%Mo steel.[6]

Obviously, some carbon is required to form the carbide precipitates that are essential for the long-term creep strength of low alloy steels but the amount needed is very small. In general, the carbon content is between 0.1% and 0.4% in most of these alloys.

2.2.2.3. Phosphorous

Phosphorous has a negative effect on the strength of steels in general and is considered an impurity in steels. The phosphorous content is generally minimized as much as is economically feasible. The presence of phosphorous is also believed to reduce the creep resistance of alloy steels, mostly by promoting the development of coarse carbides that are less effective in precipitation strengthening. It has been shown that phosphorous in a 2.25%Cr-1%Mo steel promoted the precipitation of M_6C carbides at the expense of dispersions of finer M_2C carbides.[10,11] Another study found a much higher concentration of large M_3C particles in a 1%CrMoV steel to which 0.1%P had been added compared to high purity material, which contained fine MC and M_2C carbides.[12]

A more recent study examined the effect of adding 0.02%P to a 1%Cr-1%Mo-0.75%V steel doped with 0.08%Ti.[13] There was little observable difference between those steels containing additional titanium and phosphorous and those with only titanium. The carbide composition of the steel doped with phosphorous seemed to shift somewhat

towards greater molybdenum content compared to the purer steel, which contained vanadium-rich carbides. The additional phosphorous appeared to have no effect on the size of the carbide precipitates.

2.2.3. Effect of Heat Treatment

Heat treatment can have a large effect on the microstructure of a low alloy steel and thus can influence the creep resistance. In general, bainitic structures have the best creep resistance while pearlitic structures have the worst creep resistance. Figure 9 illustrates the effect of initial microstructure on the creep strength of a 2.25%Cr-1%Mo steel. Obviously, an initial heat treatment that produces a completely bainitic microstructure is optimal for high creep strength.

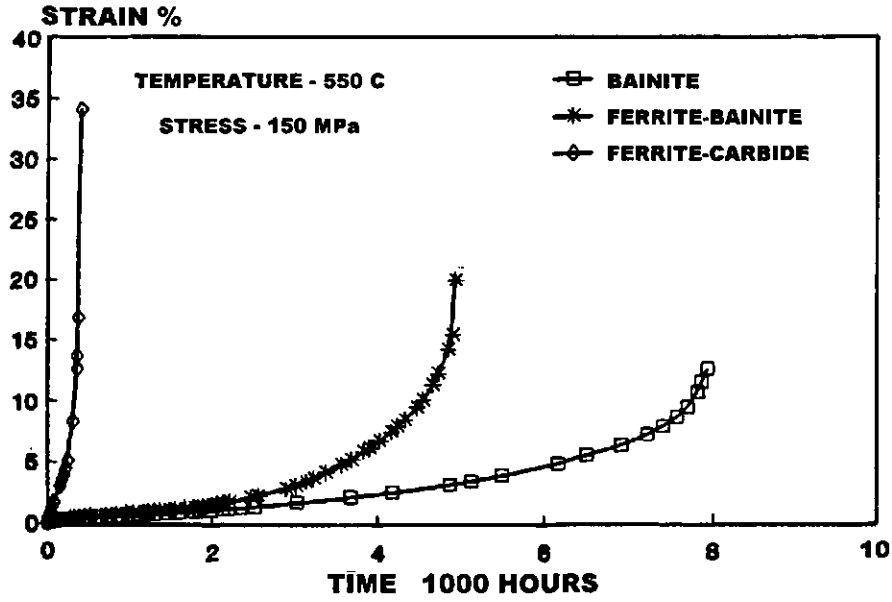

Figure 9: Typical creep curves for 2.25%Cr-1%Mo steel with different initial microstructures.[5]

Whether isothermal transformation or normalizing produces greater creep strength than a quenching and tempering treatment is unclear. It would seem that specimens that undergo isothermal transformation tend to experience higher creep rates while specimens that are quenched and tempered appear to have a shorter creep life.[6,8]

It is clear that tempering seems to reduce the overall creep life and reduces long-term creep strength. This is most likely due to the fact that some precipitation occurs during

tempering so that precipitate particles tend to age more rapidly during creep and coarsen to the point where they no longer enhance creep resistance sooner. The contribution of solid solution strengthening to the overall creep strength of a tempered specimen is minimal even in the initial stages of creep, as the precipitation strengthening contribution becomes dominant much earlier. These observations are illustrated in Figure 10.

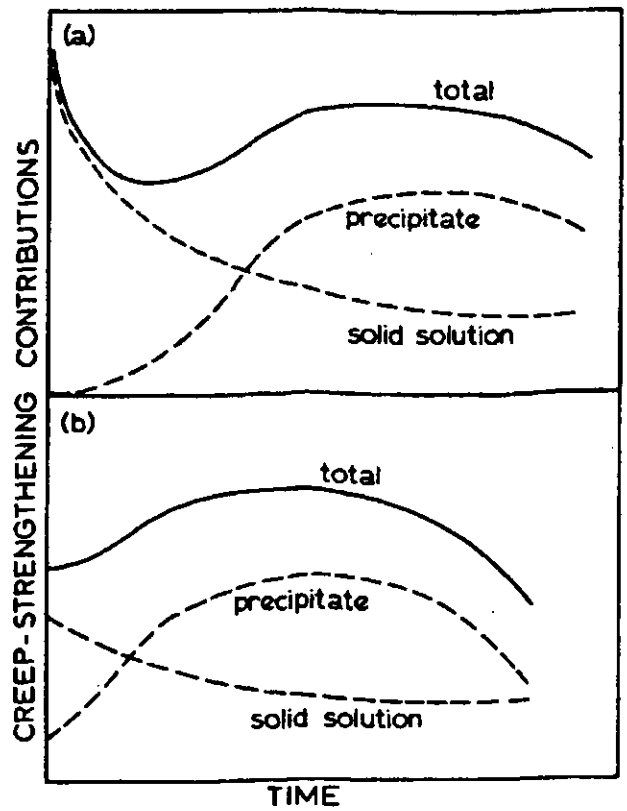

Figure 10: Creep strengthening contributions.[7]

These transient effects obviously become less important at lower stresses such as those seen in service. The creep life is much longer and the impact of the initial heat treatment and microstructure is minimal when compared to the total creep life.

2.2.4. Creep Behaviour

Creep is a very complex phenomenon that is controlled by a number of mechanisms, most of which are not fully understood. Unfortunately, the creep behaviour of alloys is even more complex than that of pure metals.

2.2.4.1. Stages of Creep

As discussed in Section 2.2, the creep behaviour of many materials is characterized by three distinct stages, which differ with respect to the derivative of the strain rate. For most pure metals, the second stage of creep, which displays a constant strain rate, is dominant. However, this is untrue for many alloys, which may have a very short secondary stage or may be missing it altogether.

A study which attempted to create isochronous, or constant time, stress versus strain curves for a 2.25%Cr-1%Mo low alloy steel from a compilation of stress-rupture data from many sources found that the tertiary creep stage commenced at very low strains.[14]. Another source examining the mechanisms of creep behavior for the same low alloy steel also reported a prominent tertiary creep region as shown by the typical creep curves in Figure 9. These curves display a region of continuously increasing creep rate, which extends over a major portion of the creep life.

The strain rate tends to increase for much of the creep life of low alloy steels due to the coarsening of the precipitate particles that provide much of the creep strength of these steels. For CrMo steels, the optimum creep strength is derived from a uniform distribution of fine needle-like Mo_2C carbides, which can be achieved by a suitable heat treatment. However, Mo_2C is not a thermodynamically stable carbide and during creep it eventually transforms to coarser carbides such as $M_{23}C_6$ or M_6C, which are not as effective in resisting creep.[4] These carbides also coarsen with time until eventually they are ineffective and provide no precipitation strengthening. A similar process affects the vanadium compounds that occur in the low alloy steels containing vanadium. However, these compounds are more resistant to coarsening than those of molybdenum or chromium.

The precipitation and coarsening of precipitate particles is enhanced by creep and is not simply a high temperature aging process. The precipitation of M_2C particles in specimens of a 1%Cr-0.5%Mo steel subjected to a creep stress at 560°C was observed to be significantly greater than in specimens aged at the same temperature in the absence of stress.[15]

2.2.4.2. Creep Mechanisms

It has been observed that the creep behavior of low alloy CrMoV steels can be divided into two distinct regions based on the magnitude of the applied stress in which two

different mechanisms appear to be operating. Figure 11, which displays the stress dependence of the creep rate and the time to fracture for a 0.5%Cr-0.25%Mo-0.25%V steel, demonstrates this behaviour.

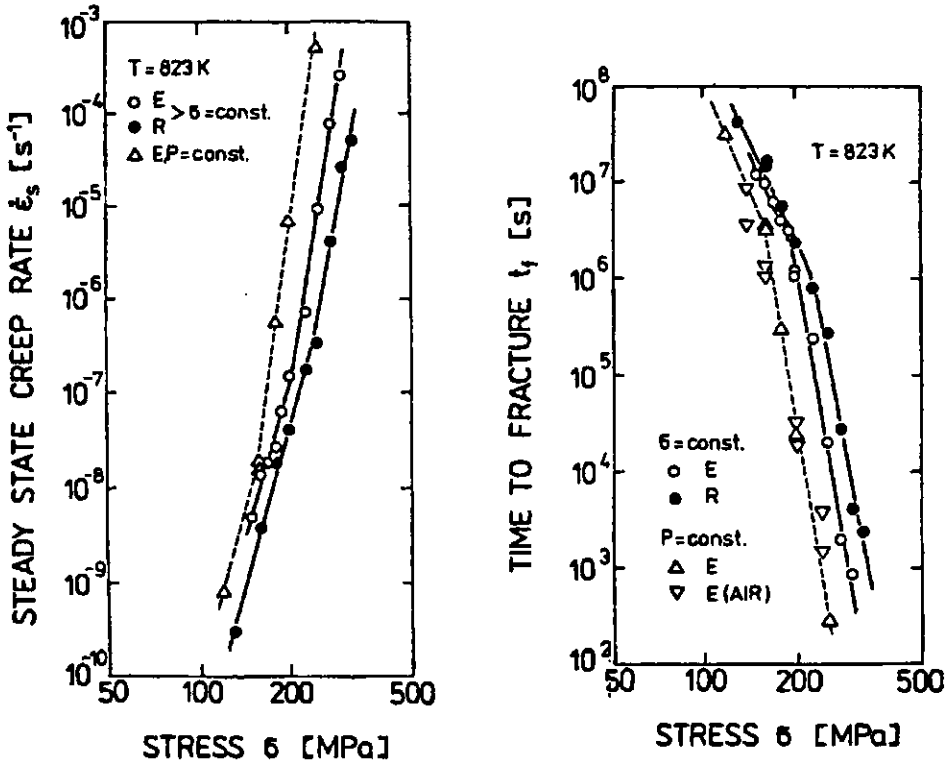

Figure 11: Stress dependence of a) creep rate, and b) time to fracture, for CrMoV steel.[16]

The specimens used in this study were taken from a steam tube that had been subjected to creep in service and had undergone plastic strain of approximately 1%. Condition E denotes specimens tested in the as-received condition. Condition R denotes specimens subjected to a regenerative austenitizing heat treatment with the goal of restoring the pre-service microstructure.

In this study and others examining low alloy CrMoV steels, the stress exponent for the secondary creep phase in the low stress region was found to be $n \cong 5$, while at higher stresses, $n \cong 11$.[16] It is important to note that the secondary creep phase refers to the portion of the creep curve with the minimum creep rate and may not be steady state. The change in the stress exponent would indicate that the mechanism controlling creep changes at a critical stress. Above this critical stress, the creep strength increases as the interparticle spacing decreases, or the number of precipitate particles increases.

Below this critical stress, the interparticle spacing was found to have little effect on the creep strength.

Examination of the microstructure of fracture specimens revealed that transgranular fracture was predominant in the high stress region, while intergranular fracture prevailed at low stresses. The main obstacles to dislocation creep, which is characterized by transgranular fracture, are obstructions such as precipitate particles.[17] This explains the dependence of creep strength on interparticle spacing at high stresses.

It is believed that intergranular cavities are nucleated due to grain boundary sliding at geometrical irregularities where high local stress concentrations can develop. The fraction of grain boundaries with observable grain boundary sliding and the mean displacement due to grain boundary sliding were measured for the 0.5%Cr-0.25%Mo-0.25%V steel mentioned earlier. The results are displayed in Figure 12 and show that grain boundary sliding increases as the stress decreases.

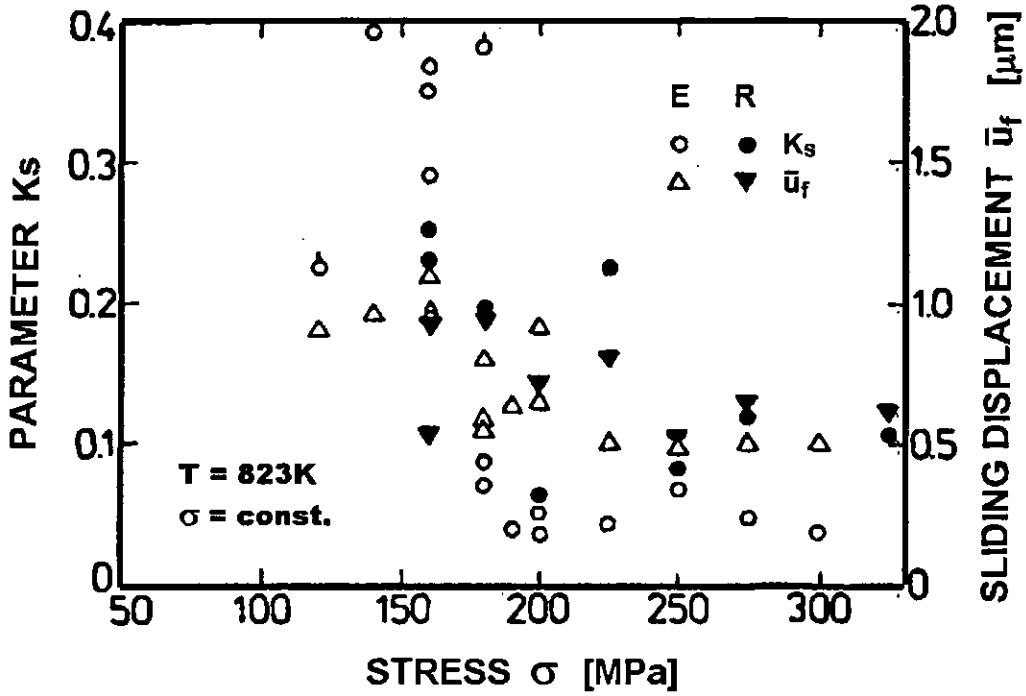

Figure 12: Stress dependence of the fraction of grain boundaries, k_s, with observable grain boundary sliding, and the mean displacement due to grain boundary sliding.[16]

From Figures 11 and 12 it appears that the critical stress which corresponds to the transition between dislocation creep and diffusion creep (or grain boundary sliding) is approximately 200 MPa for this steel. Under the normal service conditions of these steels, diffusion creep would likely be the controlling mechanism.

Another elevated temperature phenomenon which must be considered is embrittlement, or more specifically, reverse temper embrittlement. Elements in the fourth, fifth and sixth main groups in the periodic table such as phosphorous and sulfur, which are found as trace elements in steels, are the main contributors to this process. Reverse temper embrittlement is an ageing process similar to creep which was found to occur at a maximum rate between 450 and 460°C in a 1%Cr-0.02%V steel.[18] The presence of molybdenum and a low impurity content reduce the embrittlement rate considerably.

2.3. Martensitic Stainless Steels

The addition of large amounts of chromium to steel has long been used to improve the corrosion resistance of steels. However, the high alloy content of stainless steels also provides them with much greater creep resistance than plain carbon steels. Stainless steels are often used for applications that require greater resistance to high temperature oxidation than low alloy steels can provide.

There are several classes of stainless steels but only tempered martensitic stainless steels are considered in this thesis. Tempered martensitic stainless steels generally have a chromium content between 9 and 12% and are characterized by a martensitic microstructure, which differentiates them from ferritic stainless steels. Ferritic stainless steels generally have similar chemical compositions but contain less nickel so they do not form martensite upon quenching from the austenitic range. Tempered martensitic stainless steels often contain smaller amounts of other elements as well such as molybdenum and tungsten.

As their name suggests, tempered martensitic stainless steels are quenched from the austenitic range to form martensite, and then tempered to reduce internal stresses. The microstructure after tempering consists of martensitic lath subgrains, with fine precipitate particles at subgrain boundaries.

Tempered martensitic stainless steels are less expensive than austenitic stainless steels, which have a high nickel content to stabilize the austenite phase at low temperatures. Tempered martensitic stainless steels are preferred for many

applications in the power generation industry because of their lower cost and lower coefficient of thermal expansion compared to austenitic stainless steels.[19]

2.3.1. Major Alloying Additions

Tempered martensitic stainless steels are similar in composition to most low alloy CrMo steels except that they contain a much larger amount of chromium for improved corrosion resistance. Tempered martensitic stainless steels derive their creep resistance from two main sources:

1) the solid solution strengthening effects of certain elements, and
2) precipitation strengthening caused by the precipitation of fine carbide and nitride particles.

2.3.1.1. Solid Solution Strengthening

Most tempered martensitic stainless steels have a chromium content between 9 and 12%, as this appears to provide the best combination of creep strength and oxidation resistance. Higher levels of chromium tend to result in the formation of δ-ferrite, which is undesirable.[20] Chromium mainly provides solid solution strengthening.

Molybdenum has traditionally been added to tempered martensitic stainless steels to provide solid solution strengthening, which accounts for much of the inherent creep strength of these steels.[7,20] Tungsten also contributes to solid solution strengthening and is used in addition to molybdenum in many steels.[21,22] The molybdenum equivalent is given by

$$\text{Mo equivalent} = \%\text{Mo} + \tfrac{1}{2}\,\%\text{W} \qquad (3)$$

and the optimum level is around 1.5%.[23] For a given Mo equivalent level, increasing the tungsten content results in an increase in creep strength.[24] However, a tungsten content of 1.8% is optimal as the strengthening effect is near maximum at this level and increasing the amount of W beyond this point results in significant loss in toughness. Increasing the W content also leads to the formation of Laves phase, which consists of coarse precipitate particles of $Fe_2(Mo,W)$.

The effect of Laves phase on creep strength is a subject of some disagreement. One study found that the continuous precipitation of this phase in a 11%Cr-0.15%Mo-2.6%W-0.2%V steel provided intergranular precipitation strengthening and was an important factor in maintaining high creep strength.[25] However, formation of the Laves

phase also results in a reduction of the amount of molybdenum and tungsten in solid solution thus decreasing the solid solution strengthening effects of these elements. Another study found that Laves phase precipitation reduces the creep rupture life by about a factor of two compared to the effects of precipitate particle coarsening.[26]

2.3.1.2. Precipitation Strengthening

Much of the creep resistance of tempered martensitic stainless steels is derived from the precipitation of fine particles throughout the microstructure. Some of these precipitates are formed during heat treatment. However, the microstructure of tempered martensitic stainless steels continues to evolve during service under the influence of temperature and stress. More precipitates form which provide much of the long-term creep life of these steels. These precipitates increase creep strength by blocking the movement of dislocations and retarding subgrain growth. Eventually the growth of both subgrains and precipitate particles results in the degradation of the creep strength and eventual failure.

Molybdenum forms carbides that contribute to precipitation strengthening. Vanadium is also often added as it forms fine nitride particles which are much more stable than molybdenum compounds. A small amount of niobium of approximately 0.06% has been found to aid in the formation of a small volume fraction of carbides that are even more stable and can result in a significant strengthening effect.[27]

One of the main precipitates in martensitic stainless steels is the $M_{23}C_6$ carbide. The M represents metal and can be filled by chromium, iron, molybdenum, or tungsten. These precipitates form on subgrain boundaries during tempering and increase creep strength by retarding subgrain growth.

Another common precipitate produced during tempering is the MX phase, which consists mainly of vanadium, niobium, and nitrogen. These particles precipitate within subgrains, both during tempering and during creep, and increase creep strength by pinning down free dislocations. These precipitates are very fine and have excellent thermal stability, and thus play an important role in the long term creep strength of martensitic stainless steels.[28]

Other phases such as M_2X and M_3X have much lower thermal stability and are considered undesirable, as they interfere with the distribution of the MX phase. The

addition of vanadium, niobium, and nitrogen in stoichiometric ratios necessary to form MX phase is known to increase creep strength for this reason.[28]

Other phases such as Laves phase and Z-phase begin to precipitate during long-term ageing or creep. Laves phase, which was mentioned earlier, contains molybdenum and tungsten, and its effect on creep strength seems unclear. Studies have found that Laves phase precipitates improve creep strength. However, it is known that these phases coarsen relatively rapidly and thus their creep strengthening effect may be limited in the long term. Z-phase has only been observed in specimens subjected to long term creep exposure in the order of 10 000 hours or more, and contains high concentration of chromium and vanadium. This phase may affect the stability of chromium rich $M_{23}C_6$ and VN particles.[29]

2.3.1.3. Other Elements

The addition of small amounts of boron has been observed to improve creep strength and ductility in austenitic steels although the strengthening mechanism is not fully understood. Boron has also been added to some tempered martensitic stainless steels in concentrations of around 0.01%.[30] One study found that a large percentage of the boron in a 12%Cr steel tended to be concentrated in $M_{23}C_6$ particles.[31] This phenomenon has also been observed in austenitic steels although its significance is unknown.

Cobalt is known to reduce the formation of δ-ferrite and thus has been added to some steels with high chromium content. Cobalt also is thought to provide solid solution strengthening in concentrations up to 3%.[23]

The addition of nickel as an alloying element to martensitic stainless steels results in a decrease in creep resistance and can reduce long term microstructural stability. However, it is added at a level below 1% to delay transformation during cooling to allow a complete martensitic microstructure to form upon quenching. At times it is desired for applications requiring a lower impact transition temperature than that provided by regular ferritic steel. Increasing the nickel content also reduces the temperature of transformation to austenite and increases the tempering resistance. Figure 13 shows the effect of nickel content on the creep strength of a 12%Cr-Mo-V-Nb steel.[32] The creep strength decreases as the nickel content increases.

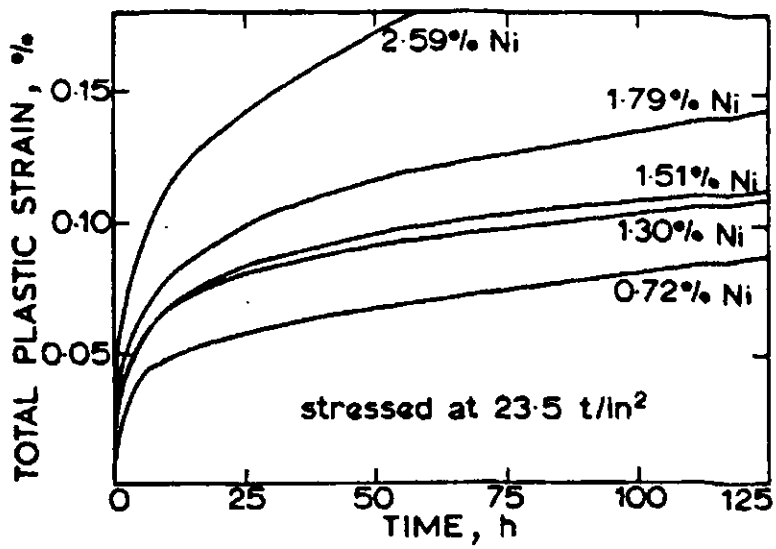

Figure 13: Effect of nickel content on creep strength of FV448 at 450°C.[32]

The use of dispersion hardening techniques can provide even greater creep resistance than those techniques already mentioned and can be effective at temperatures as high as 700°C. One study showed a significant increase in creep strength in a 13%Cr-1.5%Mo steel when titanium was added due to the formation of TiO_2 oxides.[33]

2.3.2. Creep Behaviour

2.3.2.1. Creep Mechanisms

Tempered martensitic stainless steels such as ASTM A437 Grade B4B are complex alloys that display similarly complex creep behaviour. Many pure metals and simple alloys have a very pronounced secondary creep region characterized by a steady state strain rate. However, most tempered martensitic stainless steels have an insignificant secondary phase or none at all, and the majority of the creep deformation occurs in the tertiary region of accelerating strain rate. This behaviour was observed for 12%CrMoV[34], 9%CrMoV[35], and 9%CrW steels.[36] The microstructure of these steels continues to evolve during creep, which results in decreasing creep strength with time.

Tempered martensitic steels are heated into the austenite range and then liquid quenched to form martensite. These steels are then tempered at a temperature somewhat above the expected operating temperature to relieve some of the internal stresses caused by the transformation to martensite and to increase the ductility and toughness. The initial microstructure of these steels after the tempering treatment is

characterized by tempered martensite laths with coarse $M_{23}C_6$ precipitate particles at subgrain boundaries.[26,35,37] There are usually finer MX or M_2X precipitates as well both at grain boundaries and within the grains themselves.[26,37] The composition of these fine precipitates depends on the overall composition of the steel. The majority of these precipitates are usually VN particles. V. Foldyana et al state that M_2X particles form at tempering temperatures below 700°C while at higher temperatures the MX phase is preferred.[38]

The effect of these precipitate particles is to prevent movement of subgrain boundaries, to impede knitting reactions between free dislocations and subgrain boundaries, and to pin subboundary dislocations, thus providing a strengthening effect.[39]

Under the influence of stress and temperature during service, the microstructure of these steels continues to evolve. The degradation of the creep strength with time is mainly due to the coarsening of both subgrains[40] and the precipitate particles themselves.[41] The coarsening of carbides is dependent on both stress and temperature, and will occur at a greater rate if either stress or temperature is increased. The coarsening of carbides is theorized to cause cavity generation once a critical carbide size is reached as it weakens the interface between the carbide and matrix.[42]

Similar to low alloy steels, the creep behaviour of most tempered martensitic stainless steels appears to be controlled by two different mechanisms at high and low stress. This behaviour was observed for Grade P92, a 9%Cr-0.5%Mo-1.8%W-0.02%V steel, as can be seen in Figure 14.

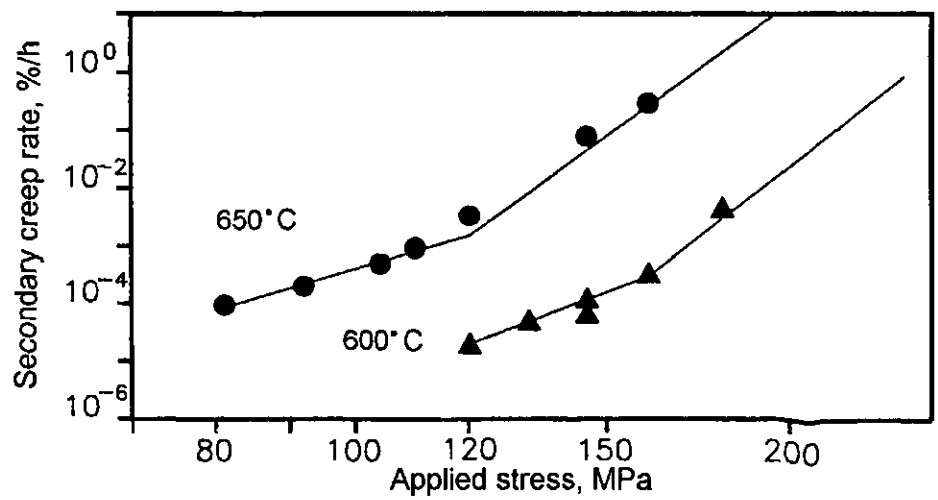

Figure 14: Secondary creep rate as a function of applied stress for P92.[42]

The stress exponent, n, in the lower stress region was found to be 6, while at higher stresses it increased to 16. Another study found that the stress exponent decreased from 6.8 to a lower value at stresses below 90 MPa for a 12%CrMoV steel.[34]

2.3.2.2. Effect of Oxidation

Oxidation must also be considered for many service applications. Corrosion in steam and combustion gas environments was found to lead to a significant decrease in creep strength due to loss of wall thickness for Grade P92 steel.[43] Figure 15 displays the predicted effect of oxidation on various wall thicknesses in long term service for this steel.

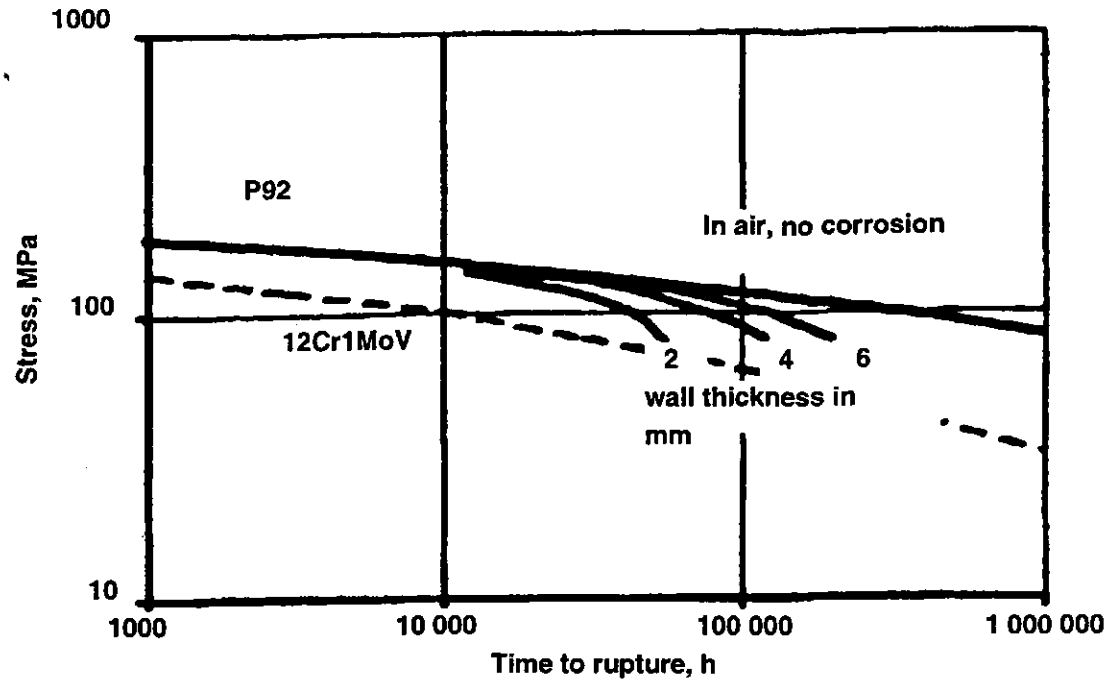

Figure 15: Stress rupture strength at 600°C for P92 taking into account effect of oxidation in simulated coal combustion environment.[43]

As can be seen in Figure 15, 12%CrMoV steel has a significantly lower creep strength than Grade P92. However, in corrosive environments this difference may be negated due to the considerably better corrosion resistance of 12%Cr steels.

2.4. Life Prediction

Prediction of the life of materials undergoing creep deformation is a topic of great practical interest as it aids in the design of parts which will be subjected to high operating temperatures. These methods are also useful for the assessment of the remaining life of parts in service. Many different life prediction methods have been developed.

2.4.1. Time-Temperature Parametric Methods

The most common life prediction methods utilize a time-temperature parameter such as the Larson-Miller, Sherby-Dorn, or Manson-Haferd parameters. These methods use data obtained from creep rupture tests at different stresses and temperatures to obtain a master curve of stress plotted versus the fore-mentioned parameters. These master curves are then used to estimate long-term rupture strength.

2.4.1.1. Larson-Miller Parameter

The Larson-Miller Parameter, which was one of the first time-temperature parameters developed and one of the most commonly used, has the form of

$$P_{L-M} = T(\log t + C) \qquad (4)$$

where T = temperature (K),
t = rupture time (hours), and
C = a constant with a value around 20.

This parameter was developed based on the Arrhenius equation mentioned earlier, which assumes that creep is governed by rate-process theories. The parameter states that for a given stress the time to rupture is related to temperature by the above equation.

The originators of this parameter assert that the value of the constant, C, is independent of stress.[44] This can be seen if log t is plotted against the reciprocal of the absolute temperature for constant stress. The result should be a straight line, which crosses the ordinate when 1/T = 0, or log t = -C. As shown in Figure 16, which contains a number of constant stress curves for the same material, the point at which the curves cross the ordinate is the same for all stresses. The value of the constant, C, can then be determined for a given material by creating a number of constant stress curves as

shown. The point at which these curves cross the ordinate is equal to the value of the constant. Note that the axis of log t is inverted.

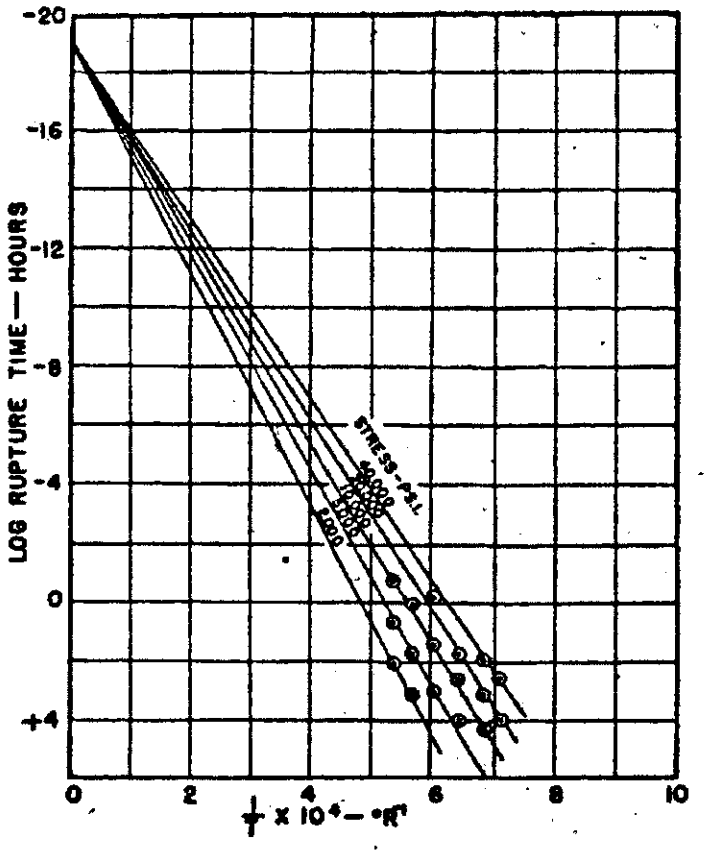

Figure 16: Constant stress curves for Larson-Miller parameter.[44]

Once the value of the constant C is determined, a master curve can be created by plotting the stress versus the Larson-Miller parameter for each test performed. Using this curve, long term rupture times at low temperatures may be predicted from short term test data at higher temperatures.

A value of 20 for the constant C is typical for many materials, and in the absence of sufficient test data to allow the determination of this constant for a particular material, this value may be used without introducing significant error in many cases.[44]

2.4.1.2. Other Parameters

Many other time-temperature parameters have been developed in attempts to address the shortfalls of the Larson-Miller parameter or to apply parametric methods to other materials.

The Manson-Haferd parameter is given by the expression

$$P_{M-H} = \frac{\log t - \log t_A}{T - T_A} \qquad (5)$$

which predicts that a constant stress plot of log t versus T yields a family of straight lines which converge at a point as shown in Figure 17. The coordinates of this point represent the values of the constants, log t_A and T_A, for that particular data set.

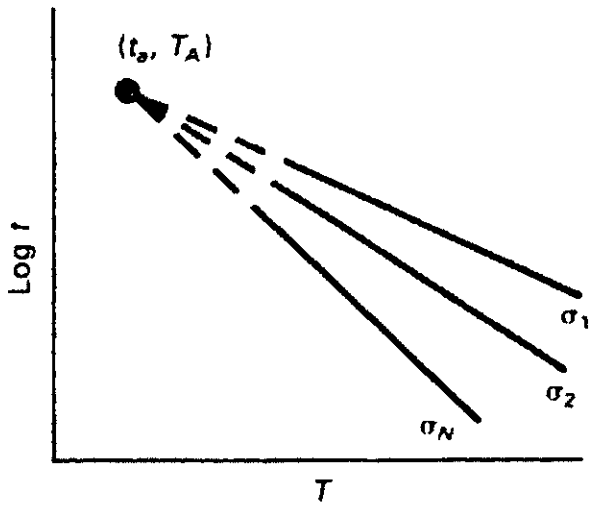

Figure 17: Constant stress curves for Manson-Haferd parameter.[45]

The Goldhoff-Sherby parameter is similar, except that it uses the inverse of the absolute temperature as the Larson-Miller parameter does. The parameter

$$P_{G-S} = \frac{\log t - \log t_A}{1/T - 1/T_A} \qquad (6)$$

predicts that a constant stress plot of log t versus 1/T should yield a family of straight lines which converge at a point, much like the Larson-Miller parameter. However, the point of convergence will not occur on the ordinate axis as shown in Figure 18, and the coordinates of this point will represent the values of the constants, log t_A and $1/T_A$.

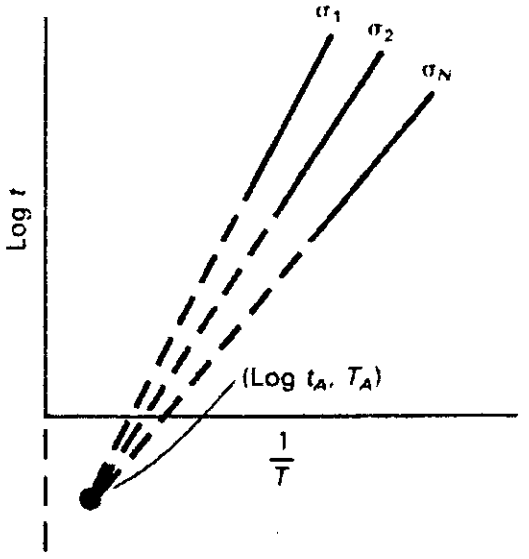

Figure 18: Constant stress curves for Goldhoff-Sherby parameter.[45]

Other time-temperature parameters include the Manson-Succop and Orr-Sherby-Dorn models.[45]

2.4.1.3. Shortfalls of Parametric Methods

Time-temperature parametric methods are often used to predict long-term creep life from short-term rupture tests. However, these methods often predict optimistic values for creep life for alloy steels due to their microstructural instability.[46]

The relationship between stress and time to rupture is very complex for alloy steels. After long-term creep deformation, strengthening effects depending on microstructural morphology, such as precipitation strengthening, lose their effectiveness and eventually disappear. For very long creep times, the inherent creep strength of alloy steels may then become the dominant factor that determines the remaining creep strength.[47] Short-term creep strength is very dependent on composition and the resultant microstructure. However, the inherent creep strength is much less dependent on microstructure and as shown in Figure 19, is very similar for steels with varying compositions.

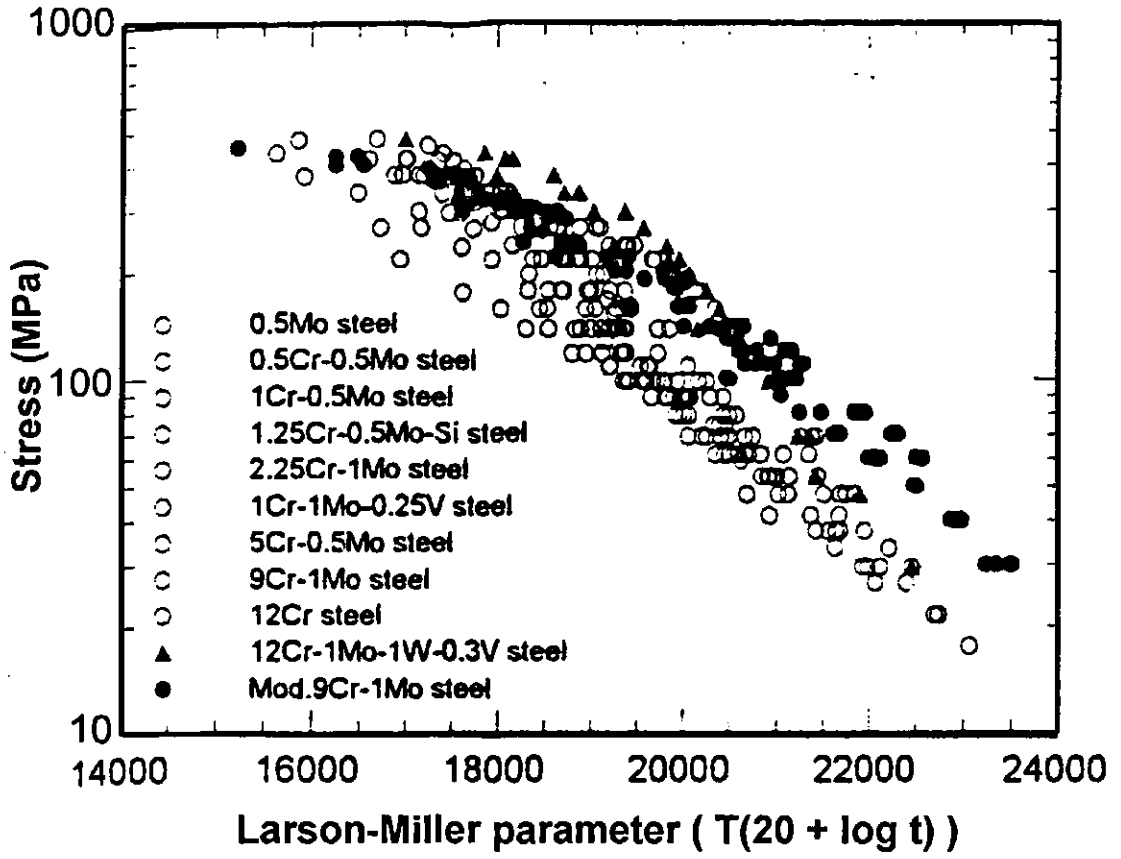

Figure 19: Creep rupture strength for 11 types of ferritic steels.[47]

The plot of stress versus the Larson-Miller parameter in Figure 19 shows that low alloys steels that display a wide scatter in terms of their short-term creep life have a tendency to converge to a narrow range in long term creep. Even the 12%Cr-1%Mo-1%W-0.3%V steel, which has better short term creep rupture strength, displays a fairly abrupt decrease so that its inherent creep strength appears to be very close to that of the low alloy steels. The modified 9%Cr-1%Mo steel appears to be an exception but its excellent long-term creep strength is due to its better microstructural stability. The inherent creep strength of ferritic steels results in a relationship between stress and rupture time that displays sigmoidal inflection, which makes it difficult to predict long term creep life from short term data using parametric methods.

Another study, which assessed the creep rupture strength of three tungsten-alloyed 9-12% Cr steels, found that using the Larson-Miller parameter led to an overestimation of long-term creep rupture strength.[48] The reason for this is the microstructural instability

of these steels. The microstructure of these steels will change considerably during creep, and is dependent greatly on time and temperature. This suggests that the premise of the Larson-Miller parameter that time and temperature can be considered interchangeable cannot be applied realistically to these steels.

2.4.2. Other Methods

Other life prediction methods that use a numerical basis have also been developed in an attempt to more closely predict the life of alloys steels, such as the initial strain method.[49]

Many mathematical models of creep, which attempt to describe creep behaviour in one or more of its stages, also have application to life prediction. The θ-projection model has been widely used within the power generation industry and its basic equation is given by

$$\varepsilon = \theta_1\left(1 - e^{-\theta_2 t}\right) + \theta_3\left(e^{\theta_4 t} - 1\right) \qquad (7)$$

where ε = creep strain,

θ_n = uniaxial parameters, and

t = time.

The θ parameters are determined from a series of uniaxial creep tests and are stress dependent. The creep rate can be obtained by differentiating Equation 7 and this model can also be extended to a multiaxial case. The θ-projection model does not give the value of strain to failure but different criteria have been used such as assuming failure to occur when the creep rate is x times the minimum creep rate.[50]

A recent study by Yokobori et al developed a master curve for the life prediction of CrMoV steel.[51] The master curve, which was developed for smooth, notched and precracked specimens, is shown in Figure 20. The data for smooth specimens and notched specimens are multiplied by 0.4 and 4, respectively.

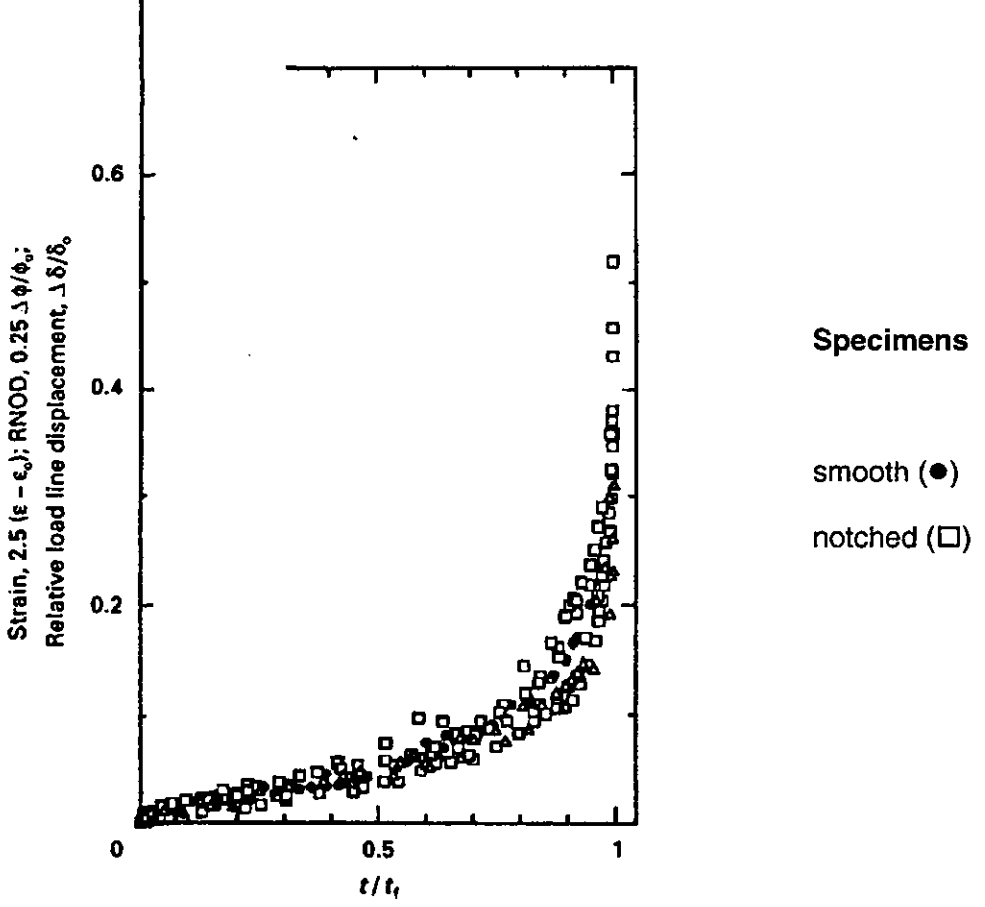

Figure 20: Experimental data plotted against the ratio of stress applied time, t, to creep fracture life, t_f.[51]

The fracture life can be determined from this curve if the creep deformation is known in creep under any applied stress and temperature.

2.5. ASTM A193 Grade B16

2.5.1. Background

Many different low alloy CrMo steels have been developed. However, steels containing vanadium are less common. Vanadium is added to these steels to produce VN precipitate particles, which are finer than those produced by Cr and Mo. These finer particles are more stable and more effective in precipitation strengthening.

ASTM A193 Grade B16 is a low alloy CrMoV steel that was developed as a bolting material for high-temperature service. The composition of this steel, which is given in Table 1, is similar to the classic CrMoV steel.

Table 1: Composition of ASTM A193 Grade B16.[52]

Element	C	Mn	P	S	Si	Cr	Mo	V
%	.36 -.47	.45 -.70	< .035	< .040	.15 -.35	.80 -1.15	.50 -.65	.25 -.35

The heat treatment for A193 Grade B16 is as follows:

1) immediately after rolling or forging, the material is to be allowed to cool to a temperature below the cooling transformation range,
2) uniformly reheated to a temperature between 925 and 954°C,
3) oil quenched, and
4) uniformly reheated for tempering to a temperature not less than 650°C.

2.5.2. Creep Data

2.5.2.1. Data Available

As stated earlier, CrMoV low alloy steels are less common than CrMo steels that do not contain vanadium, such as ASTM A193 Grade B7. As a result, available creep data are more plentiful for plain CrMo steels. No creep data for ASTM A193 Grade B16 was found.

However, the National Research Institute for Metals (NRIM) in Japan is gathering long-term creep and rupture data for heat resisting steels in the Creep Data Sheet Project.[53] One of the materials being examined is a 1%Cr-0.5%Mo-0.25%V steel for bolting applications which is similar to ASTM A193 Grade B16.[54] Creep rupture data for up to 10,000 hours and short-time tensile properties are available and the results were published in Creep Data Sheet #44 in 1997. An attempt to obtain these results is ongoing.

As well, a master creep curve was found for a 1.25%Cr-0.5%Mo-V steel in the open literature on the elevated-temperature properties of chromium-molybdenum steels.[55] A limited amount of creep rupture data for this steel is also available from the same source.

A large amount of creep data is available for plain CrMo steels such as the 1%Cr-0.5%Mo and 2.25%Cr-1%Mo steels.

2.5.2.2. Analysis of Data

A master curve and creep rupture data to 1000 hours for several low alloy steels was found in the ASTM Special Technical Publication mentioned in the previous section. A comparison of the 1.25%Cr-0.5%Mo-V steel with a 1.25%Cr-0.5%Mo steel and a 2.25%Cr-1%Mo steel provides some insight into the creep behaviour of CrMoV steels.

The short term creep strength of the 1.25%Cr-0.5%Mo-V steel and the 1.25%Cr-0.5%Mo steel are quite similar. Figures 21 and 22 contain the curves predicting rupture in 1000 hours as a function of stress and temperature for these two steels.

The amount of stress required to cause rupture in 1000 hours for these two steels is very similar for any given temperature. At a service temperature of 538°C (1000°F), the CrMoV steel could withstand approximately 33 ksi for 1000 hours while the CrMo steel would handle about 30 ksi. Obviously these values are only estimates but they display the comparative creep strength of these steels. The CrMoV steel is in the as-cast condition. The creep strength of the CrMo steel in the as-cast condition appears in general to be lower than that of annealed stock.

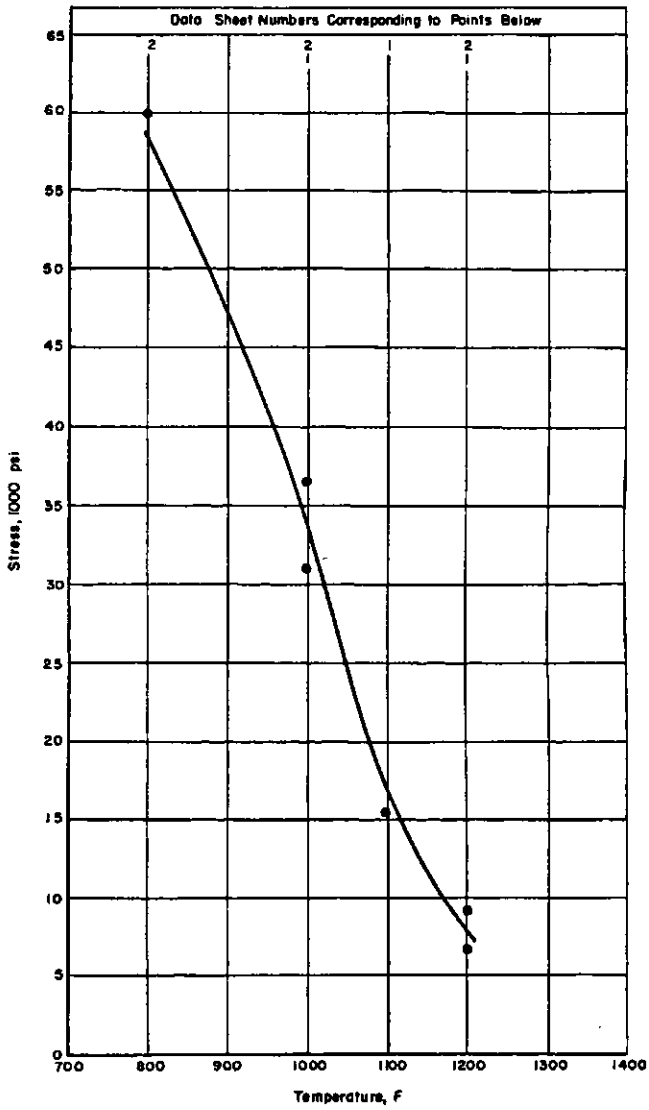

Figure 21: Rupture in 1000 hours, 1.25%Cr-0.5%Mo-V steel.[55]

In short term creep, the addition of vanadium may provide some additional creep strengthening although it is not a significant amount. For lower stresses and longer testing times, the CrMoV steel would likely display considerably better creep strength than the CrMo steel due to the greater stability of the vanadium precipitates.

Surprisingly, when the 1000 hour rupture curve for the 2.25%Cr-1%Mo steel is examined it appears to offer less creep strength than the 1.25%Cr-0.5%Mo steel. For a temperature of 538°C (1000°F), the curve would predict that a stress of approximately 23 ksi would result in failure in 1000 hours.

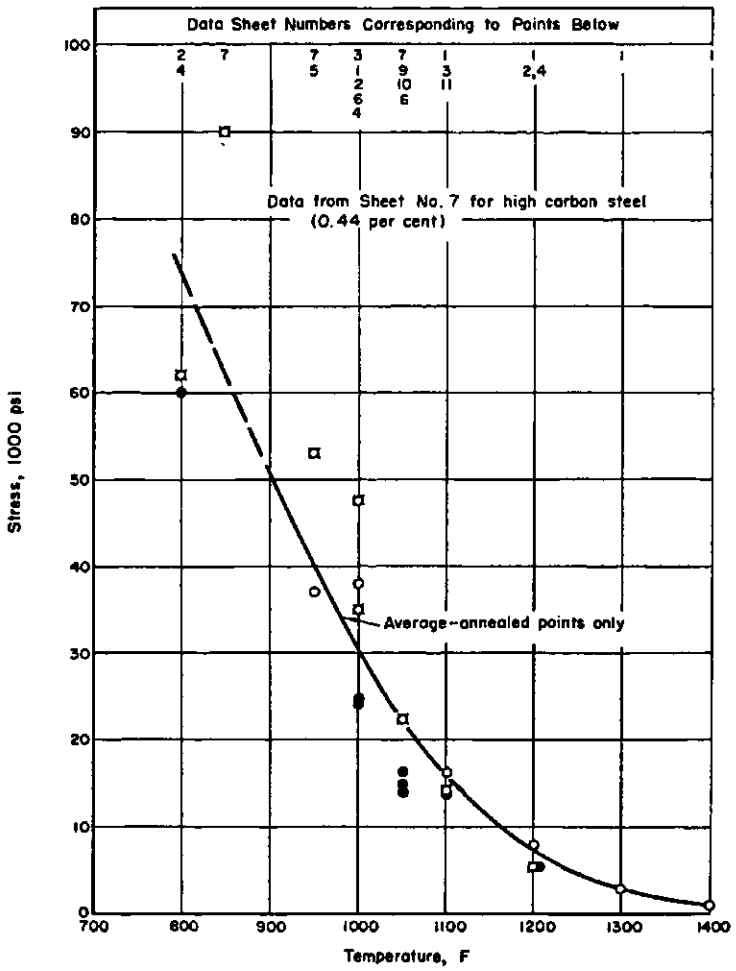

Figure 22: Rupture in 1000 hours, 1.25%Cr-0.5%Mo steel.[55]

2.6. ASTM A355 Class A

2.6.1. Background

Surface nitriding of steels is performed to provide a material that has a high surface hardness yet still displays good ductility and toughness. ASTM Standard A355 was written for very specific steels that have optimal properties for surface nitriding. All of these steels have a significant amount of aluminum added to form nitride precipitates, which provide the hardening effect. The composition of ASTM A355 Class A is given in Table 2.

Table 2: Composition of ASTM A355 Class A.[56]

Element	C	Mn	P	S	Si	Cr	Al	Mo
%	.38 -.43	.50 -.70	< .035	< .040	.15 -.35	1.40 – 1.80	.95 – 1.30	.30 -.40

All A355 steels are to be liquid quenched and then given a tempering treatment not lower than 600°C to produce a fine spheroidized structure.

2.6.2. Creep Data

As discussed earlier, a significant amount of creep data is available for low alloy CrMo steels. However, no information was found for steels with a high aluminum content similar to ASTM A355 Class A. The effect of this addition on the creep behaviour is uncertain. As well, it is likely that the tempering time required to form the spheroidized bainitic microstructure specified would be longer than the tempering treatment given to most steels. This could have a large effect on the creep behaviour of the material as a significant amount of ageing may already have occurred before the material is put into service.

CrMo steels with such a combination of chromium and molybdenum are also uncommon. Most low alloy CrMo steels with no vanadium content tend to have compositions similar to either 1%Cr-0.5%Mo or 2.25%Cr-1%Mo steels. However, a master creep curve was found for an annealed 1.25%Cr-0.5%Mo steel in an ASTM publication on the elevated-temperature properties of chromium-molybdenum steels.[55] A limited amount of creep rupture data for this steel and a 1.75%Cr-0.5%Mo steel is also available from the same source.

2.7. ASTM A437 Grade B4B

2.7.1. Background

ASTM A437 Grade B4B is a tempered martensitic stainless steel designed for turbine-type bolting materials that is specially heat treated for high-temperature service. The composition of this steel is given in Table 3.

Table 3: Composition of ASTM A437 Grade B4B.[57]

Element	C	Mn	P	S	Si	Ni	Cr	Mo
%	.20 -.25	.50 -1.00	< .025	< .025	.20 -.50	.50 -1.00	11.0 -12.5	.90 -1.25

Element	V	W	Al	Ti	Sn
%	.20 -.30	.90 –1.25	< .05	< .05	< .04

The heat treatment for A437 Grade B4B is as follows:

1) material to be heated to a temperature between 1025 and 1050°C,
2) liquid quenched to below 316°C,
3) uniformly reheated for tempering for a minimum of 2 hours at a temperature at least 55°C higher than the proposed operating temperature but not less than 620°C, and
4) air or furnace cooled to room temperature.

2.7.2. Creep Data

2.7.2.1. Available Data

ASTM A437 Grade B4B is a specialized steel designed for bolting applications only, and no creep data for this specific steel were found. However, this steel is very similar in composition to AISI Type 422 steel for which a significant amount of creep information is available. The only difference in composition is that the Type 422 steel has slightly higher chromium content than the A437 Grade B4B steel.

The ASTM Data Series Publication DS 59 contains creep rupture data for AISI Type 422 steel.[58] However, most tests recorded had a duration of less than 1000 hours and none exceeded 10 000 hours. As well, there is little data on the secondary creep rate.

The NRIM Creep Data Sheet Project also has published creep data for similar steels.[54] A 12%Cr-1%Mo-1%W-0.25%V steel for bolting applications is being tested in conjunction with the low alloy bolting steel mentioned in the previous section. Creep Data Sheet #44, which was published in 1997, contains creep rupture data up to 10 000 hours and short-time tensile properties for this steel. As well, a 12%Cr-1%Mo-1%W-0.3%V steel for turbine blade applications is also being tested. This steel is manufactured according to JIS Standard SUH 616-B, which is similar to ASTM A437 Grade B4B.[59] Creep Data Sheet #10B, which was published in 1997, contains creep rupture data for up to 100 000 hours, as well as minimum creep rates, short-time tensile

data, and evaluation of short-time tensile strength and long-term creep rupture strength. An attempt to obtain these data sheets is ongoing.

Much of the current testing being performed centers on 9%Cr steels such as Type P92, which is similar to A437 Grade B4B but has a 2% W and 0.5% Mo content. There is a significant amount of recent creep data available for these steels, as much of the recent development work has been related to these steels.

2.7.2.2. Analysis of Data

The creep rupture data available for AISI Type 422 in ASTM DS 59 demonstrate a considerable increase in creep strength compared to the low alloy steels discussed in Section 6.2. The 1000 hour creep rupture curve for this steel predicts that a stress of about 55 ksi would cause failure for a service temperature of 1000°F.[58] The short term creep strength of 12%CrMoWV would appear to be almost double that of the low alloy steels.

The creep strength of Type 422 is also significantly greater than that of 12%Cr steels. Creep rupture data for these steels would suggest that a 12%Cr steel could withstand only about 25 ksi for 1000 hours at 538°C (1000°F). Obviously, the solid solution strengthening of molybdenum and tungsten and the precipitation strengthening of molybdenum and vanadium provide a considerable increase in creep resistance as expected.

12%CrMoWV tempered martensitic steels are especially desirable for their excellent oxidation resistance. They also demonstrate better creep resistance than most alloy steels.

2.8. New Developments

Chromium molybdenum steels are commonly used in many steam turbine applications because of their excellent elevated temperature behaviour and relatively low cost compared to other steels or alloys with similar creep performance. Chromium-molybdenum steels have evolved over the last century and the addition of various alloying elements such as vanadium and tungsten has resulted in improved creep resistance and stability. Much of the current research is focused on the development of improved 9-12% Cr tempered martensitic stainless steels.

The efficiency of steam turbines is greatly dependent on their operating temperature. However, increasing the operating temperature requires either increasing the amount of material used or else using materials with greater creep resistance. There are economical and functional limits on the thickness of parts; therefore the search for materials with improved behaviour at high temperatures continues. Current developments are aimed at producing materials capable of withstanding operating temperatures in excess of 600°C.

Austenitic steels offer similar or better creep strength than tempered martensitic steels but they are more expensive and have higher coefficients of thermal expansion, lower thermal conductivity and higher susceptibility to stress corrosion cracking.[60] As a result of these limitations, the demand for improved tempered martensitic stainless steels still exists.

Much of the current development involves finding the optimum concentration of the various elements that provide creep strengthening effects. The effect of adding less common elements such as boron and titanium in small amounts is also being studied. A new grade of 9.5%Cr martensitic stainless steel has been developed which contains a uniform dispersion of titanium carbide precipitates formed in austenite prior to martensite transformation.[61] These carbides are very small and have high thermodynamic stability, and thus result in very high creep strength. Steels containing up to 3% palladium have also been studied, which contain fine FePd based precipitates labelled α''.[62] These precipitates have been shown to be stable even after aging at 700°C, thus providing creep strengthening at temperatures considerably higher than any power generation plants currently operate at.

Another important factor in the creep strength of tempered martensitic stainless steels is the heat treatment they receive prior to service due to the effect of microstructural evolution, which occurs both during the heat treatment and during service. As a result, research to determine the most suitable tempering treatment is also being attempted.

3. EXPERIMENTAL METHODS

3.1. Materials

Three alloy steels were obtained representing the three ASTM grades discussed in the previous section.

ASTM A193 Grade B16 was obtained from CSC, Warren, OH through Castle Metals, Toronto, ON as 25.4 mm (1 in.) diameter barstock. Nitralloy 135G Modified, which corresponds to ASTM A355 Class A, was obtained from Crucible Materials Corporation, Camillus, NY as 31.75 mm (1.25 in.) diameter barstock. Carpenter 636, which is equivalent to ASTM A437 Grade B4B, was obtained from Carpenter Technology Corporation, Reading, PA as 28.57 mm (1.125 in.) diameter barstock. For the remainder of this thesis, these materials will often be referred to using the applicable standard number only, such as A355.

The material test sheets for these materials are in Appendix A.

3.1.1. Creep Tensile Specimens

Cylindrical threaded-end creep tensile specimens were machined from each steel grade. These specimens were manufactured in accordance with ASTM E139-96 with the dimensions shown by the drawing in Figure 23. Shoulders were machined on each specimen at either end of the gauge length to allow the attachment of an extensometer for strain measurement purposes.

The gauge length of each test specimen was polished in a lathe using emery paper to improve the surface finish. The final surface roughness was achieved using 600 grit paper.

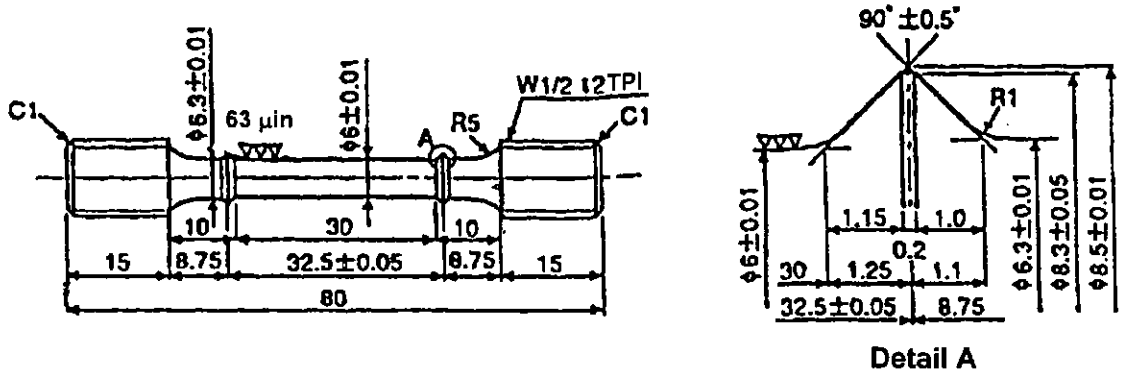

Figure 23: Creep test piece dimensions.

The specimens were color coded at the time of machining according to the barstock from which they were machined. At the time of testing, each test specimen was further identified using a two digit alphanumeric code. The first digit was a number between 1 and 6 corresponding to the original color coding, as shown in Table 4. The second digit was a letter assigned at the time of testing to differentiate the specimen from other specimens machined from the same barstock.

Table 4: Code used for Barstock Identification

Code	Material	Barstock
1	ASTM A355 Class A	Black
2		Green
3	ASTM A193 Grade B16	Grey
4	ASTM A437 Grade B4B	Prime
5		Red
6		Yellow

Using Specimen 2C as an example, the '2' would indicate that the specimen was machined from the green coded barstock of ASTM A355 Class A, and the 'C' would denote the fact that it was the third specimen tested from that particular barstock.

3.1.2. Low Temperature Tensile Specimens

Cylindrical threaded-end tensile specimens were also machined from each steel grade. These specimens were manufactured in accordance with ASTM E8-98 and the dimensions were: overall length = 152.5 mm, gauge length = 50 mm, and gauge diameter = 12.5 mm.

3.2. Experimental Test Procedures

The major portion of the experimental testing undertaken in this project was creep testing of the three steel grades already mentioned. However, a number of other tests were also performed for verification of material properties and to aid in understanding the high temperature behaviour of the steels under consideration.

3.2.1. Creep Testing

Creep testing was carried out according to standards ASTM E139-96, JIS Z 2271, and JIS Z 2272. All tests were constant load tensile tests at elevated temperatures.

3.2.1.1. Experimental Setup

Ten Satec M3 creep frames, as shown in Figure 24(a), were used to carry out all tests. These creep frames consisted essentially of a tensile load application mechanism and a furnace. A data acquisition system monitored the tests and recorded measured data. A schematic diagram of the creep testing apparatus is shown in Figure 24(b).

The load was applied through a 10:1 lever arm ratio, and an automatic load levelling system maintained the load as the specimens lengthened during creep testing. Three Type R thermocouples were used in each furnace to monitor temperature. The junction of each thermocouple was coated with a ceramic paste to provide a good insulating barrier. Each furnace contained three elements, and three corresponding PID controllers. The temperatures measured by the thermocouples were relayed to the controllers and to the data acquisition system.

Five of the creep frames were equipped with extensometers and SLVC sensors for measuring specimen strain during creep. The extensometers attached to the shoulders at both ends of the gauge length of each specimen. As the specimen deformed during creep, the SLVC sensor measured the change in distance between the specimen shoulders, or the change in the specimen gauge length. Each extensometer was also equipped with a dial gauge for manual verification of the SLVC sensor strain measurements.

All ten creep frames were equipped with digital clocks which measured the test time from when the load was applied until each test was terminated due to rupture or manual shutdown.

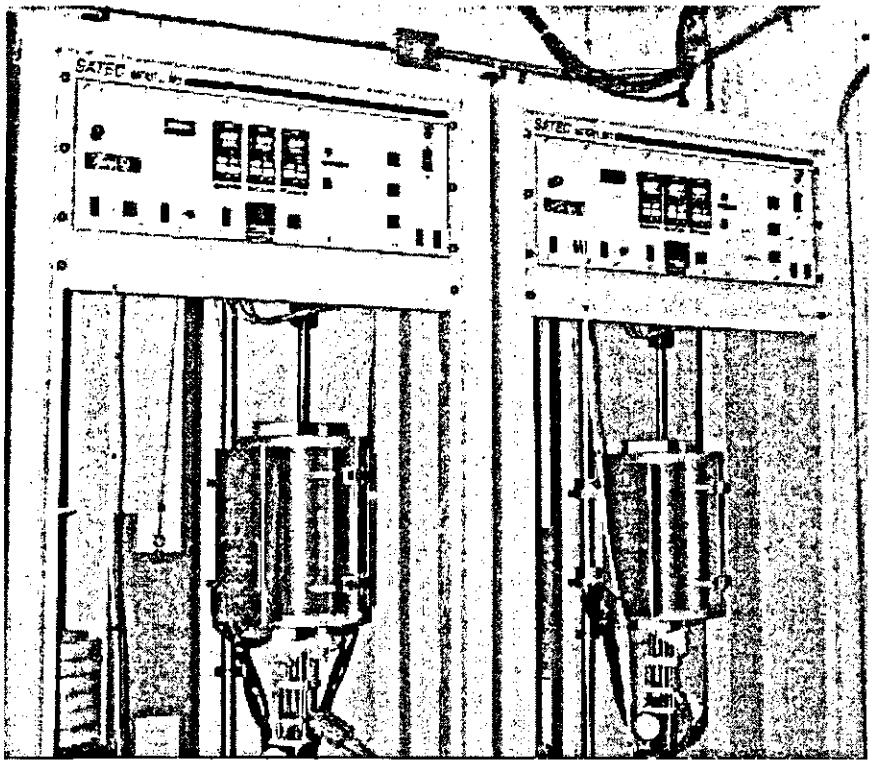

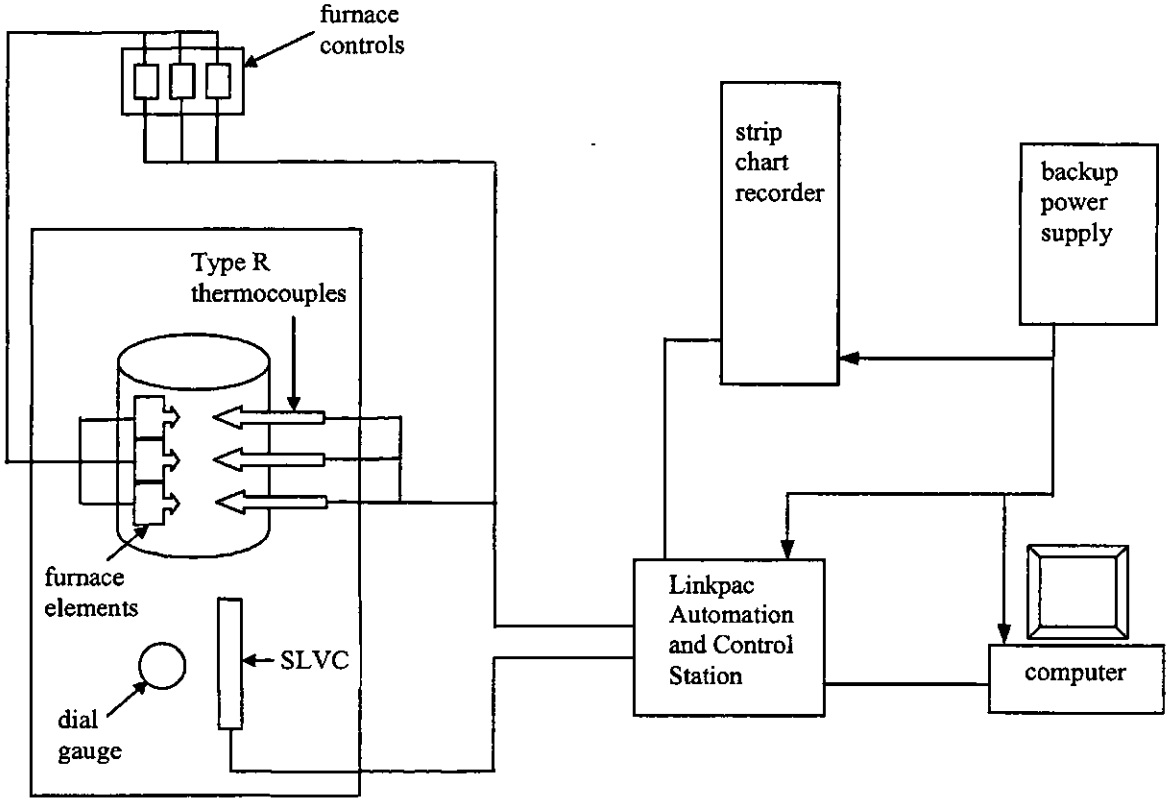

Figure 24: a) Satec M3 creep frames, and b) Schematic diagram of creep testing apparatus.

The tests performed using the extensometer equipped creep frames will be referred to as creep tensile tests. The tests performed using the other frames will be called stress rupture tests, as the only information obtained was time to rupture.

The data acquisition system used was called the LinkPac Data Acquisition and Control System for Creep and Stress-Rupture Testing designed for use with the Satec M3 creep frames. The system consisted of a Pentium computer and a LinkPac Model F16 Automation and Control Station. LinkPac software installed on the computer was used to monitor all ten creep frames, provide real time reports of temperature and strain, and record temperature and strain data in text files at regular intervals for each test.

A strip chart recorder was used to provide a backup record of temperature and strain data for each test. A backup power supply was connected to the computer and strip chart recorder to maintain data acquisition in the event of a power failure.

3.2.1.2. Experimental Procedure

Two measurements of the gauge diameter were taken at three locations along the gauge length of each specimen. The diameter was recorded as the average of the diameters at all three locations according to JIS Z 2271 and JIS Z 2272.

Each creep tensile specimen was then washed with methanol and attached to the specimen couplers. This assembly is called the load train. The threads of each specimen and associated couplers were coated with high temperature "anti-seize" to prevent oxidation and seizure during testing.

If the specimen was intended for creep tensile testing, an extensometer was then clamped to the specimen shoulders. The threads of the small extensometer bolts were also coated with "anti-seize". The three Type R thermocouples were then attached directly to the specimen using 80%Ni-20%Cr thermocouple wire at the locations shown by the arrows in Figure 25.

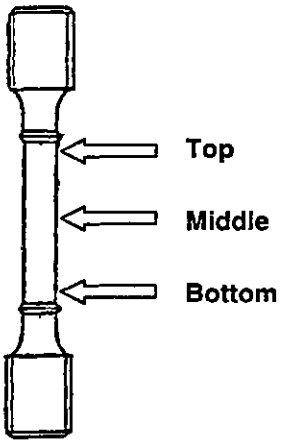

Figure 25: Attachment points of thermocouples to specimen gauge section.

The entire assembly was then installed in the creep frame. Once the pertinent test data such as specimen diameter, test temperature, and applied load is entered into the LinkPac software, the test is ready for commencement.

The furnace controllers were set to a ramp output to bring the specimen temperature up to 50°C below the test temperature at a rate of 7°C per minute. ASTM E139-96 specifies that the ramp rate must be such that the time to reach the test temperature is greater than one hour. The temperature was allowed to stabilize and then the furnace controllers were set to PID control. The specimen temperature was then slowly raised to the desired test temperature.

According to ASTM E139-96, the indicated temperature is not to exceed the nominal test temperature by more than 2°C at any time before the load is applied or for the duration of the test. The LinkPac software was set to terminate a test if the indicated temperature exceeded this limit.

Once the specimen temperature reached the desired test temperature, the specimen was allowed to soak for at least 16 hours before the load was applied to allow equilibrium conditions to be reached. Upon fulfilling the required soak time, the prescribed load was applied to the specimen, at which point the clock started recording the elapsed test time.

The LinkPac software was set to record the specimen strain at every 0.01% strain interval. Any change in the specimen temperature was also recorded.

Manual strain readings from the dial gauge and SLVC sensor were taken prior to the start of each test and then on a daily basis thereafter to provide a basis for assessing the validity of the results.

Upon specimen rupture, the furnace automatically turned off and was allowed to cool to room temperature. After cooling, the furnace was opened and the specimen removed. The two halves of the ruptured specimen were placed back together and the gauge length and total length of the specimen were measured.

3.2.1.3. Test Schedule

A test schedule was developed to provide a basis for performing individual tests. The proposed schedule contained tests at three different temperatures from 538°C (1000°F) to 649°C (1200°F). The goal was to perform tests with rupture times varying between 56 hours and 3200 hours for the purpose of constructing a Larson-Miller master curve for each steel. The proposed test schedule is shown in Table 5.

Table 5: Proposed test schedule.

Temperature		Life (hr)							
(°C)	(°F)	18	32	56	180	320	560	1800	3200
538	1000	1	1	1	1	1	3	1	1
593	1100	1	1	1	1	1	1	1	1
649	1200	1	1	1	1	1	3	1	1

The schedule also made provision for assessing the repeatability of the test results through multiple tests at a rupture time of 560 hours for at least two temperatures for each steel.

The stresses required to obtain the proposed rupture times were estimated from rupture data available for similar steels. A Larson-Miller master curve created from creep test data for 1.25%Cr-0.5%Mo-V steel published in the ASTM Special Technical Publication No. 151, mentioned in Section 2.5, was used to estimate the required stresses for A193.[55] Similar master curves for 1.25%Cr-0.5%Mo and 2.5%Cr-0.5%Mo steels contained in the same publication were used for A355. Since no data was available for steels with the same chromium and molybdenum contents as A355, stress values were estimated using the average value obtained from the two master curves. Stress rupture data provided by Carpenter Technology Corporation was used to estimate test stresses for A437.

3.2.1.4. Verification of Thermocouples

A Type K thermocouple was used to verify the temperatures measured by the Type R thermocouples. The Type K thermocouple was calibrated using an Ectron 1100 thermocouple simulator calibrator.

The Type K thermocouple was then attached to a creep specimen between the top and middle Type R thermocouples prior to installing the specimen in one of the creep frames. A test was then carried out according to the standard procedure. At approximately twenty four hours after the test load was applied to the specimen, the temperature displayed by the Type K thermocouple and the three Type R thermocouples was recorded. This procedure was repeated for each creep frame.

3.2.2. Tensile Testing

Room temperature tensile testing was performed on all three steels to verify material properties. The low temperature tensile specimens were tested at room temperature using a standard Instron testing machine at a strain rate of 5 mm/min. Tensile strength and percent elongation were calculated in accordance with ASTM E8-98. The percent elongation was based on an initial gauge length of 50 mm marked on the undeformed specimens. Load-extension curves were recorded by means of an autographic device attached to the Instron machine.

3.2.3. Hardness Measurements

Hardness testing was performed on all three steels in the as-received condition to verify material properties. Slices cut from the original barstock were metallurgically polished using 6 micron diamond paste. Hardness testing was also performed on representative creep tensile specimens after rupture. Slices cut from the gauge length cross section of ruptured specimens were metallurgically polished using 6 micron diamond paste.

Vickers microhardness measurements were then carried out on the polished surfaces using a Buehler Micromet II microhardness tester with a direct load of 500 g applied for 11 s.

At least twelve microhardness measurements were taken at various points in the cross section. Eight of these measurements were taken just inside the outer circumference as the surface hardness was of most interest. Hence, the results cited in this work are the average values from such multiple measurements.

The absolute hardness value was obtained according to the following equation:

$$HV = 1854\frac{F}{d^2} \qquad (8)$$

where HV = Vickers hardness,

F = test load (g), and

d = arithmetic mean of the two diagonals d1 and d1 (μm).

The hardness values obtained using the Vickers microhardness test were converted to equivalent Brinell hardness values for comparison with various standards. The Brinell hardness conversions were based on a 3000 kg load with a 10 mm ball indenter.

3.2.4. Metallography

Scanning electron and transmission electron microscopy was used to examine microstructural characteristics and fracture surface morphology.

3.2.4.1. Scanning Electron Microscopy

Fracture surfaces of ruptured creep specimens were examined using a PhillipsXL30 ESEM scanning electron microscope in order to characterize the fracture mode and any fine scale features on the fracture surface. The fracture surfaces were removed from the ruptured creep specimens using an abrasive diamond saw.

Pieces of the original barstock and slices cut both transversely and longitudinally from ruptured creep specimens using an abrasive diamond saw were polished to 1 μm. These samples were then examined using a Jeol JSM-5900LV scanning electron microscope. EDX analysis was performed on these samples using Oxford Instruments INCA Suite 1.02 software in order to characterize the chemical composition of any intermetallic compounds observable. Some fracture surfaces were also examined using this microscope for the purpose of performing EDX analysis on observable particles.

3.2.4.2. Transmission Electron Microscopy

Thin foils of ruptured creep specimens were examined using a Jeol JEM-2000FX transmission electron microscope in order to characterize the controlling creep mechanisms and microstructural features.

The procedure used to produce the thin foils was as follows. The outside diameter of a ruptured creep specimen was reduced to 3 mm. Slices approximately 0.2 mm in

thickness were then cut from the specimen using a low speed diamond saw. Each slice was then polished to a thickness of approximately 0.12 mm using 600 grit emery paper. Electropolishing of the thin foils was accomplished using a solution of 90% perchloric acid and 10% glacial acetic acid at 20 V and 288 K.

4. EXPERIMENTAL RESULTS AND DISCUSSION

Three alloy steels were examined in this study. A presentation of all test results and a discussion thereof will be given for each of these steels.

4.1. Verification of Material Properties

The three steel alloys purchased for testing purposes are purported by their manufacturers to satisfy the requirements of the applicable ASTM standard. Several tests were performed on these steels in the as-received condition to verify that their material properties and chemical composition do indeed meet the ASTM standard.

4.1.1. ASTM A193 Grade B16

4.1.1.1. Composition

Spectrochemical analysis was performed to verify the chemical composition of each steel. The results of the analysis for the steel purchased as ASTM A193 Grade B16, along with the reported chemical composition, are presented in Table 6.

Table 6: Spectrochemical analysis of ASTM A193 Grade B16.

Element	C	Mn	S	P	Si	Cu	Ni	Cr	V	Mo	Al
	(wt%)	(wt%)	(wt%)	(wt%)	(wt%)	(wt%)	(wt%)	(wt%)	(wt%)	(wt%)	(wt%)
Test Results	0.386	0.530	0.018	0.015	0.235	0.181	0.155	0.931	0.277	0.495	0.007
Reported	0.42	0.53	0.016	0.017	0.22	0.16	0.16	0.93	0.28	0.52	0.003

The results showed that the composition of this steel was in accordance with the requirements of the ASTM standard, as previously listed in Chapter 2.

4.1.1.2. Tensile and Hardness Properties

Tensile and hardness tests were performed on all three materials under consideration to examine their mechanical properties at room temperature. The results of these tests for A193 are shown alongside the requirements of the ASTM standard in Table 7.

Table 7: Tensile test results for ASTM A193 Grade B16.

Property	0.2% Offset Yield Strength (MPa)	Ultimate Tensile Strength (MPa)	Elongation (%)	Reduction of Area (%)	Brinell Hardness, max
ASTM Standard	725	860	18	50	321 HB
Test Results	925	974	22.6	58.0	279 HB

This steel met all of the mechanical requirements of ASTM Standard A193 Grade B16, although the tensile strength of the material was significantly greater than required.

4.1.2. ASTM A355 Class A

4.1.2.1. Composition

The results of the spectrochemical analysis for Nitralloy 135G Modified, which was purchased as an equivalent to ASTM A355 Class A, along with the reported chemical composition, are presented in Table 8.

Table 8: Spectrochemical analysis of Nitralloy 135G Modified.

Element	C	Mn	S	P	Si	Cu	Ni	Cr	Mo	Al
	(wt%)	(wt%)	(wt%)	(wt%)	(wt%)	(wt%)	(wt%)	(wt%)	(wt%)	(wt%)
Test Results	0.367	0.660	0.016	0.010	0.283	0.165	0.185	1.621	0.384	0.600
Reported	0.38	0.67	0.014	0.009	0.27	0.17	0.18	1.75	0.35	1.16

All elements were present in the amount required by the ASTM standard, as previously listed in Chapter 2, except for aluminum. ASTM A355 Class A calls for an aluminum content between 0.95 and 1.30 weight percent, yet the spectrochemical analysis results showed an aluminum content of only 0.6% in the steel tested. The manufacturer reported that the aluminum content was much higher at 1.16%, which is within the range required by the ASTM standard.

4.1.2.2. Tensile and Hardness Properties

The results of the tensile and hardness tests for Nitralloy 135G Modified are shown in Table 9.

Table 9: Tensile test results for Nitralloy 135G Modified.

Property	0.2% Offset Yield Strength (MPa)	Ultimate Tensile Strength (MPa)	Elongation (%)	Reduction of Area (%)	Brinell Hardness
Reported	726	902	21.2	60.4	269 HB
Test Results	740	896	24.0	57.4	266 HB

ASTM A355 Class A has no mechanical requirements listed except that the Brinell hardness must fall within the range of 223 to 269 HB. The Nitralloy 135G Modified satisfies this requirement. The mechanical properties of the steel tested also appear to conform closely to those claimed by the manufacturer.

4.1.3. ASTM A437 Grade B4B

4.1.3.1. Composition

Carpenter 636 is reported by its manufacturer to meet the requirements of ASTM A437 Grade B4B. The results of the spectrochemical analysis performed on this steel are shown in Table 10.

Table 10: Spectrochemical analyses of Carpenter 636.

Element	C	Mn	S	P	Si	Ni	Cr	V	Mo	W	Cu	Al
	(wt%)	(wt%)	(wt%)	(wt%)	(wt%)	(wt%)	(wt%)	(wt%)	(wt%)	(wt%)	(wt%)	(wt%)
Test Results	0.219	0.729	<.005	0.019	0.337	0.905	11.30	0.234	1.090	1.140	0.100	0.023
Reported	0.21	0.73	0.001	0.014	0.33	0.85	11.82	0.22	1.09	1.03		

The results showed that the composition of this steel was in accordance with the requirements of the ASTM standard, as previously listed in Chapter 2.

4.1.3.2. Tensile and Hardness Properties

The results of the tensile and hardness tests performed on the Carpenter 636 steel are displayed in Table 11.

Table 11: Tensile test results for Carpenter 636.

Property	0.2% Offset Yield Strength (MPa)	Ultimate Tensile Strength (MPa)	Elongation (%)	Reduction of Area (%)	Brinell Hardness, max
ASTM Standard	720	1000	13	30	331 HB
Test Results	845	996	20.6	56.7	298 HB

The tensile test and hardness test results seem to show that the steel tested had slightly lower strength and greater ductility than would be expected. A decrease in tensile strength is very likely to be mirrored by a decrease in creep strength.

4.2. Creep Testing Results

The primary focus of this project was to characterize the high temperature behaviour of the three alloy steels under consideration. The principal method used to achieve this goal was creep testing at elevated temperatures. Half of the tests were performed as creep tensile tests in which the strain as a function of time was measured. The remaining tests were stress rupture tests in which the only measured parameter was time to rupture.

The time to rupture results of all tests will be presented first, followed by the results of the creep tensile tests.

4.2.1. ASTM A193 Grade B16

4.2.1.1. Stress Rupture Results

The time to rupture was measured for all tests from the time the load was applied to the specimen until the time when fracture occurred. These results are presented graphically for the A193 steel as a function of stress in Figure 26. A summary of all tests performed can be found in Appendix B.

As would be expected, the time to rupture tended to decrease as the applied stress or the test temperature was increased.

When compared with the stress rupture data for a 1.25%Cr-0.5%Mo-V steel, the A193 steel demonstrated similar creep strength at 538°C. At higher temperatures, the A193 steel appeared to suffer a considerable loss in creep strength compared to the published data. However, due to the severe oxidation that occurs at these higher temperatures, these steels should not be used in service at such temperatures. The application of the master curve to these higher temperatures may therefore have resulted in error.

Three tests were performed at the same stress level at both 538°C and 649°C to assess the repeatability of the tests. These tests can be observed in Figure 26. The difference between the shortest and longest rupture times, expressed as a percentage of the average of the three rupture times was 29.8% at 538°C and 29.1% at 649°C.

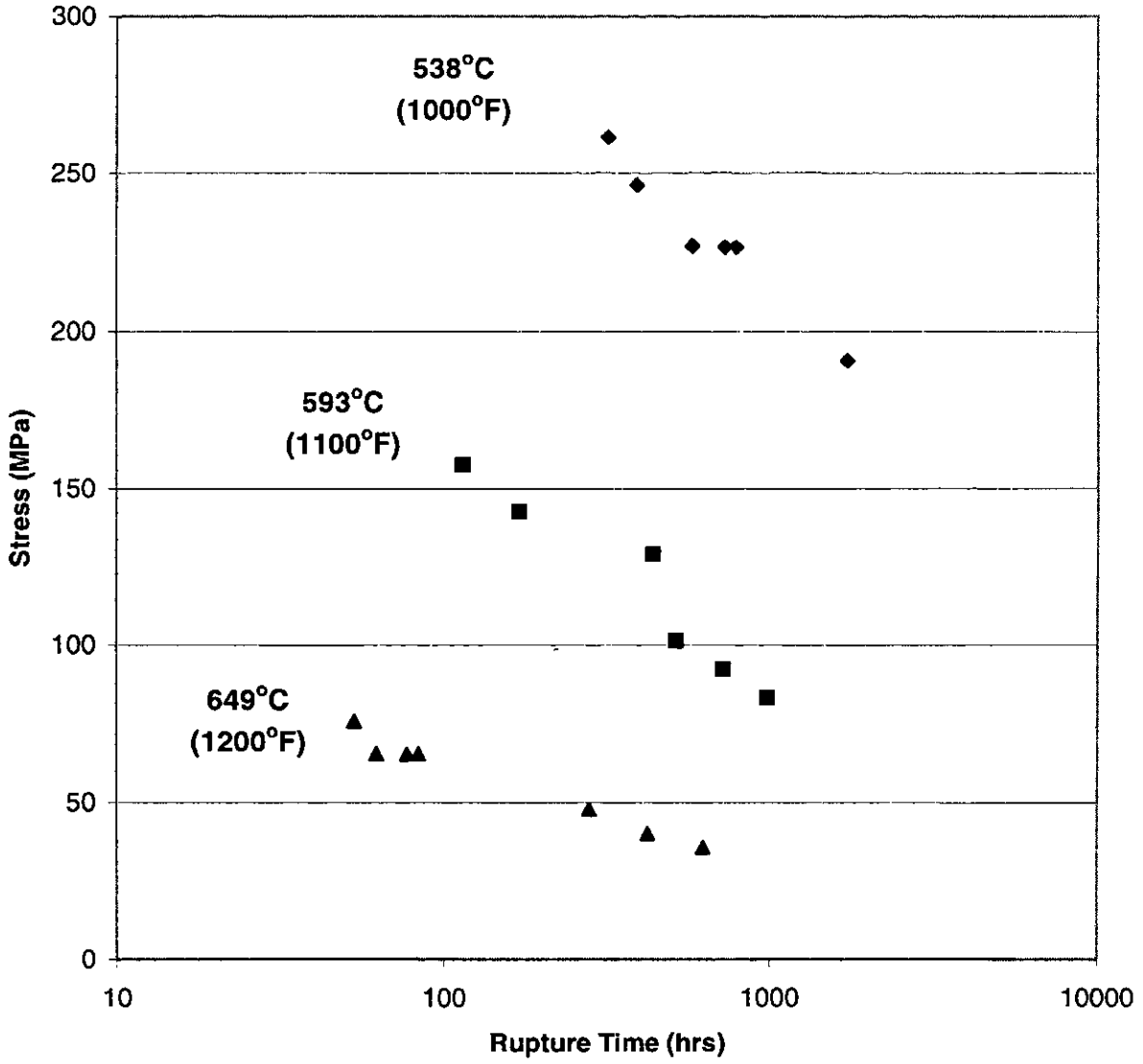

Figure 26: Stress rupture results for ASTM A193 Grade B16.

4.2.1.2. Creep Tensile Results

Much more can be learned about the creep behaviour of these steels from those tests for which the strain was measured as it changed with time. The whole creep curve can be analysed rather than just the final point. Since these steels will seldom see rupture in service, the earlier stages of the creep curve are of great importance.

The strain is plotted as a function of time for Specimen 3M in Figure 27(a), which represents a typical creep curve for this steel. Specimen 3M was subjected to an applied stress of 190.8 MPa. As can be seen, the tertiary region is very prominent as might be expected for these steels. The primary stage is very short and can be seen much more clearly if only the first 600 hours is plotted, as shown in Figure 27(b). The presence of a secondary stage, in which the strain rate is constant, is not well defined. It almost appears as if the strain rate decreases to a minimum point and then begins to increase again. The point at which the minimum strain rate is reached appears to be between 200 and 400 hours.

The creep curves of other specimens tested at 538°C are very similar. The only observable difference is in the amount of instantaneous strain that occurs, which increases as the applied load increases. This can be seen by comparing the creep curve for Specimen 3A, which was subjected to an applied stress of 246.3 MPa and is shown in Figure 28, with that of Specimen 3M, which was loaded to 190.8 MPa and is shown in Figure 27(a).

If the strain rate in the secondary stage, or minimum strain rate, is determined for each test at 538°C, and plotted as a function of stress, it appears to follow a power law relationship as shown in Figure 29. The exponent of the power law relationship, usually signified by the letter n, has a value of approximately 7.5.

The general shape of the creep curve does not appear to be affected by temperature either. This can be seen by comparing the two creep curves in Figure 30, which are for a specimen tested at 593°C and a specimen tested at 649°C, with the creep curves displayed in Figures 27 and 28.

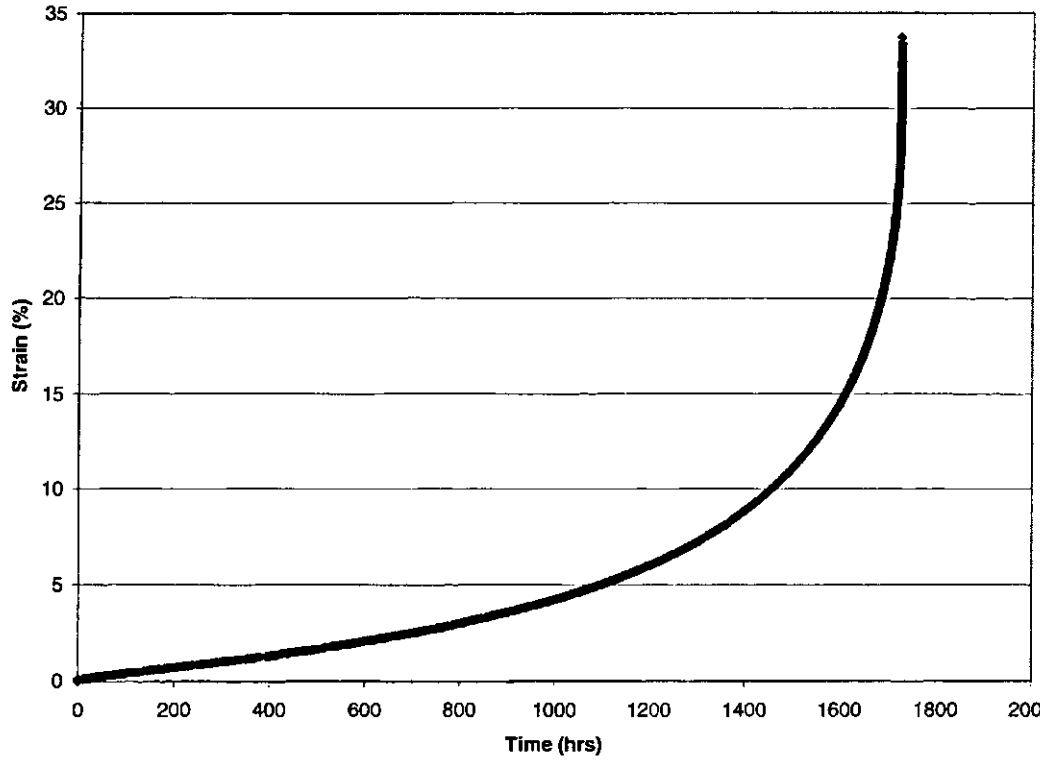

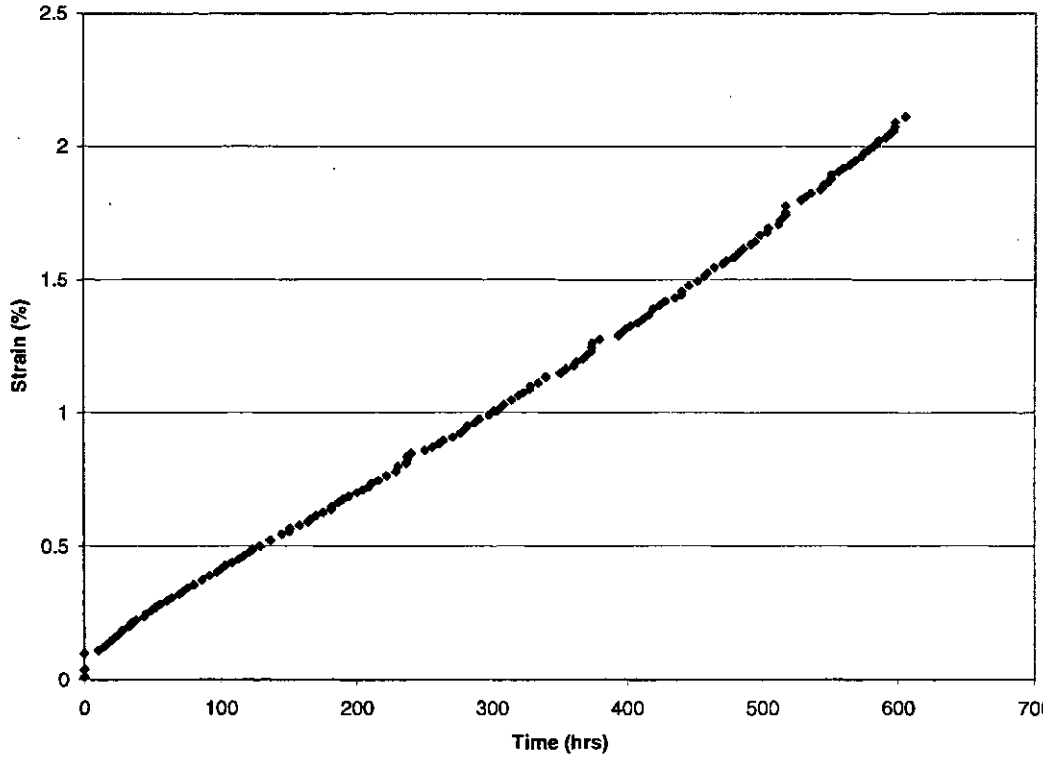

Figure 27: Strain as a function of time, Specimen 3M, 538°C, 1726 hours, a) to rupture, and b) first 600 hours.

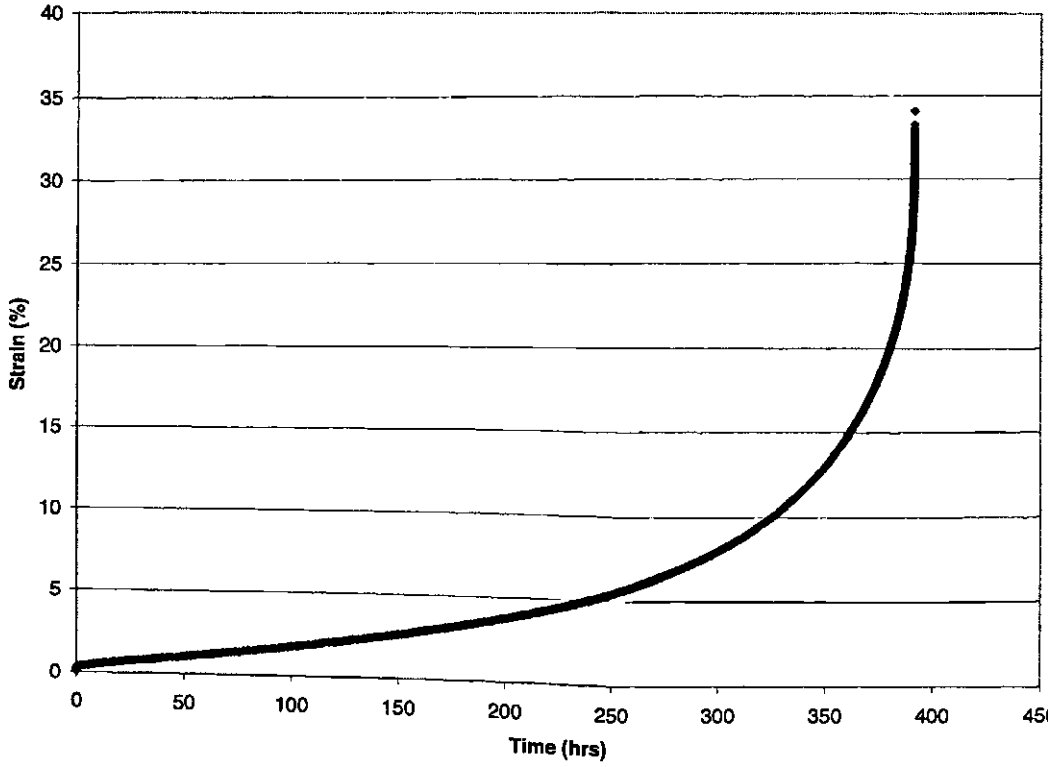

Figure 28: Strain as a function of time, Specimen 3A, 538°C, 392 hours.

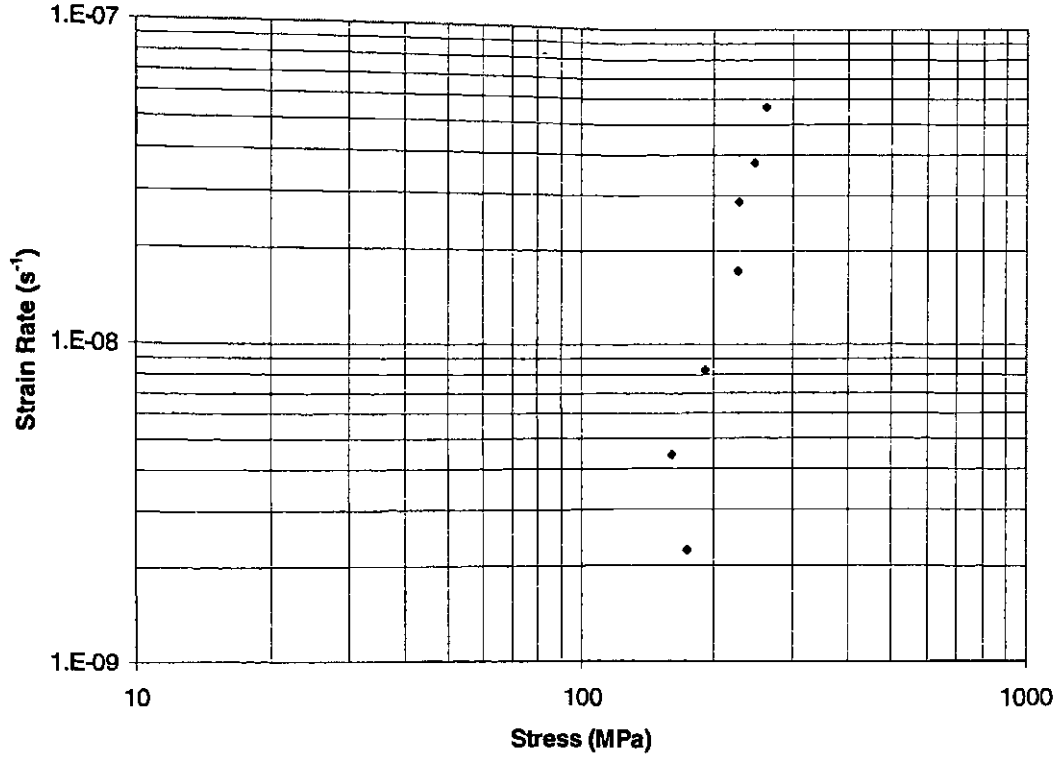

Figure 29: Minimum strain rate as a function of stress at 538°C for ASTM A193 Grade B16.

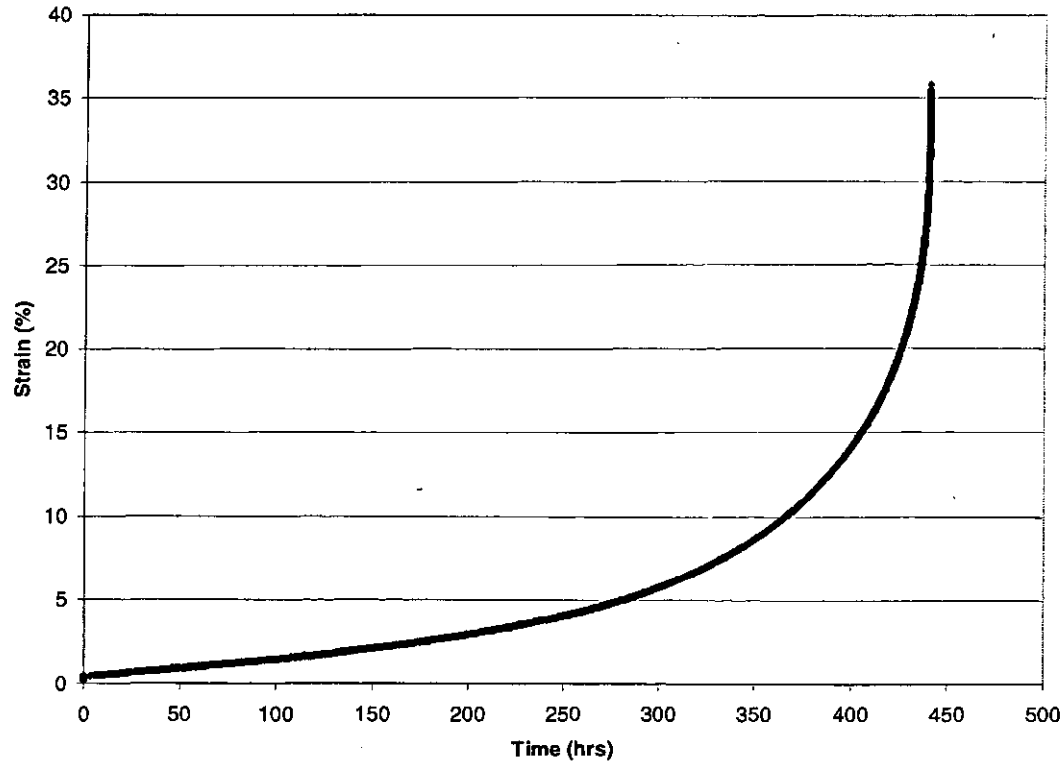

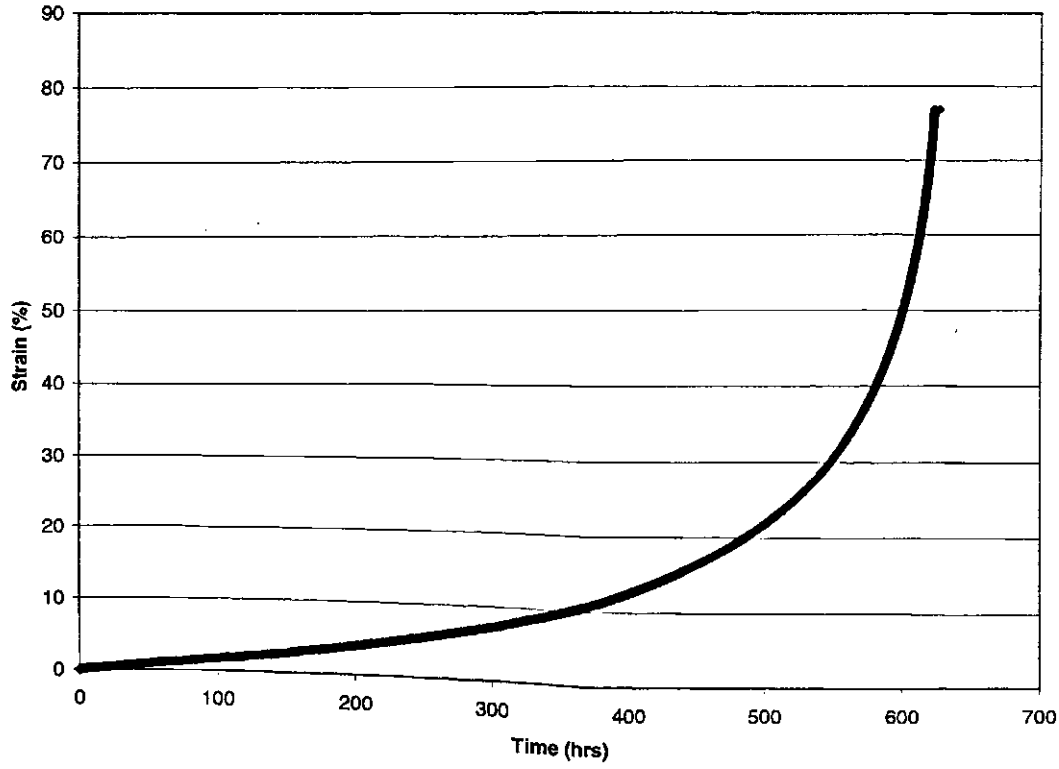

Figure 30: Strain as a function of time, a) Specimen 3I, 593°C, 440 hours, b) Specimen 3S, 649°C, 627 hours.

Although the general shape of the curves is the same, it is interesting to note the difference in the total strain reached at rupture. The total elongation of the specimen tested at 593°C was approximately the same as the total elongation of the specimens tested at 538°C. However, the amount of strain at rupture for the specimen tested at 649°C was approximately double that of the other specimens shown.

4.2.1.3. Elongation at Rupture

The elongation of each specimen was measured after rupture and the results were plotted as a function of stress in Figure 31. Although there is a large amount of scatter present in the elongation results, general trends can be observed.

It seems that there is a trend towards increasing elongation at rupture as the temperature is increased, although the difference in elongation between specimens tested at 538°C and those tested at 593°C is minimal. However, as noted in the previous section, there appears to be a fairly dramatic increase in elongation at rupture for those tests performed at 649°C compared to tests performed at lower temperatures.

From the data available, it is not possible to determine if there is any correlation between total elongation at rupture and applied stress. Although there may appear to be a slight trend towards increasing elongation at rupture as the stress is decreased within a given temperature band, the amount of scatter present in the data precludes one from making this conclusion.

The increase in elongation at rupture at 649°C seems to be accompanied by a significant increase in oxidation as well. Those specimens tested at 649°C displayed massive scaling on their surfaces after rupture resulting in significant material loss. The increase in temperature seemed to increase the rupture ductility of these specimens dramatically, although not without a significant loss in creep strength as demonstrated by the stress rupture data.

4.2.1.4. Master Curve

The rupture data obtained for this steel did not show good fit with the Larson-Miller time-temperature parameter. In order to use this parameter, the family of straight lines produced by creating a constant stress plot of log t versus 1/T should converge on the ordinate. However, as shown in Figure 32, the constant stress curves for the A193 test data converged significantly before the ordinate.

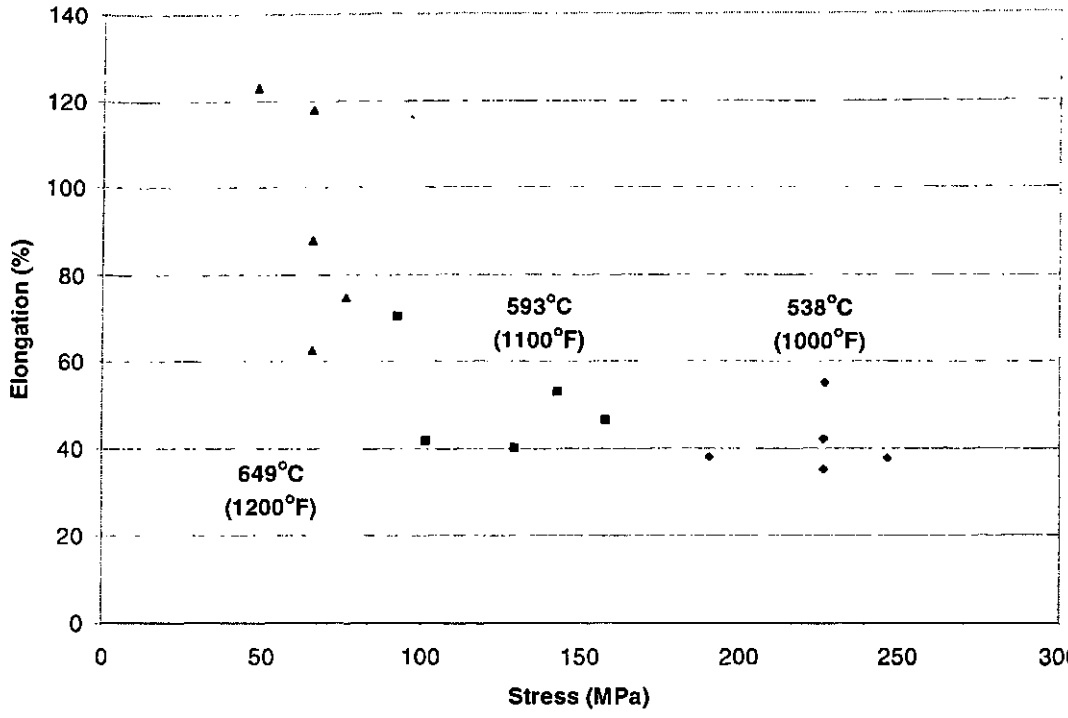

Figure 31: Elongation at rupture as a function of stress for ASTM A193 Grade B16.

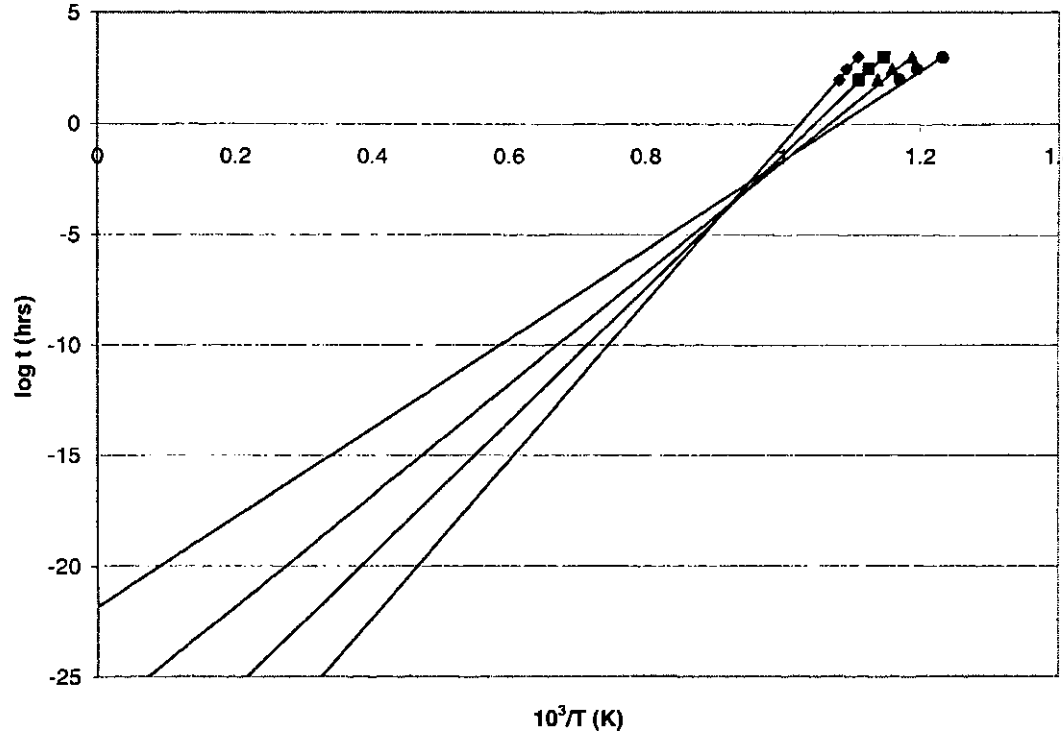

Figure 32: Constant stress curves on a plot of log t versus 1/T for ASTM A193 Grade B16.

However, this pattern is typical of the Goldhoff-Sherby parameter. The point of convergence (Ta, ta) defines the optimum constants for this particular data set.

An attempt to fit the data to other time-temperature parameters did not prove successful. The Manson-Haferd parameter predicts that the constant stress lines on a plot of log t versus T should converge at some point (Ta, ta). The constant stress lines for the A193 test data diverge.

The Orr-Sherby-Dorn parameter is good for data for which the constant stress lines on a plot of ln t versus T are parallel. However, the constant stress lines for the A193 test data converge, as would be expected when considering that the constant stress lines on a plot of log t versus T also converge, making this parameter ineffectual for modelling the data as well.

Using the Goldhoff-Sherby parameter to model the A193 test data, the values of the constants T_A and t_A were determined to be 975 K and 0.5 hours, respectively. A master curve was then plotted using this parameter as shown in Figure 33.

A master curve was also plotted using the Larson-Miller parameter as shown in Figure 34 for comparison with available data. A value of 20 was used for the constant as it has been used with reasonable success for the majority of steel alloys.[44]

Longer term test data is needed to provide more confidence in the master curves produced. Scatter contained in the test data may account for the poor fit with the Larson-Miller parameter.

4.2.2. ASTM A355 Class A

4.2.2.1. Stress Rupture Results

The test results of A355 display similar creep strength to that of A193. A graphical summary of the stress rupture results for A355 is shown in Figure 35. More detailed information for each test performed is contained in Appendix B.

Multiple tests were performed with the same applied stress at 538°C and 593°C as can be seen in Figure 35 and the results were even better than for A193. The difference between the shortest and longest rupture times, expressed as a percentage of the average of the three rupture times, was 21.4% at 538°C and only 2.9% at 593°C.

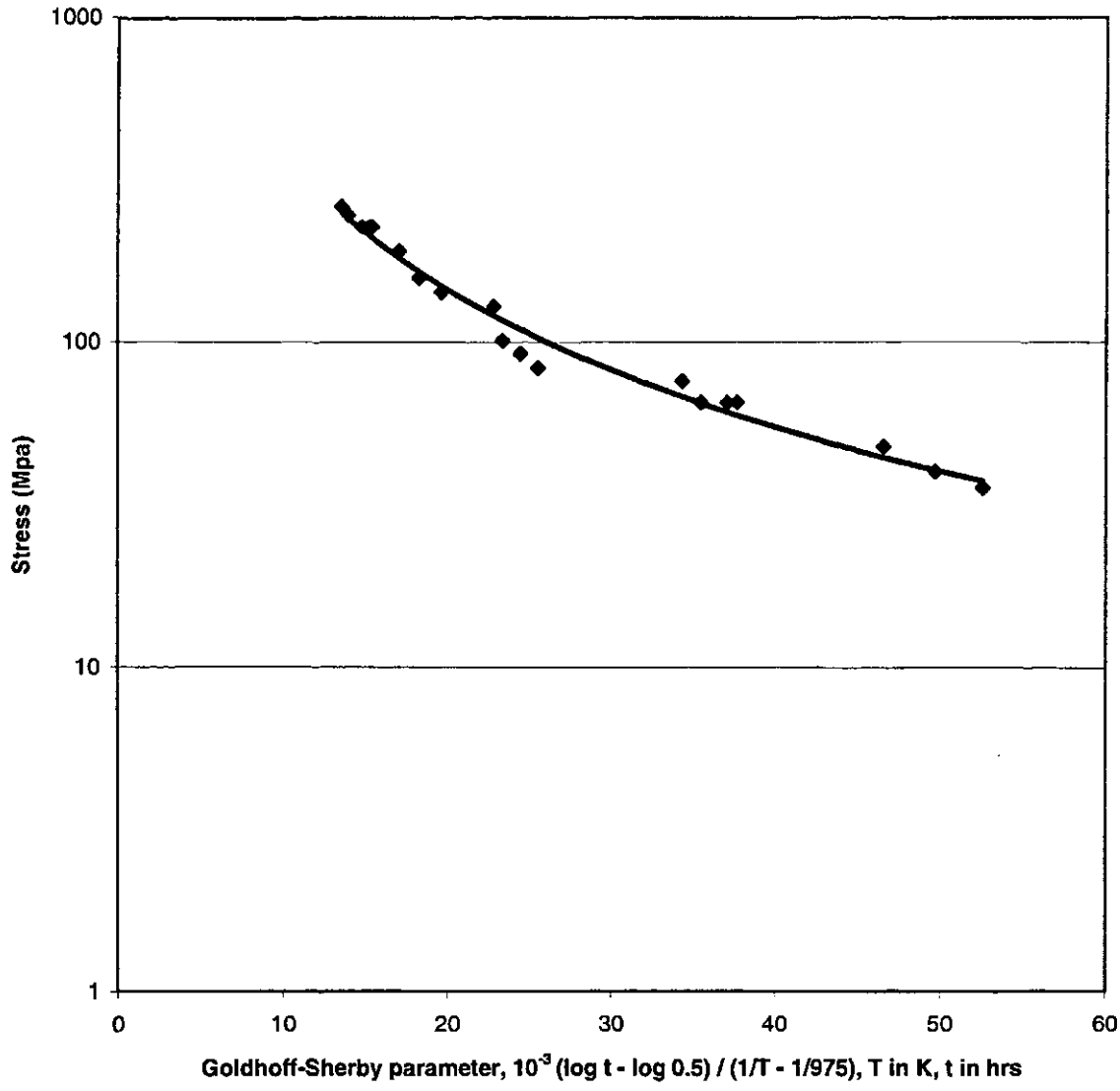

Figure 33: Goldhoff-Sherby master curve for ASTM A193 Grade B16.

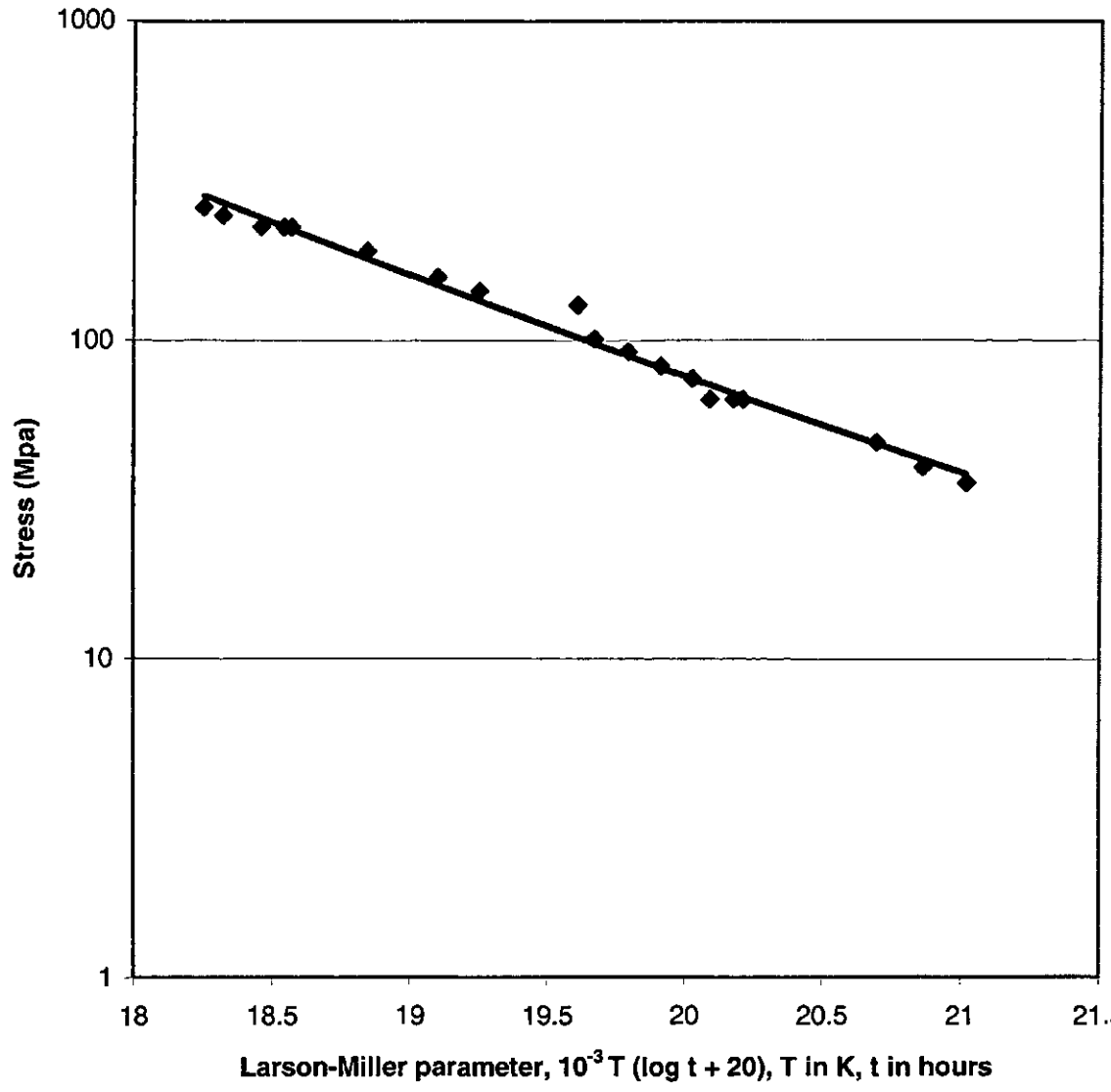

Figure 34: Larson-Miller master curve for ASTM A193 Grade B16.

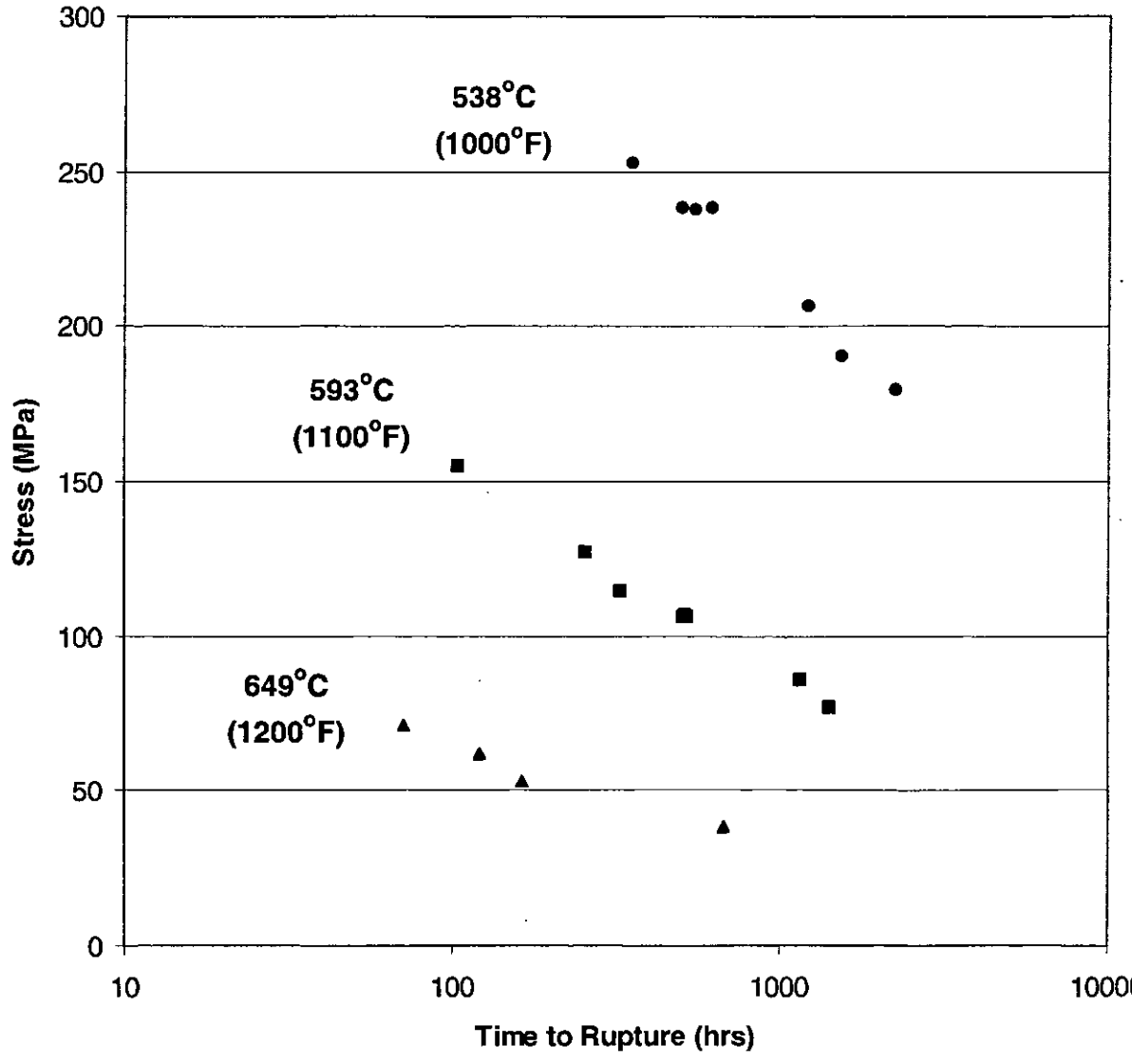

Figure 35: Stress rupture results for ASTM A355 Class A.

4.2.2.2. Creep Tensile Results

The creep curves of the A355 specimens tested seem to closely mirror those of the A193 steel, with the tertiary region being very prominent. A plot of strain as a function of time for Specimen 1D, which was subjected to an applied stress of 190.7 MPa, is shown in Figure 36(a). This specimen was tested at the same temperature and same stress as Specimen 3M, the creep curve of which was shown in Figure 27 with the creep tensile results for A193. As can be seen, the two curves are very similar although the rupture time of Specimen 1D is 170 hours shorter.

The first 600 hours of the creep curve of Specimen 1D are shown in Figure 36(b) and it can be seen that again it is difficult to identify a secondary stage that is truly steady state.

However, the minimum strain rate was determined approximately and it was found to be about 35% greater than the minimum strain rate of Specimen 3M. This is a fairly representative example of the relative creep strength of these two steels. In general, the creep strength of A193 was found to be somewhat greater than that of A355, as demonstrated by the increased strain rate and shorter rupture time.

The minimum strain rate was determined for all specimens tested at 538°C and plotted as a function of stress as shown in Figure 37. This steel appears to follow a power law relationship as well with the exponent, n, having a value of approximately 4.5. This value is significantly lower than that determined from the test data for A193.

The shape of the creep curve changes little if the temperature is increased, as shown by the plot for Specimen 2L displayed in Figure 38, although the total strain at rupture has almost doubled.

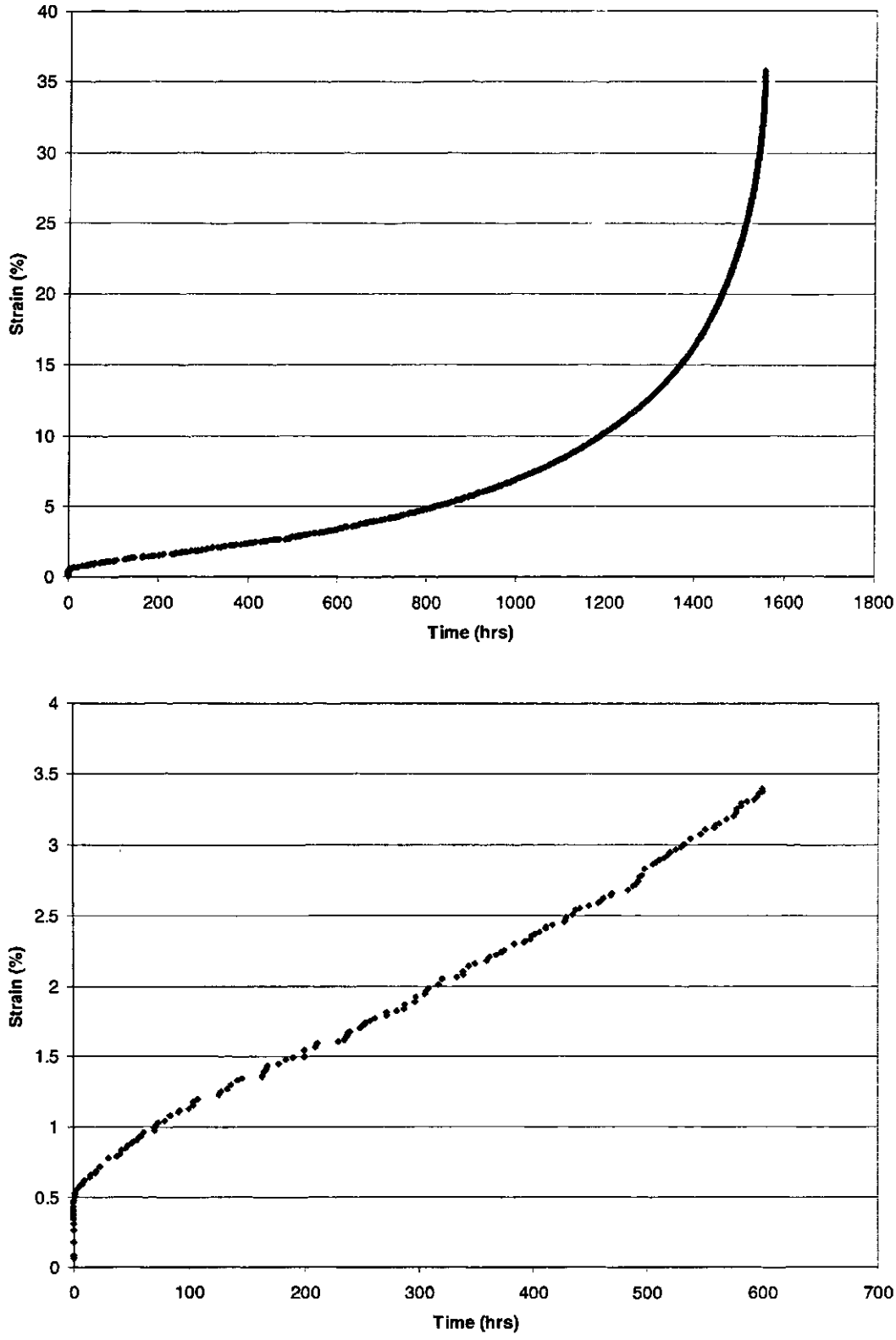

Figure 36: Strain as a function of time, Specimen 1D, 538°C, 1554 hours, a) to rupture, and b) first 600 hours.

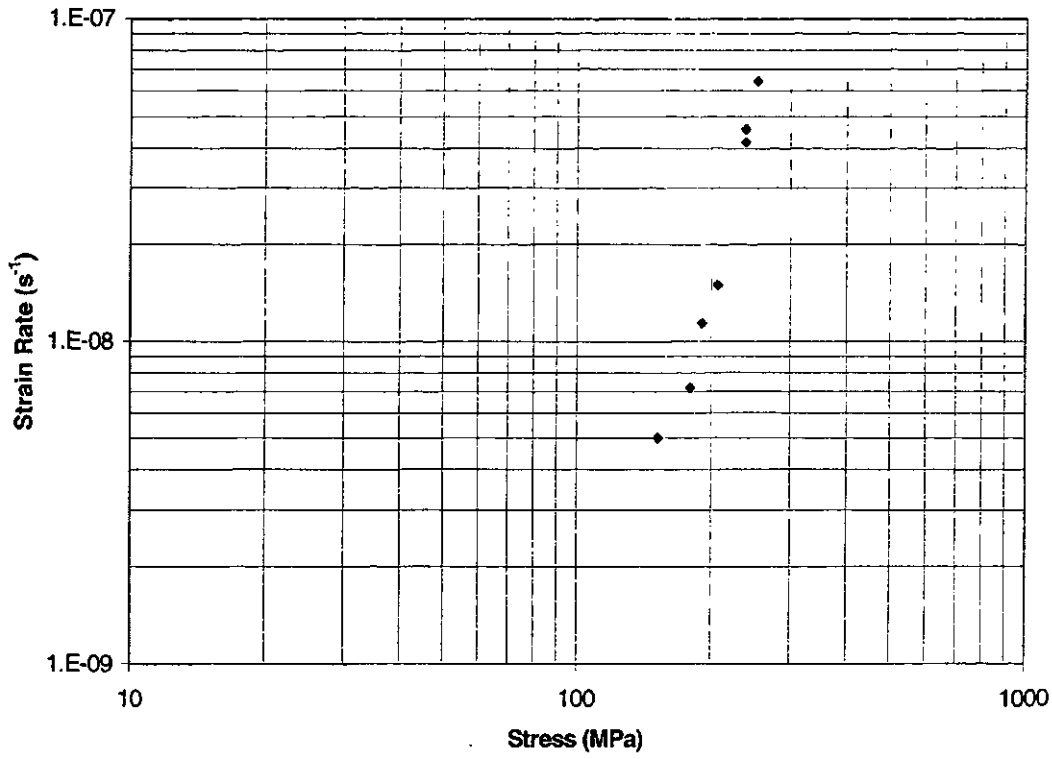

Figure 37: Minimum strain rate as a function of stress at 538°C for ASTM A355 Class A.

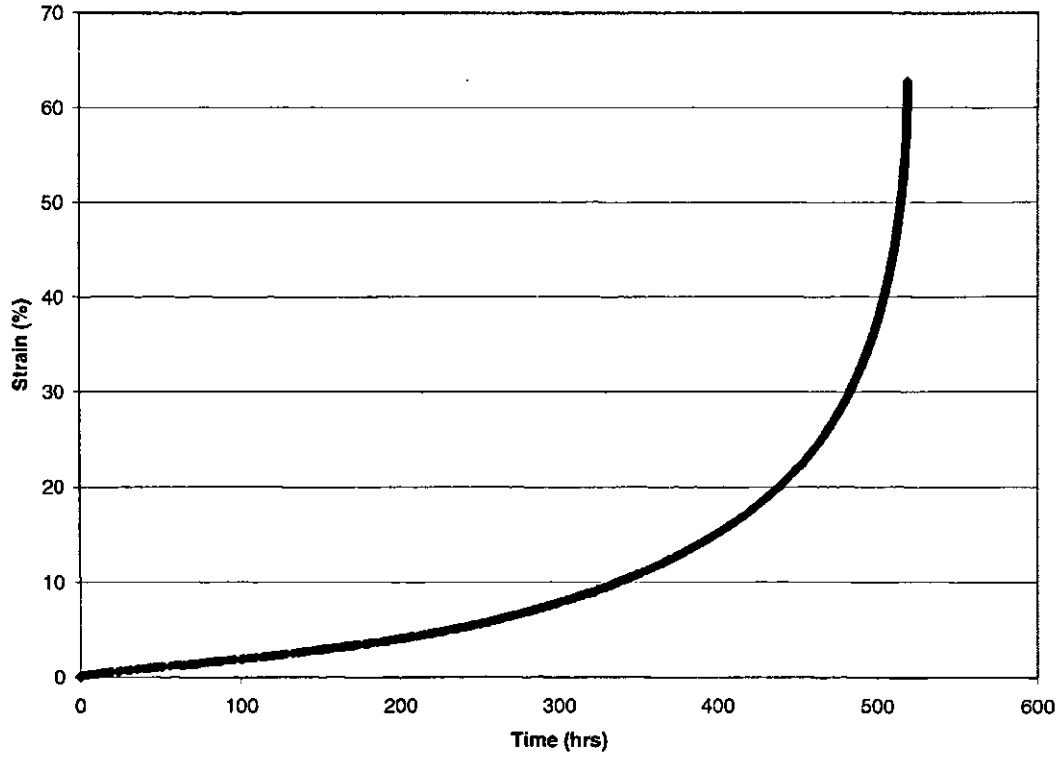

Figure 38: Strain as a function of time, Specimen 2L, 593°C, 519 hours.

4.2.2.3. Elongation at Rupture

Again, it is interesting to note the effect of temperature on the amount of elongation that occurs before rupture. Figure 39 contains a plot of the total elongation at rupture for each specimen as a function of applied stress. As observed for A193, there appears to be a general trend towards an increase in elongation at rupture as the temperature is increased.

Although the scatter in the data is fairly significant, the data might also suggest that the amount of elongation at rupture tends to increase as the applied stress is decreased. As with A193, it appeared that for those tests performed at 649°C, there was a stress below which the total elongation at rupture increased significantly, accompanied by a similar increase in oxidation.

4.2.2.4. Master Curve

Similar to A193, the test data for A355 did not produce constant stress curves that converged at the ordinate on a plot of log t versus 1/T thus making it impossible to determine the value of the constant, C, of the Larson-Miller parameter for this particular data set. The constant stress curves converged significantly before the ordinate as shown in Figure 40, at approximately the same point as the constant stress curves for the A193 data. The constants, (T_A, t_A), for the Goldhoff-Sherby parameter determined from the point of convergence thus had the same values as for A193, 975K and 0.5 hours, respectively.

The Goldhoff-Sherby parameter was then used to create a master curve for the A355 test data as displayed in Figure 41.

A master curve was also created using the Larson-Miller parameter with a constant of 20. This curve is shown in Figure 42.

The use of these curves for estimation of rupture time should be approached with caution due to the small amount of data used to create them. Longer term data would increase the level of confidence in these curves.

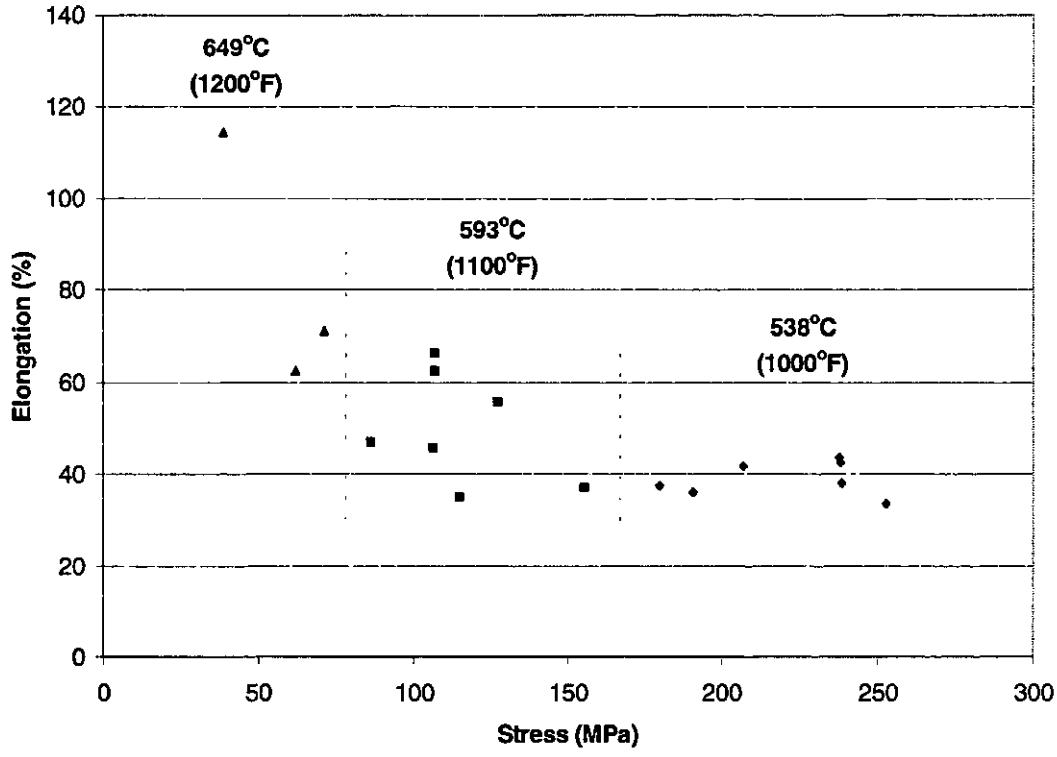

Figure 39: Elongation at rupture as a function of stress for ASTM A355 Class A.

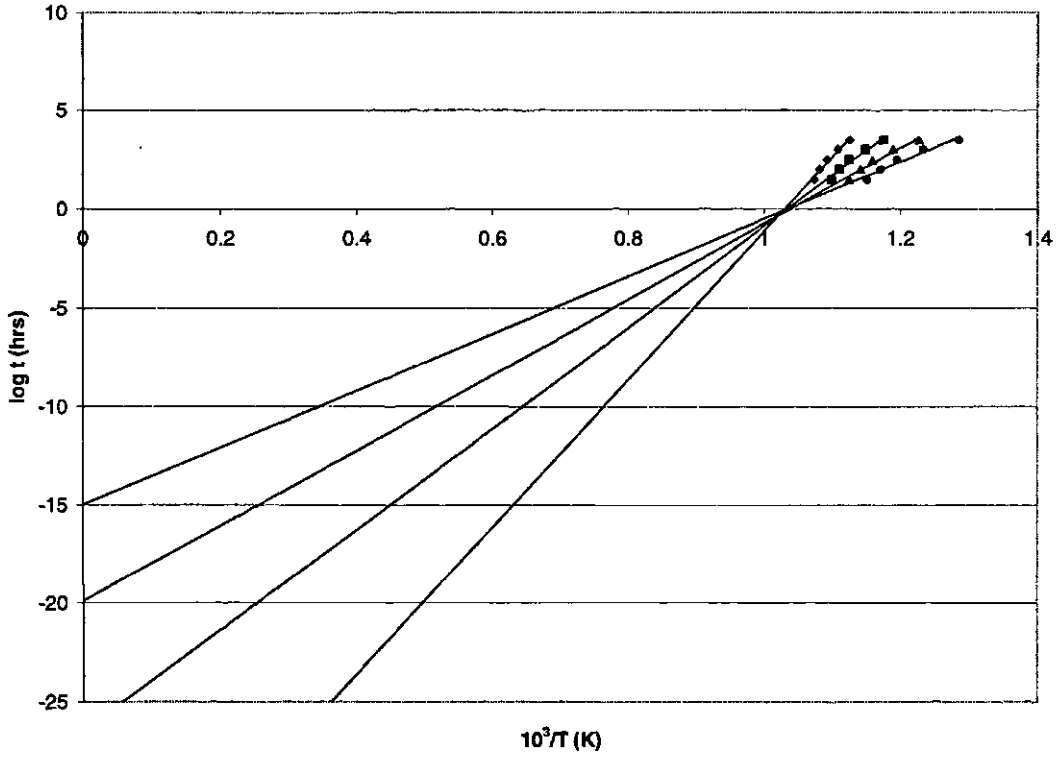

Figure 40: Constant stress curves on a plot of log t versus 1/T for ASTM A355 Class A.

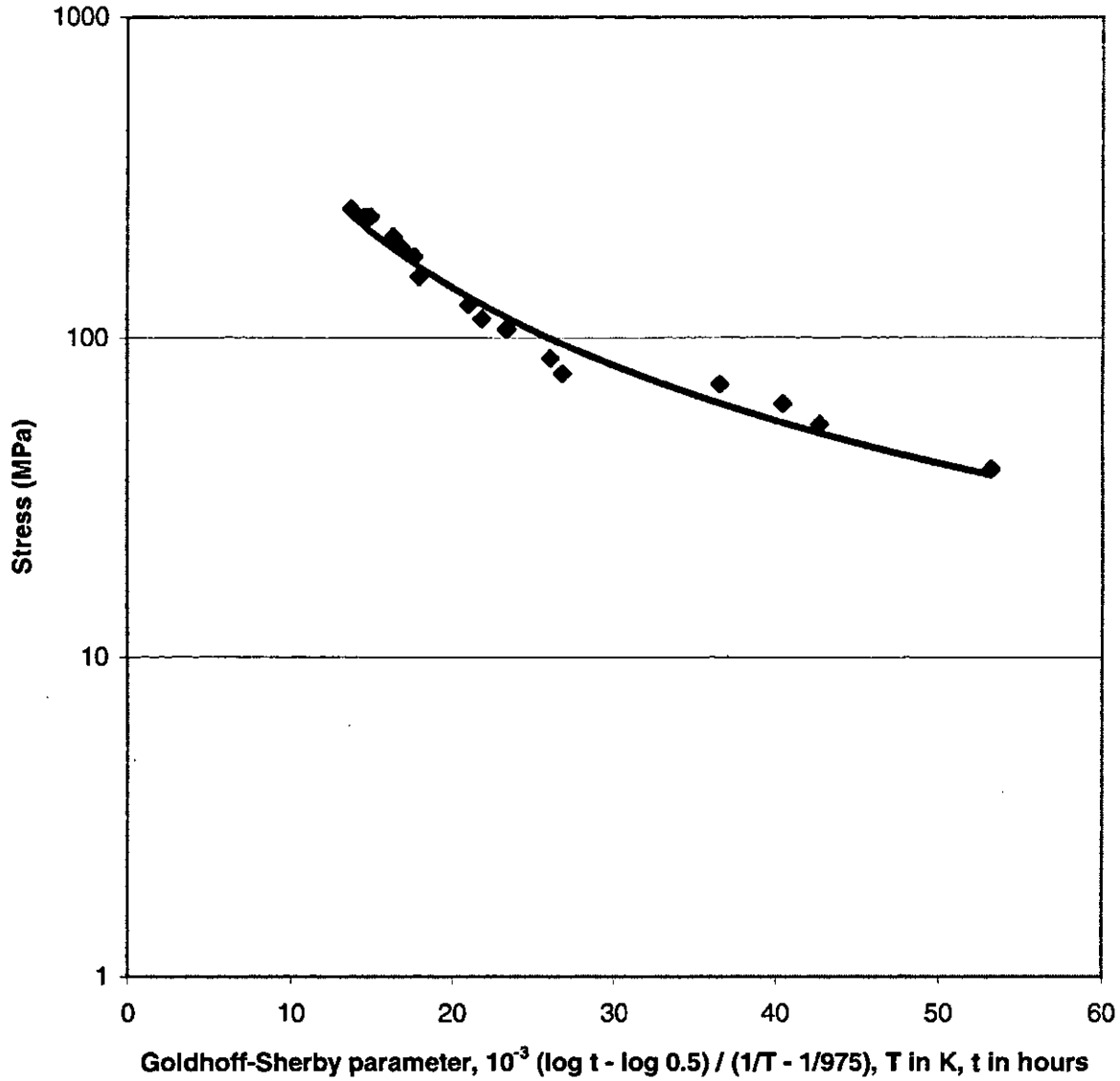

Figure 41: Goldhoff-Sherby master curve for ASTM A355 Class A.

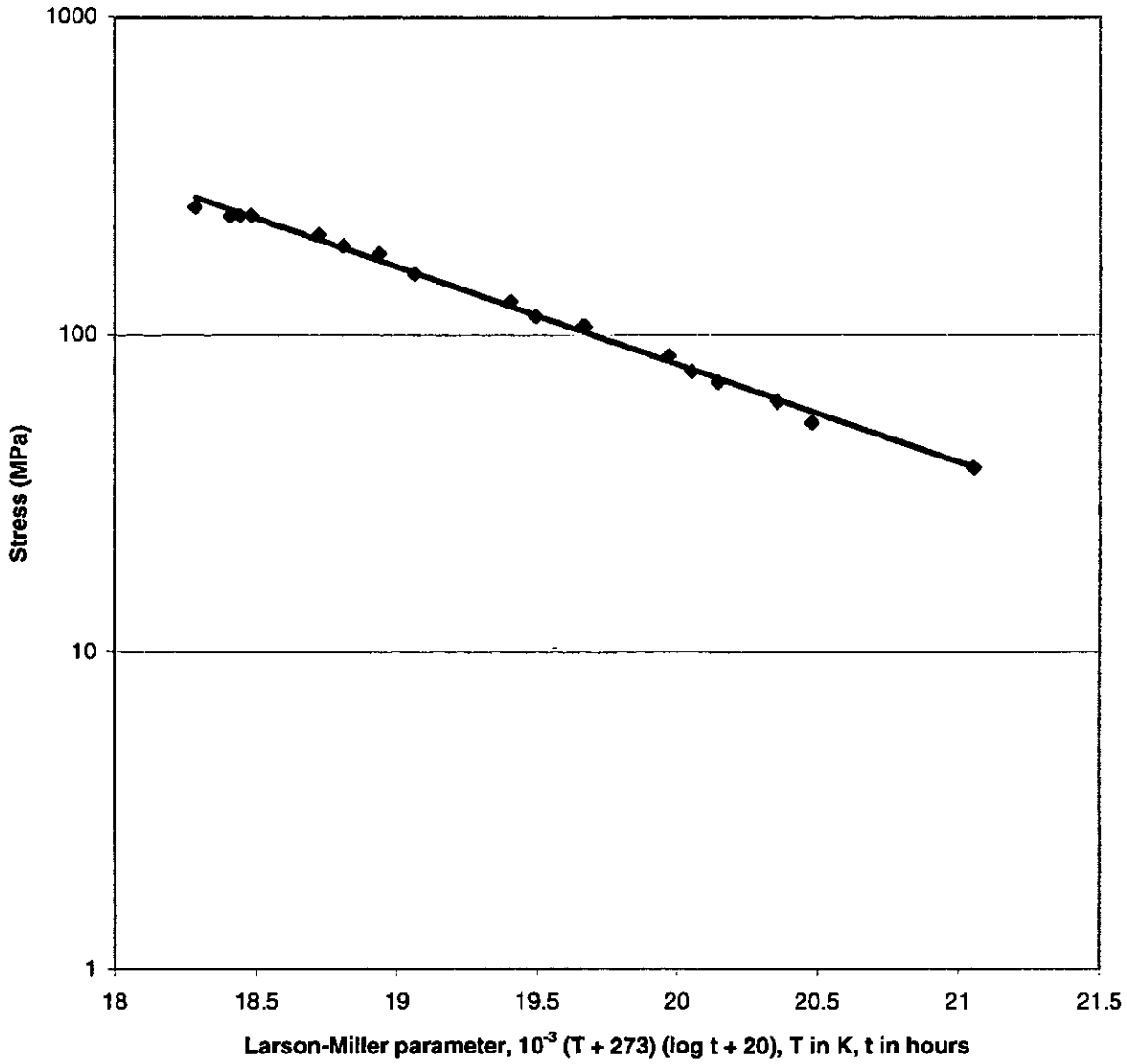

Figure 42: Larson-Miller master curve for ASTM A355 Class A.

4.2.3. ASTM A437 Grade B4B

The A437 steel is significantly different than the other two steels studied due to its high chromium content, which makes it a stainless steel. The creep strength and oxidation resistance are correspondingly much greater.

4.2.3.1. Stress Rupture Results

Stress rupture data up to 10 000 hours was provided by Carpenter Technology Corporation for the Carpenter 636 steel, which corresponds to A437. A Larson-Miller master curve was created from this data, which was then used to estimate the required stresses for the creep tests for this steel. The rupture times for all the tests performed in this study are thus shown in Figure 43 along with the estimated rupture time for each test based on the stress rupture data provided.

The agreement between the test results and the rupture data provided by Carpenter was fairly good for those tests with longer rupture times. However, it seemed that the difference between the two often became very large as the time to rupture decreased. This is very noticeable for those tests performed at 538°C and 649°C with rupture times of one hundred hours or less. This discrepancy may be partially due to the inability of the Larson-Miller parameter to provide a good estimate of creep strength in that range. However, it would appear that the very short term creep strength of the steel tested was somewhat less than that suggested by Carpenter.

Again, the repeatability of these tests appeared to be better than that of A193. Tests were repeated at the same stress level at both 538°C and 649°C and the difference between the shortest and longest rupture times, expressed as a percentage of the average of the three rupture times, was 23.4% at 538°C and only 11.2% at 649°C.

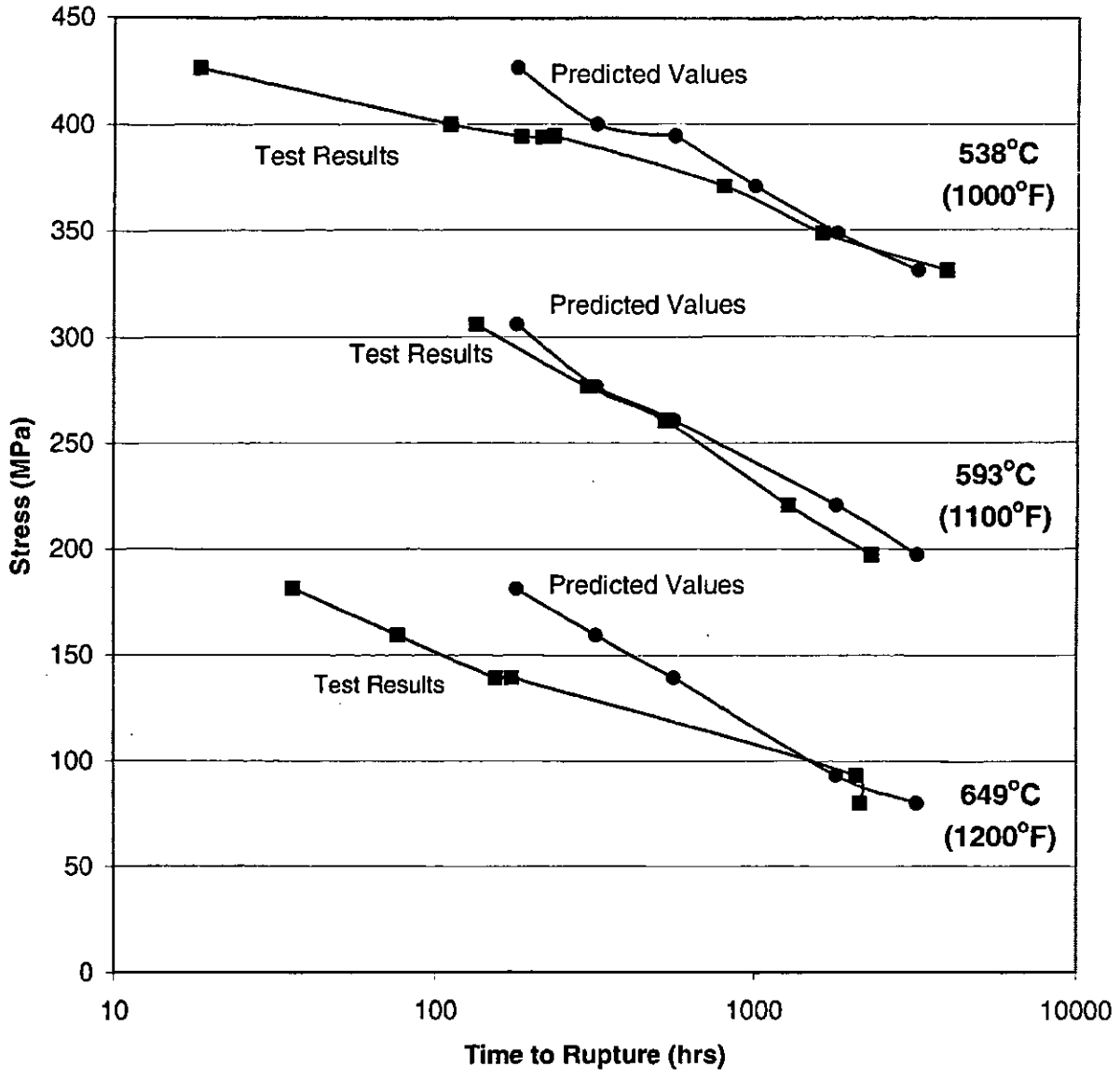

Figure 43: Stress rupture results for ASTM A437 Grade B4B.

4.2.3.2. Creep Tensile Results

As might be expected considering the substantial differences between A437 and the other two steels examined in this study, the shape of the creep curve for A437 is somewhat different from those shown earlier. A plot of strain as a function of time for Specimen 4K, which is displayed in Figure 44(a), shows a typical creep curve with three fairly distinct stages observable. The primary stage is still quite short and the tertiary stage is still very prominent, but the secondary stage is much more pronounced. The secondary stage appears to be at least as long as the tertiary stage if not longer, depending on what is defined as the onset of tertiary creep.

The steady state portion of the curve is shown in Figure 44(b), and the strain rate can be determined by finding the slope of the line. The steady state strain rate was determined for each specimen tested at 538°C and plotted as a function of applied stress as shown in Figure 45.

It is interesting to note that the slope of the line, which is equal to the value of the exponent, n, in the power law, appears to change at around 380 MPa in Figure 45. The value of n changes from approximately 5 to around 2.5. This would seem to indicate a change in the controlling mechanism of creep.

The creep curve of Specimen 4J, which was tested at 649°C, is contained in Figure 46 and it can be seen that the basic shape of the curve is unchanged from that of Specimen 4K.

The total elongation of Specimen 4J is not significantly greater than of Specimen 4K either, which is a departure from the behaviour observed earlier for the A193 and A355 steels.

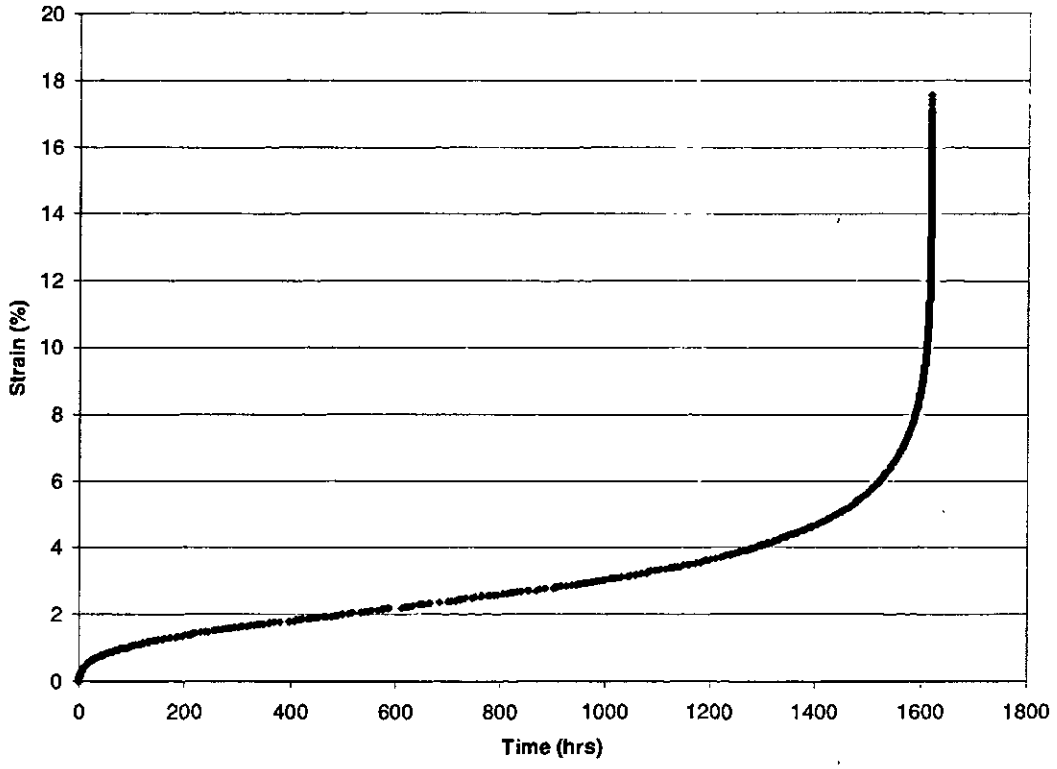

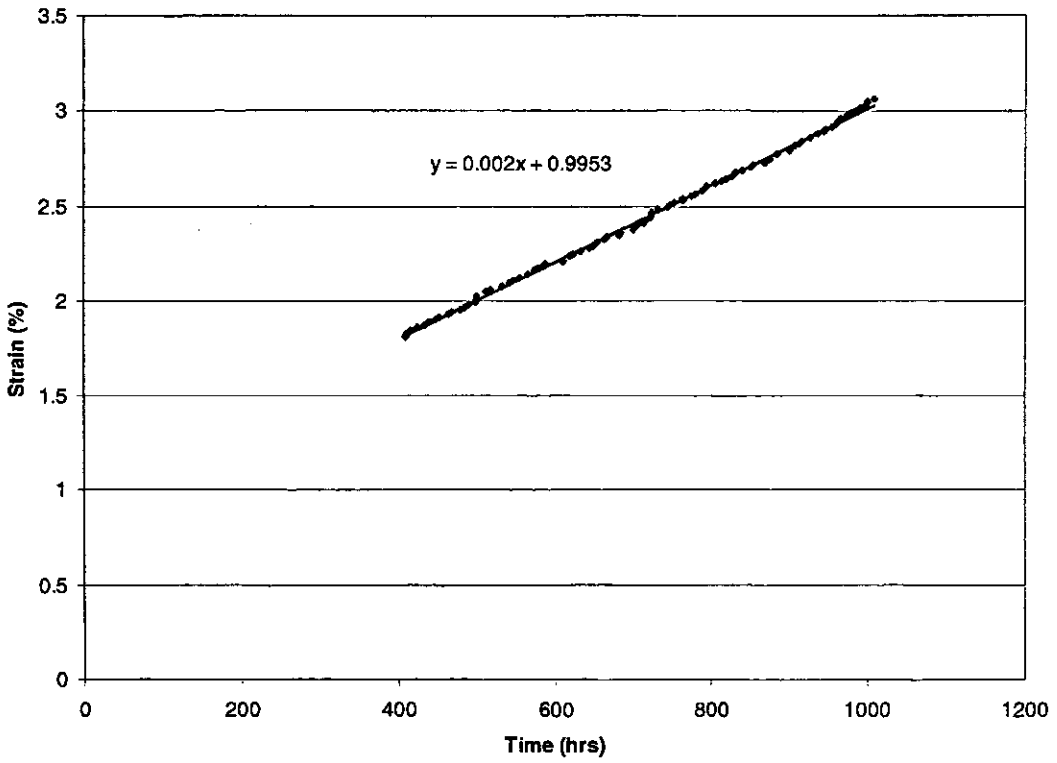

Figure 44: Strain as a function of time, Specimen 4K, 538°C, 1617 hours, a) to rupture, and b) secondary stage.

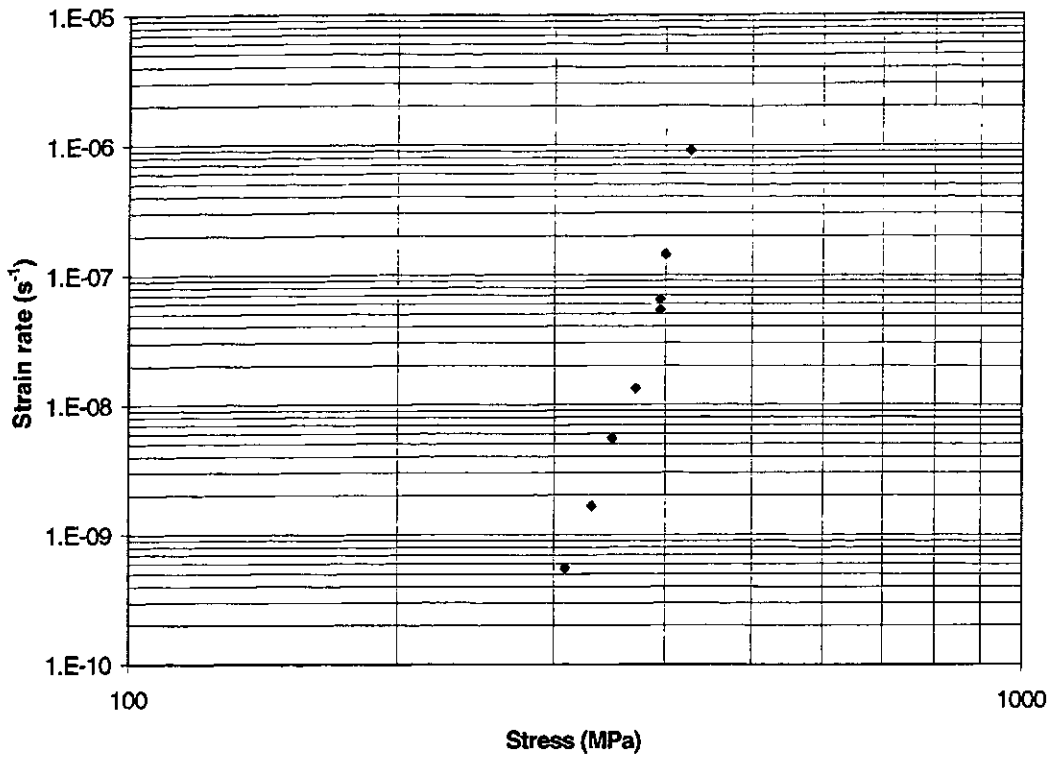

Figure 45: Minimum strain rate as a function of stress at 538°C for ASTM A437 Grade B4B.

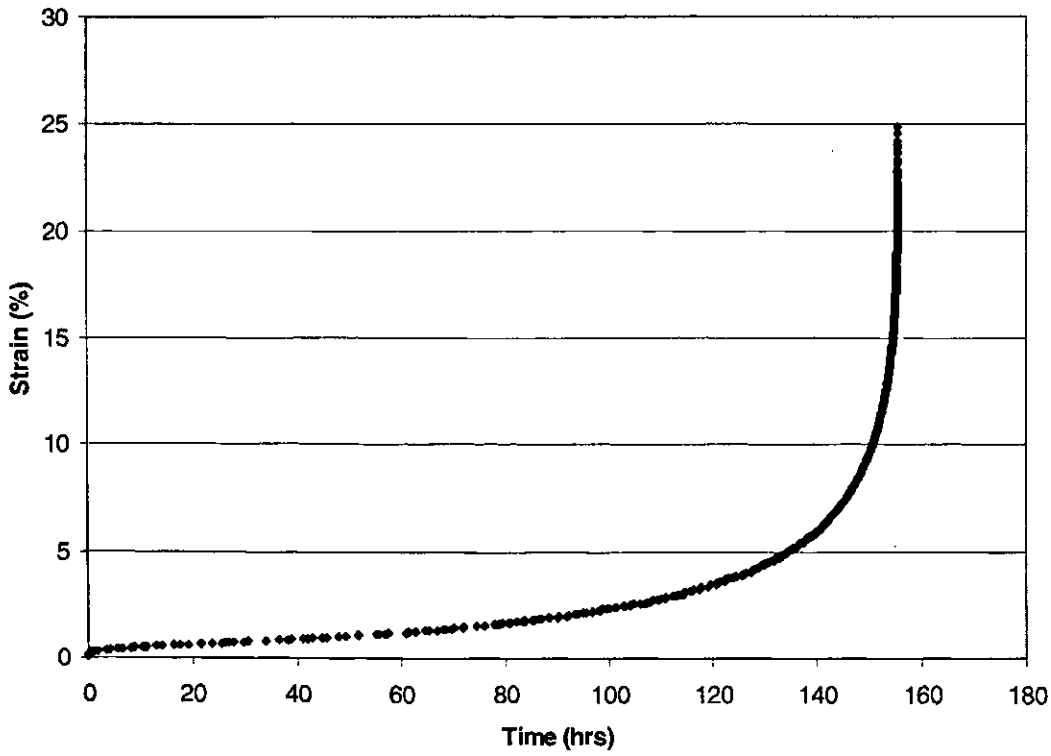

Figure 46: Strain as a function of time, Specimen 4J, 649°C, 156 hours.

4.2.3.3. Elongation at Rupture

When the elongation at rupture for each specimen tested is plotted as a function of stress for the A437 steel, it can be seen that there is no dramatic change as the temperature is increased. Figure 47 shows that the trend towards increasing elongation at rupture as the temperature is increased observed for A193 and A355 may not hold true for this steel. The average elongation at rupture does increase slightly at 649°C compared to 538°C although it is not a large increase, and the average elongation at rupture actually drops slightly at 593°C compared to 538°C.

The elongation at rupture is significantly lower overall for this steel compared to the other two as would be expected considering its greater strength and lower ductility.

4.2.3.4. Master Curve

The conditions predicted by the Larson-Miller parameter held true for the stress rupture data for A437. The constant stress curves on a plot of log t versus 1/T actually converged at the ordinate at a value of approximately –30 as seen in Figure 48. The tendency of high chromium steels to have values for the constant, C, of 25 or greater has been observed by others and thus a value of 30 is acceptable.[44]

A master curve using the Larson-Miller parameter was created and is displayed in Figure 49.

4.3. Metallography Results

Metallography should be an integral part of any study of materials and their behaviour as much can be learned from examining metal alloys at the microstructural level. The three steels in this study were examined using both scanning and transmission electron microscopes with the object of discerning the mechanisms controlling their creep behaviour and obtaining a more complete understanding of their microstructural characteristics. Fracture surfaces were also examined at high magnification to observe the prevalent fracture modes.

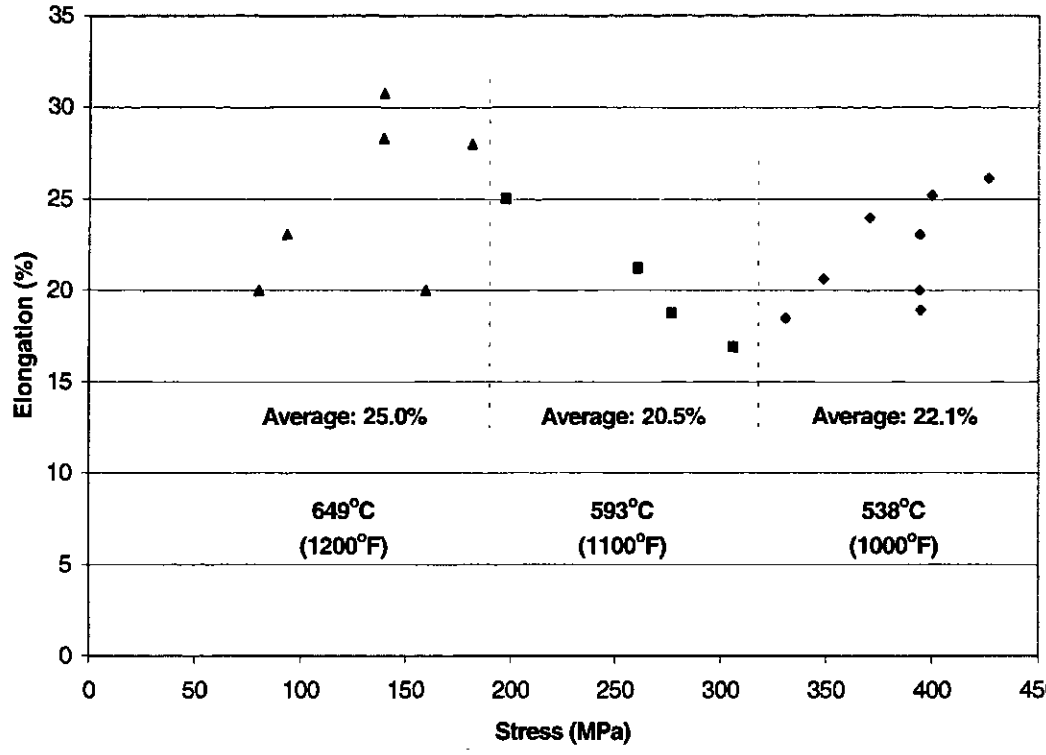

Figure 47: Elongation at rupture as a function of stress for ASTM A437 Grade B4B.

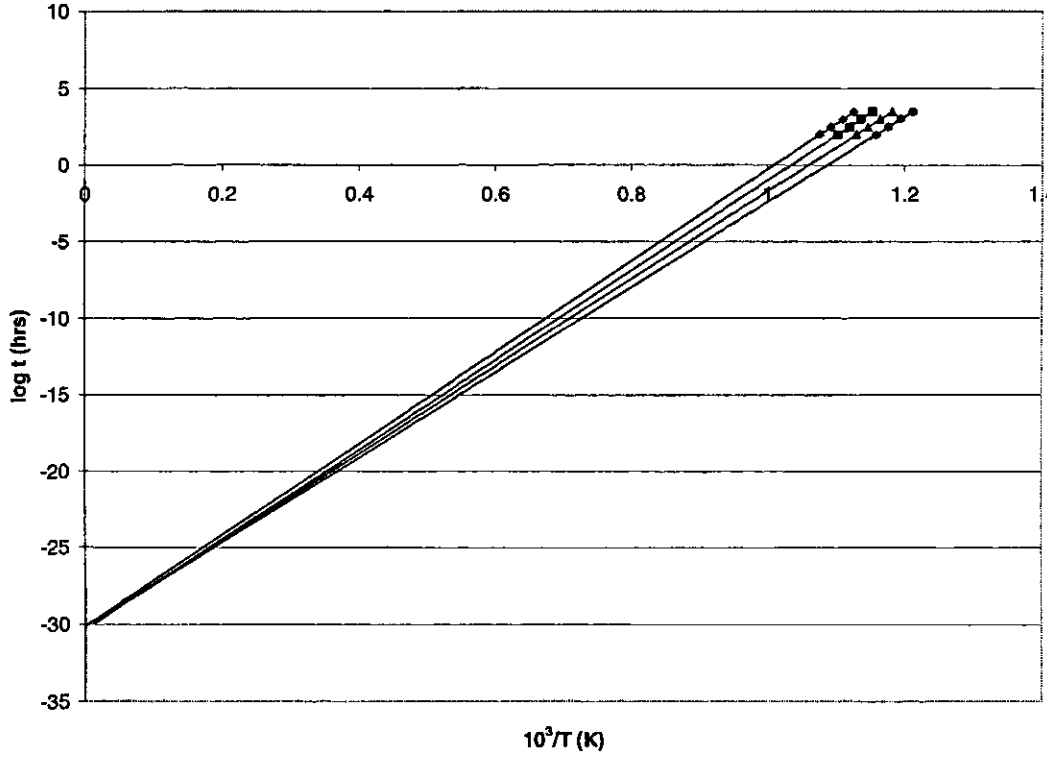

Figure 48: Constant stress curves on a plot of log t versus 1/T for ASTM A437 Grade B4B.

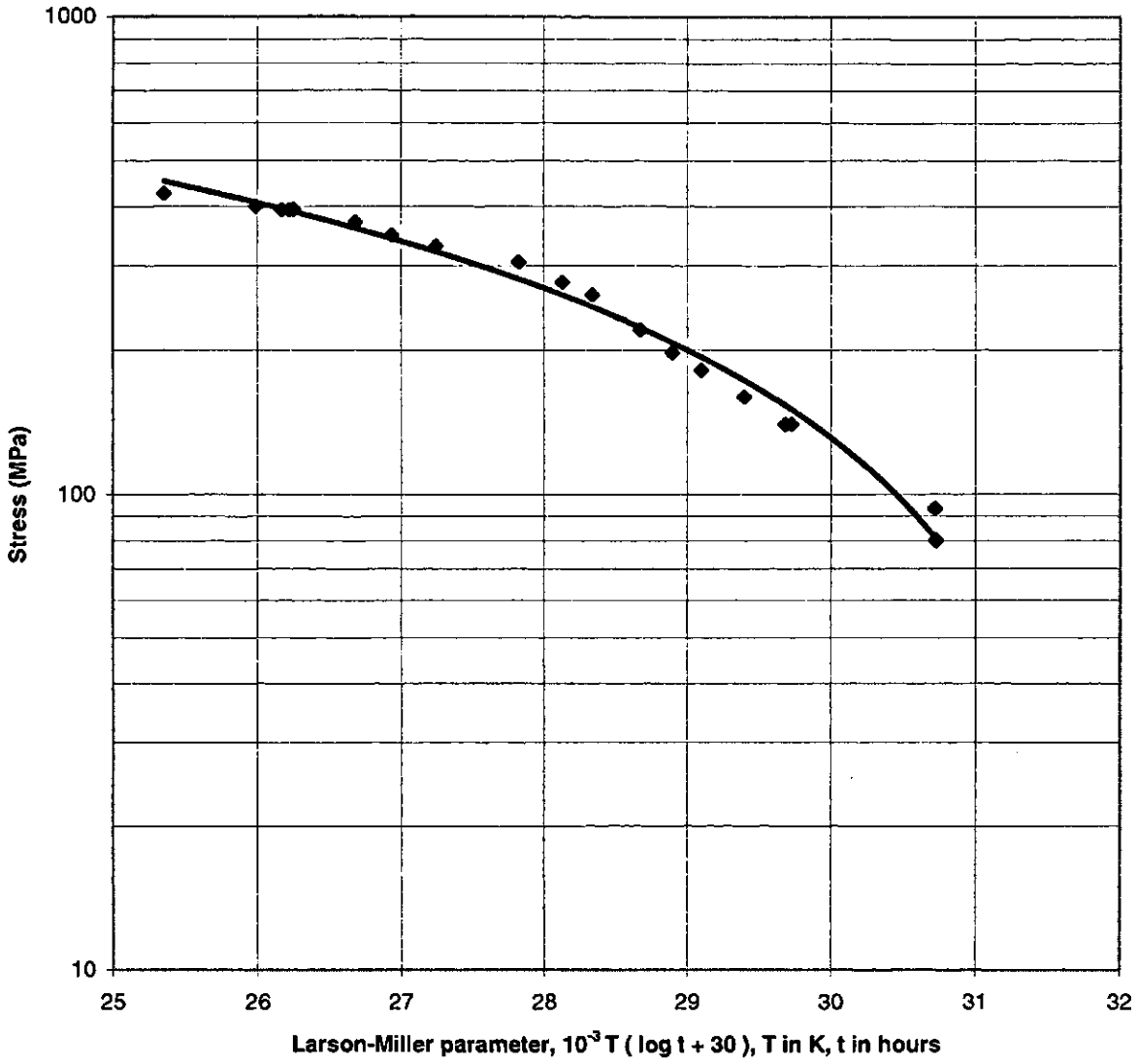

Figure 49: Larson-Miller master curve for ASTM A437 Grade B4B.

4.3.1. Fractography

A study of the fracture surface morphology of ruptured creep specimens using a scanning electron microscope revealed much useful insight into the behaviour of these steels at high temperatures. A look at some of these fracture surfaces and a discussion of their features will be put forward in the following section.

4.3.1.1. ASTM A193 Grade B16

Observation of the fracture surfaces of ruptured A193 specimens revealed that the fracture mode was a combination of brittle and ductile behaviour. Figure 50 contains images of the fracture surfaces of two specimens obtained at fairly low magnification so the entire fracture surfaces are observable. The test temperature and the time to rupture is given for each specimen in the caption. These specimens were subjected to an applied stress of 261.4 MPa and 190.8 MPa, respectively.

Each of these specimens, which were tested at the same temperature, display both brittle and ductile fracture. The region in the center of each specimen is clearly ductile in nature and displays the cup and cone morphology typical of such fractures. However, the region directly outside that is evidently the result of brittle fracture as evidenced by its relatively smooth surface which is characteristic of very quick catastrophic failure. The third concentric region furthest away from the center is simply the outer surface of the specimen displaying the significant reduction in area due to necking which occurred in the final stages of creep before rupture.

One would surmise from these fracture surfaces that the rupture commenced at the center of the specimen and proceeded outward in a ductile manner, until the energy is greater than the steel can dissipate at which point the specimen ruptures almost instantly in a brittle fracture mode. The point of succession between ductile and brittle fracture most likely occurs when a crack in the specimen becomes too large.

Although these fracture surfaces are from two specimens which have rupture times that differ by an order of magnitude, it is interesting to note how similar they are. The magnification of both images is the same allowing direct comparisons between the specimens. The overall area reduction due to necking of both specimens is very similar, as well as the percentage of the fracture surface that appears to exhibit ductile fracture characteristics.

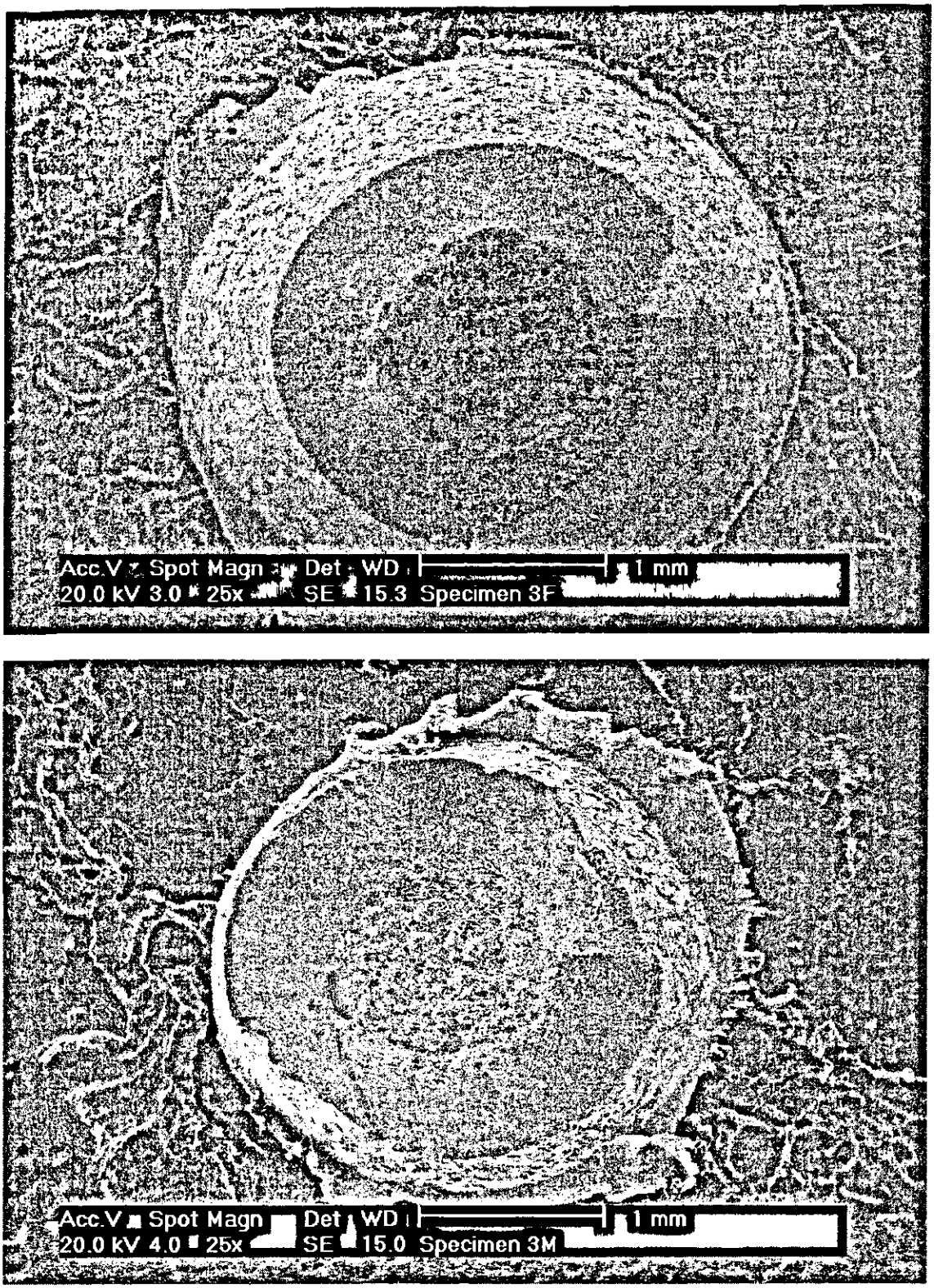

Figure 50: Fracture surfaces of a) Specimen 3F, 538°C, 321 hours, and b) Specimen 3M, 538°C, 1726 hours.

When considering these facts in conjunction with the elongation at rupture results, it would seem that the rupture ductility of this steel is not affected greatly by stress. The total elongation at rupture of Specimens 3F and 3M was about 45% and 35% respectively, which is not a significant difference considering the amount of scatter present in the elongation data.

However, one can see a definite evolution in the fracture surfaces as the test temperature is increased. The fracture surfaces of two specimens tested at higher temperatures are displayed in Figure 51.

The fracture surface of Specimen 3G displays similar features as the two specimens observed previously. However, the ductile zone covers a larger percentage of the fracture surface of Specimen 3G, and the area reduction due to necking is more severe.

Specimen 3B, which was tested at the highest temperature, displays a further evolution of the changes that occurred between Specimen 3F and Specimen 3G. The fracture mode appears to be entirely ductile in nature with no brittle region evident. As well, the reduction in area is even more significant and the size of the fracture surface is very small.

It would seem that the fracture mode of this steel appears to become more ductile at higher temperatures, as evidenced by the increase in the relative size of the ductile region and the decrease in the overall size of the fracture surface due to necking. This is reinforced by the dramatic increase in elongation for specimens tested at 649°C compared to those tested at lower temperatures.

It appears that there is a significant increase in rupture ductility and corresponding loss in creep strength for this steel at 649°C. This effect is also accompanied by much greater oxidation compared to lower temperatures. These low alloy steels would not be subjected to temperatures this high in service and it is unlikely of any profit to continue testing of this steel at this temperature.

The difference between the ductile and brittle fracture zones can be more readily seen at higher magnification as shown in Figure 52. The ductile regions of the fracture surfaces of this steel tend to contain many small holes as can be seen in Specimen 3B.

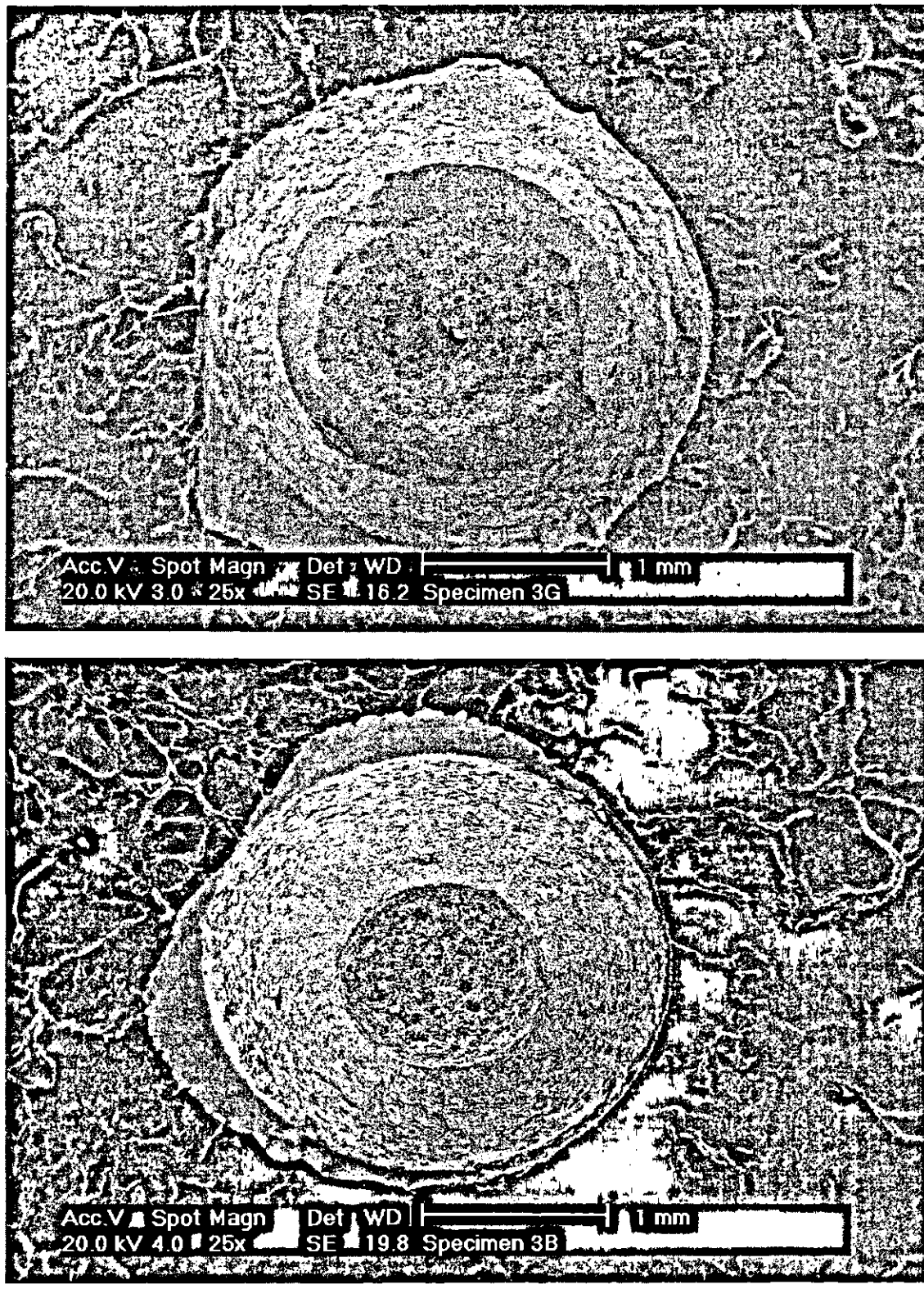

Figure 51: Fracture surfaces of a) Specimen 3G, 593°C, 518 hours, and b) Specimen 3B, 649°C, 53 hours.

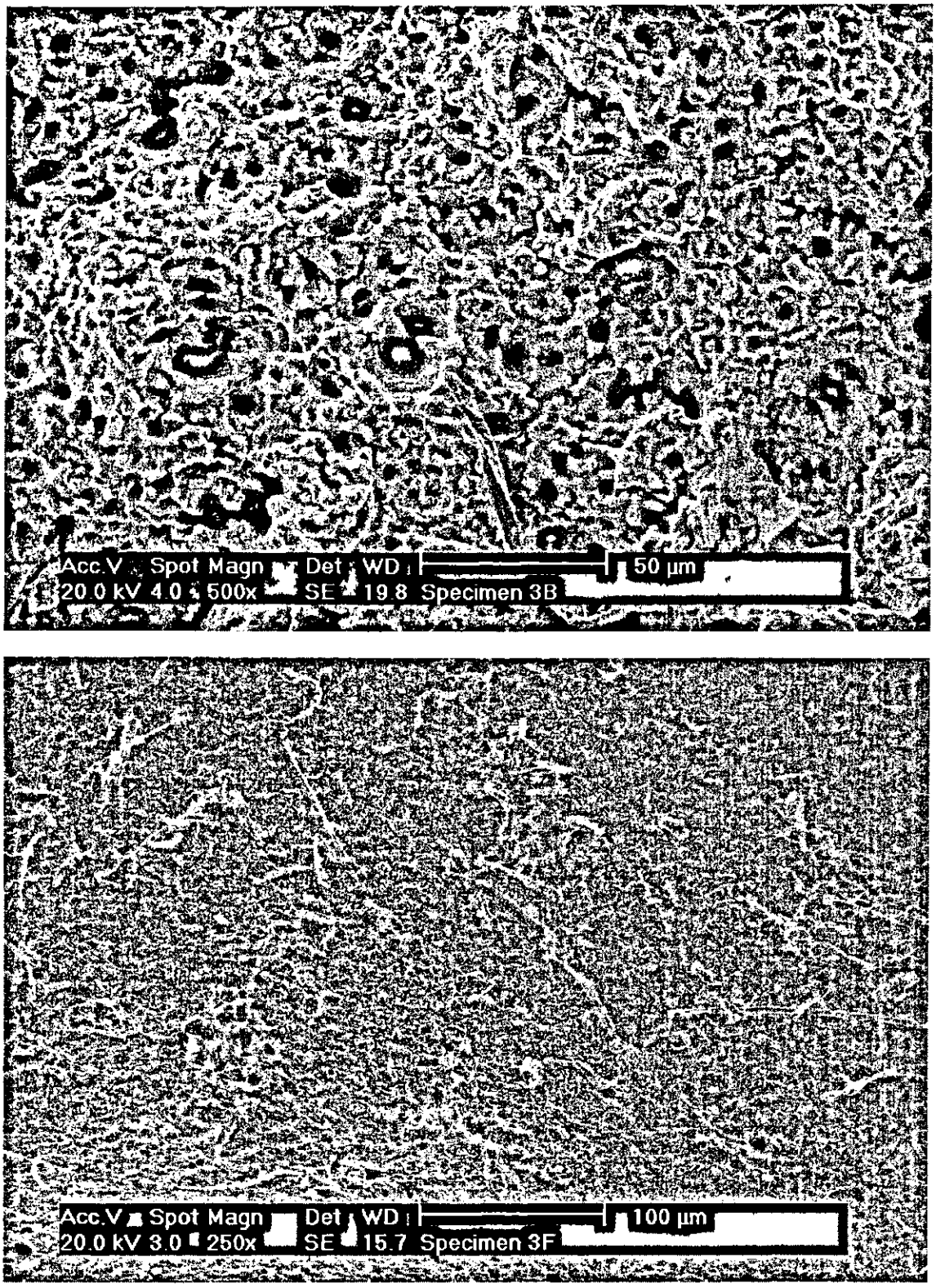

Figure 52: a) Ductile region of Specimen 3B, b) brittle region of Specimen 3F.

4.3.1.2. ASTM A355 Class A

Fracture surfaces of ruptured A355 Class A creep specimens were also observed using a scanning electron microscope. It is interesting to note that the fracture mode was completely ductile for all specimens observed, with one exception.

The fracture surfaces of two specimens tested at 538°C are shown in Figure 53. Specimen 2E displays the only fracture surface observed containing both ductile and brittle fracture zones. Specimen 1C, which had a much longer time to rupture, displays a fracture surface more typical of this steel, wherein the entire fracture surface is ductile in nature.

In a similar manner to A193 Grade B16, the rupture ductility of A355 Class A appears to increase as the test temperature is increased. This can be observed in the fracture surfaces displayed in Figure 54, both of which are obtained from ruptured specimens tested at higher temperatures than the two specimens observed previously.

As noted earlier, there is no brittle zone in either of these fracture surfaces, but the reduction in size of the fracture surface as a whole as the temperature is increased demonstrates the increase in rupture ductility.

As with A193 Grade B16, no definite conclusion could be drawn from the elongation at rupture data as to the effect of stress on the rupture ductility, although there did seem to be a slight trend towards increasing elongation as the stress was decreased. When the fracture surfaces are examined, this trend would appear to obtain further confirmation.

There is an obvious increase in the rupture ductility of Specimen 1C compared to Specimen 2E as noted earlier, although the elongation at rupture only varied between 37.5% and 33.5% for these specimens. These specimens were subjected to applied stresses of 179.7 MPa and 252.8 MPa, respectively.

A similar change can be observed if the fracture surface of Specimen 1J, which is displayed in Figure 55, is compared to that of Specimen 1G, which is shown in Figure 54. Specimen 1J was subjected to a stress of only 38.5 MPa, while Specimen 1G was subjected to a stress of 61.9 MPa. Specimen 1J displays considerably greater reduction in area, and thus greater rupture ductility, to go with its lower stress level.

The data is hardly conclusive, but it would appear that the rupture ductility of A355 tends to increase as the temperature is increased and the stress is decreased.

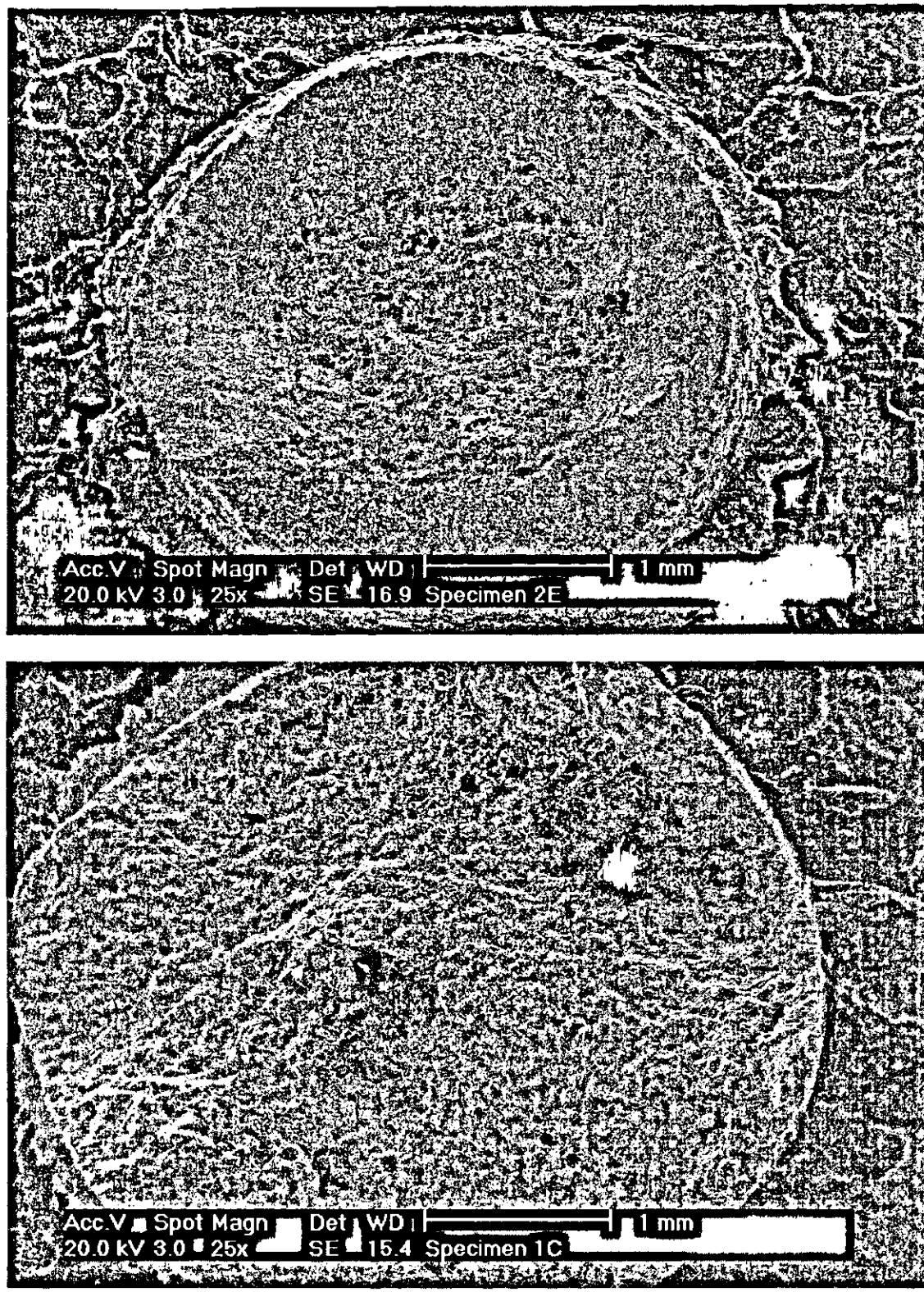

Figure 53: Fracture surfaces of a) Specimen 2E, 538°C, 352 hours, and b) Specimen 1C, 538°C, 2246 hours.

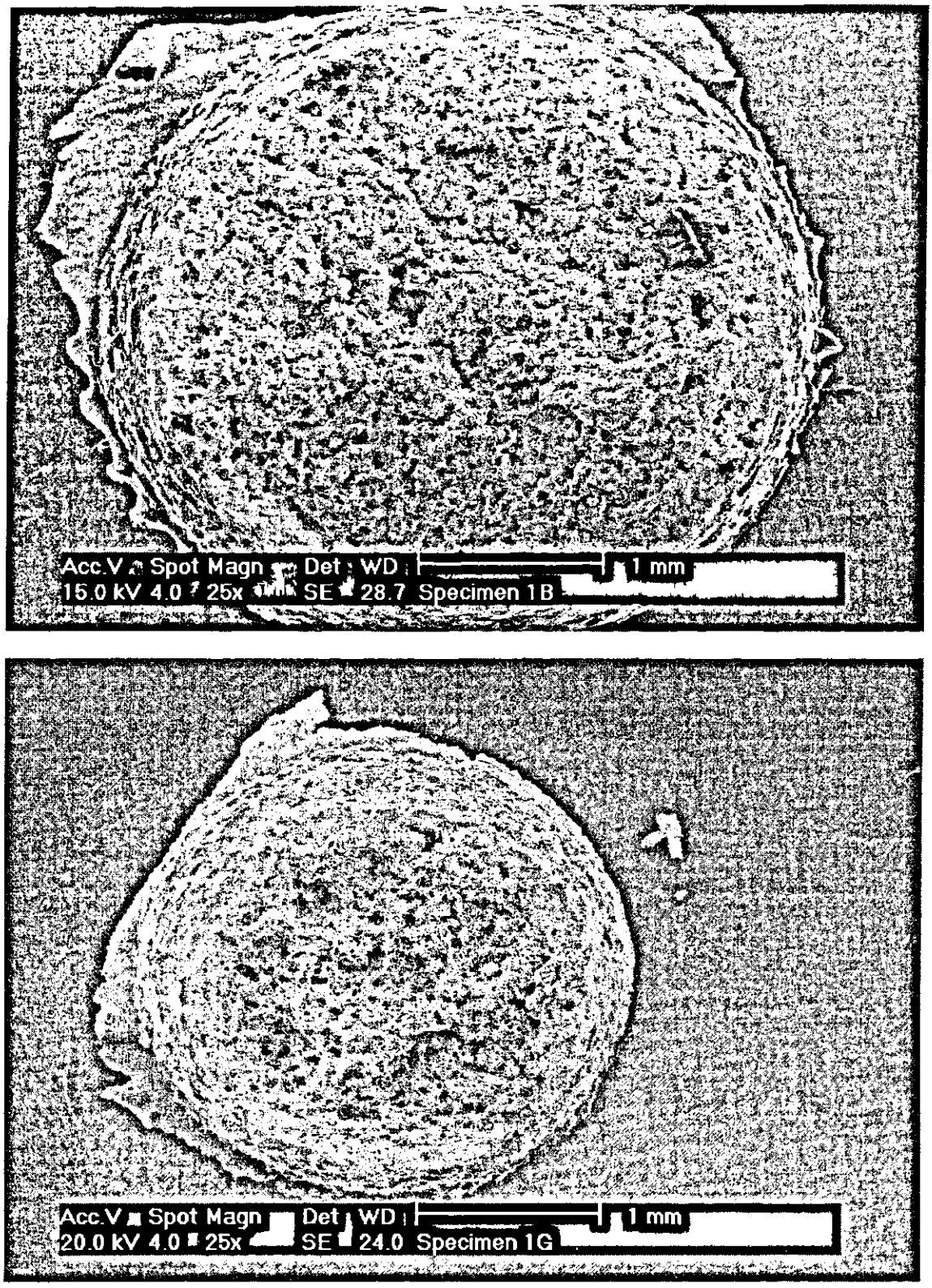

Figure 54: Fracture surfaces of a) Specimen 1B, 593°C, 326 hours, b) Specimen 1G, 649°C, 121 hours.

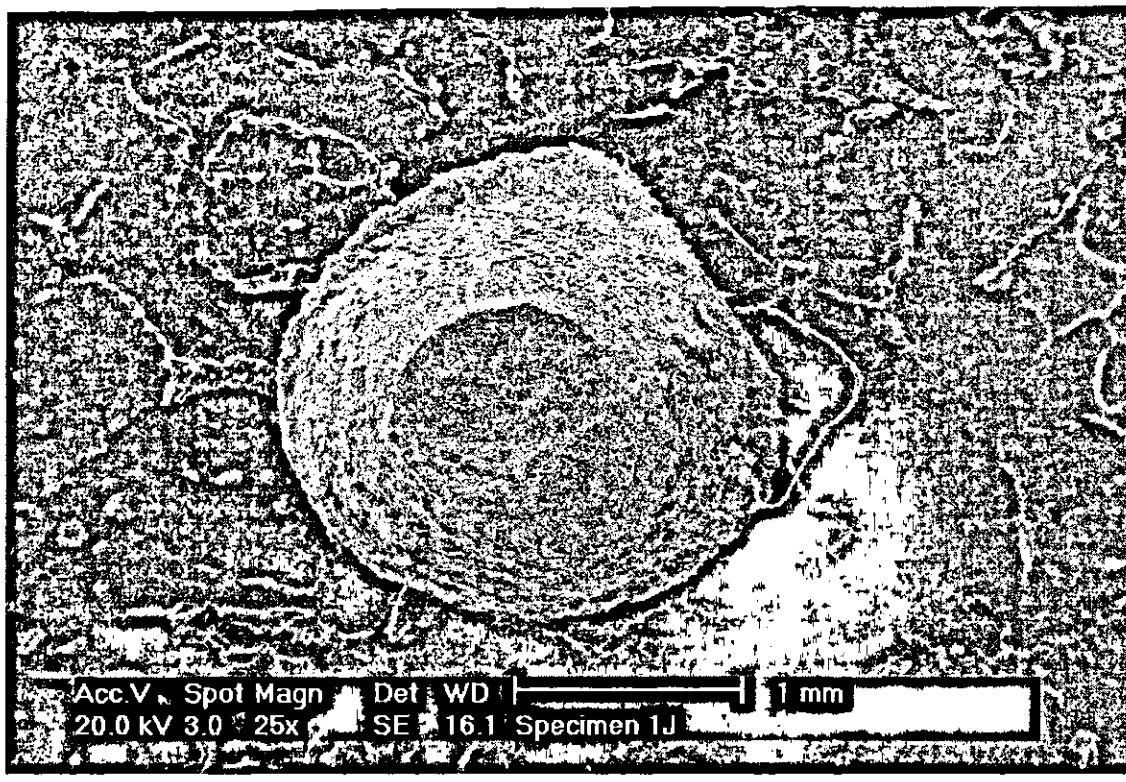

Figure 55: Fracture surface of Specimen 1J, 649°C, 681 hours.

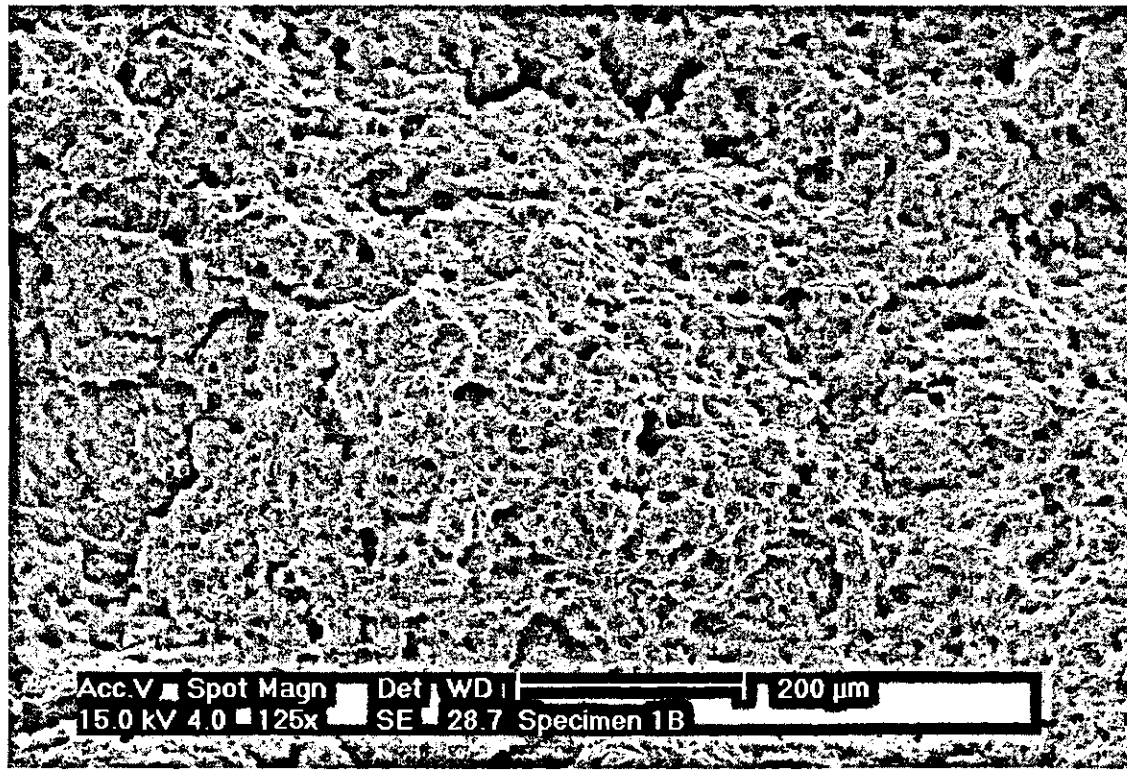

Figure 56: Ductile region of Specimen 1B.

Examining the ductile fracture regions at higher magnification reveals surface morphology very similar to that of A193, as can be seen in Figure 56. The ductile region of Specimen 1B is characterized by a cup and cone morphology, although the scale of the features is significantly larger than observed for A193.

4.3.1.3. ASTM A437 Grade B4B

The A437 steel has greater tensile strength and less ductility than the other two steels studied and this is apparent when the fracture surfaces of this steel are examined. As shown in Figure 57, the failure mode of this steel appears to be a combination of ductile and brittle fracture as observed for A193. However, the brittle zone is more dominant and the reduction in area is less pronounced.

There is little difference between the fracture surfaces of Specimen 4B and Specimen 4D, which were tested at 426.6 MPa and 370.6 MPa, respectively. Examining other fracture surfaces at higher temperatures as well, there is no evidence that the rupture ductility of this steel is affected by the applied stress. As observed earlier, the elongation at rupture results for this steel were similarly inconclusive.

The effect of test temperature, however, is very similar to that observed for A193 and A355, although perhaps not as severe. Figure 58 displays the fracture surfaces of two specimens tested at 593°C and 649°C, respectively, and the increase in the relative size of the ductile region, as well as the increase in overall area reduction, can be clearly seen.

The ductile regions of these fracture surfaces contain many voids, or worm holes, which which may be the result of cavity generation during the final stages of tertiary creep. Figure 59 contains images of the ductile regions of Specimen 4G and Specimen 4J displaying these worm holes. The image of Specimen 4J also contains a large flake-like particle observed on several of these fracture surfaces. EDX analysis was performed to try determine the composition of these particles as will be discussed in the next section.

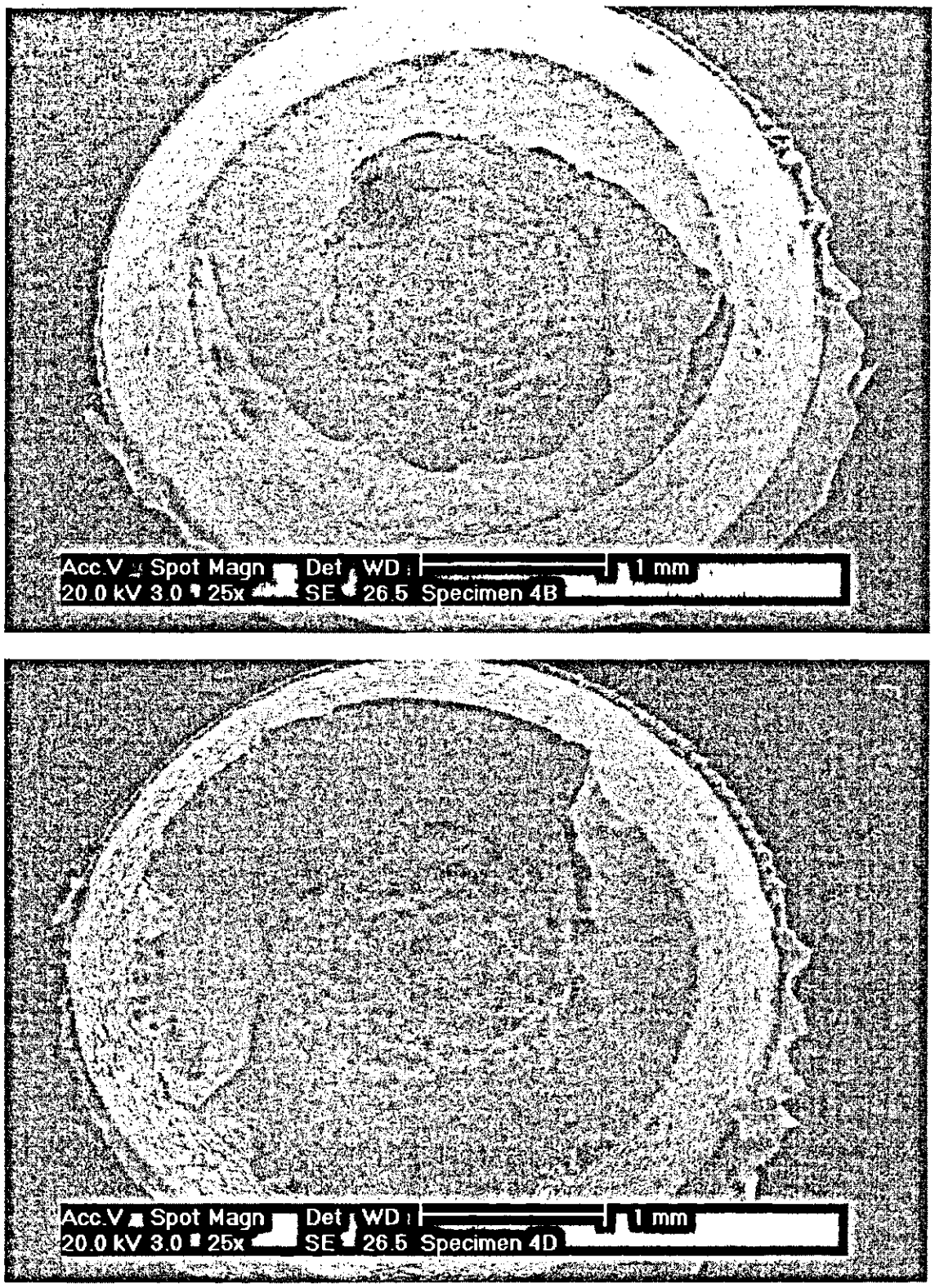

Figure 57: Fracture surface of a) Specimen 4B, 538°C, 18 hours, and b) Specimen 4D, 538°C, 798 hours.

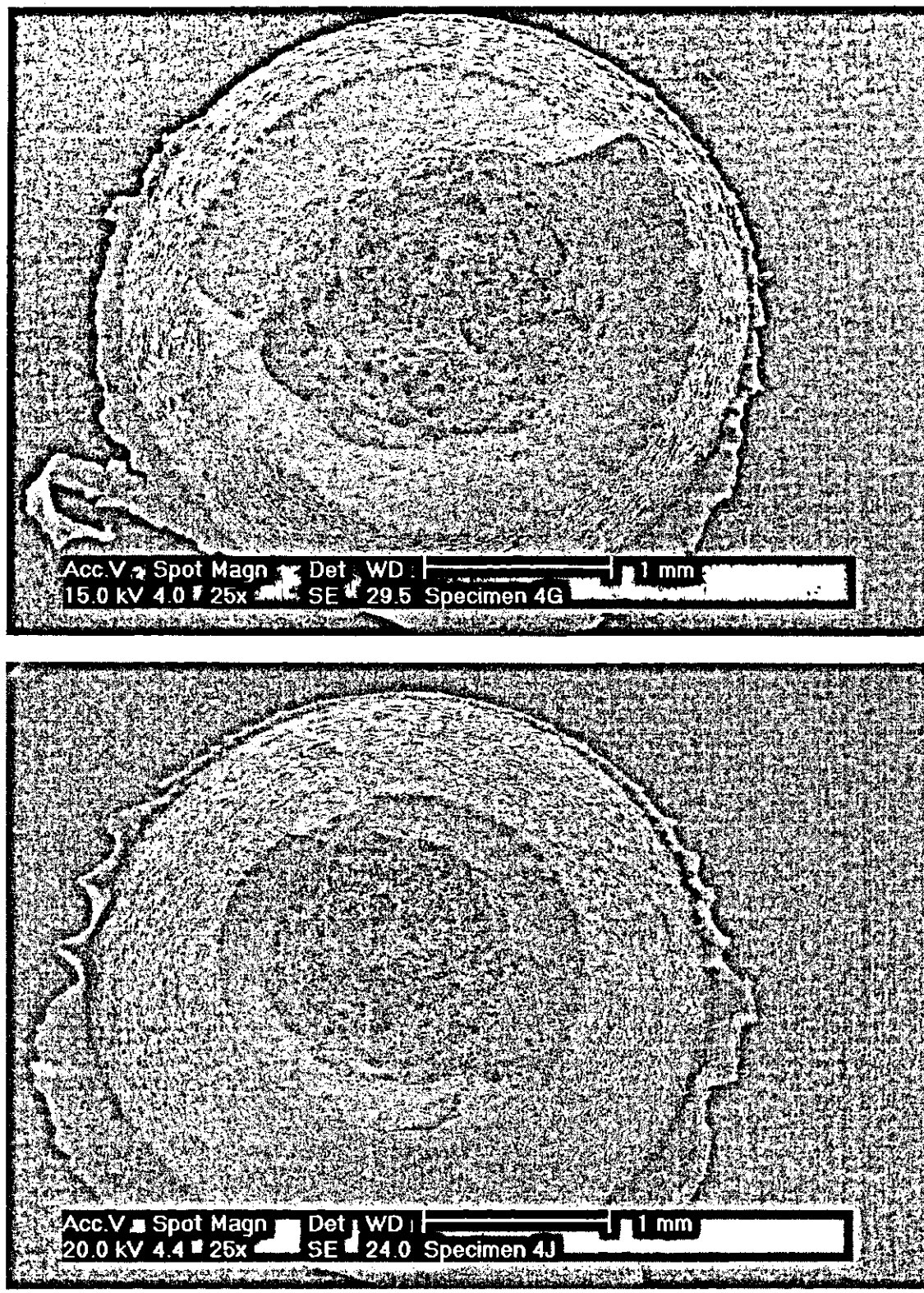

Figure 58: Fracture surface of a) Specimen 4G, 593°C, 1277 hours, and b) Specimen 4J, 649°C, 156 hours.

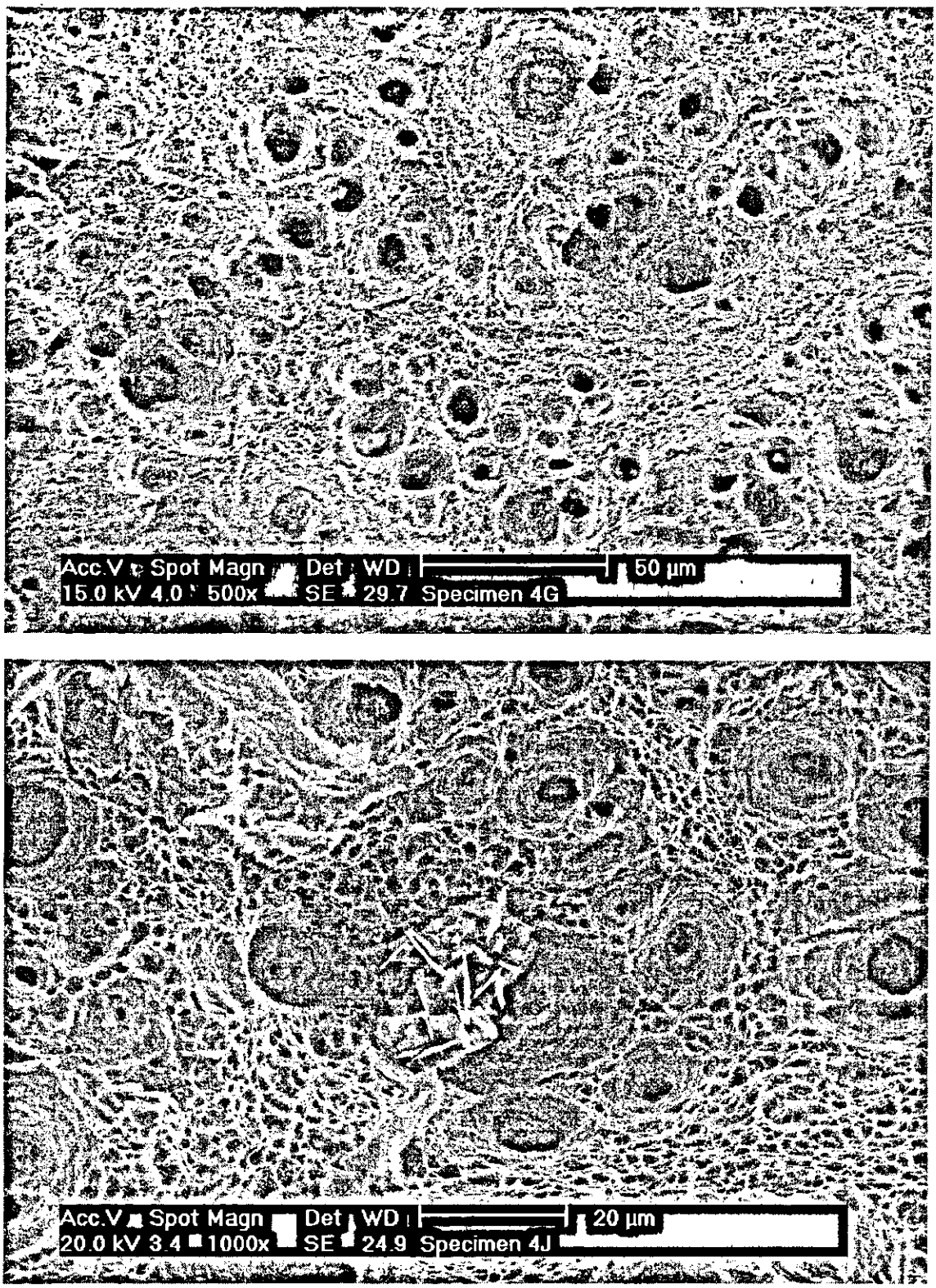

Figure 59: Ductile region of a) Specimen 4G, and b) Specimen 4J.

4.3.2. EDX Analysis

Polished surfaces of both ruptured specimen and barstock in the as-received condition, as well as fracture surfaces, were examined using a scanning electron microscope equipped with the ability to perform EDX analysis. This procedure makes it possible to identify phases and particles by determining their chemical composition.

4.3.2.1. ASTM A193 Grade B16

A slice of the original barstock of the A193 steel was polished to 6 μm and examined. A typical view of the sample is shown in Figure 60, and it reveals two large particles as well as a number of small white particles.

The large particles were examined using EDX analysis and were found to be inclusions of S-Mn and Al-O. The EDX spectrum obtained from each particle is shown in Figure 60 as well, along with the chemical composition suggested by the software package. All compositions are given in weight percent. A spectrum was also taken from the matrix area for comparison and the chemical composition was found to be representative of the nominal composition of this steel. It is important to note the high carbon content shown. This is not necessarily indicative of the actual carbon content in the material but is a result of contamination from the EDX analysis itself.

The small white particles were too small for analysis using a scanning electron microscope. They are possibly chromium carbides, which are among the largest and most common of the precipitate particles formed in these steels.

Various particles were also observed on the fracture surfaces and EDX analysis was used in an attempt to identify these particles. A large particle observed on the fracture surface of Specimen 3B was examined and its spectrum is shown in Figure 61. It appears to be a silicon carbide particle since the indicated carbon content is significantly greater than that shown in the matrix composition. EDX analysis at the point labelled Spectrum 2 in Figure 61(a) revealed mostly iron oxide, which is to be expected considering the large amounts of oxidation which occur at these temperatures.

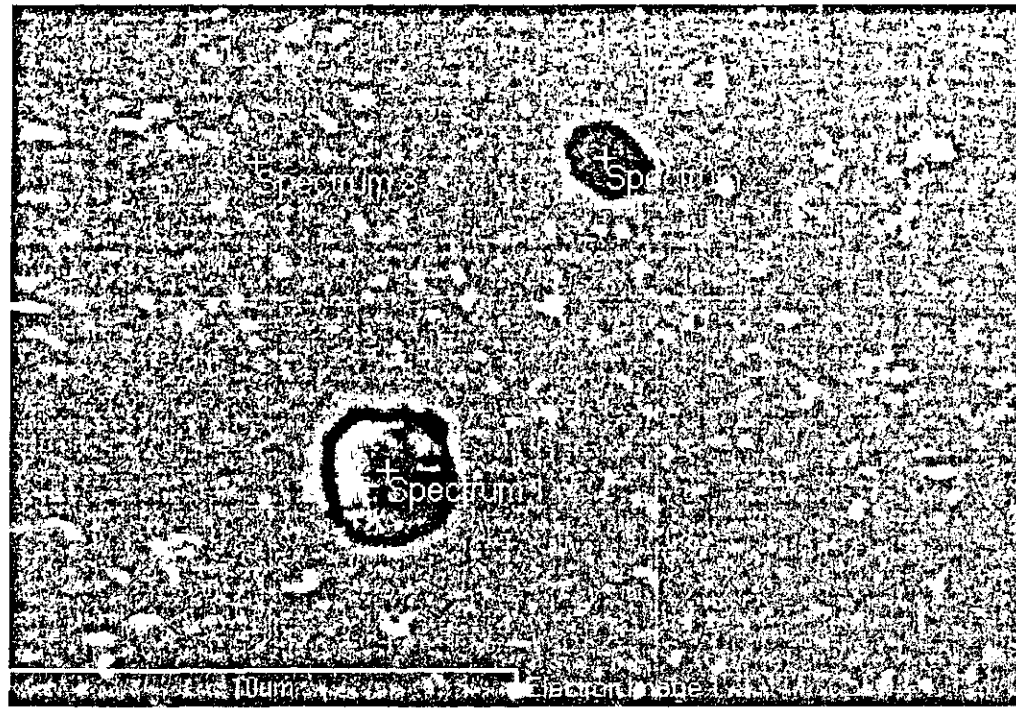

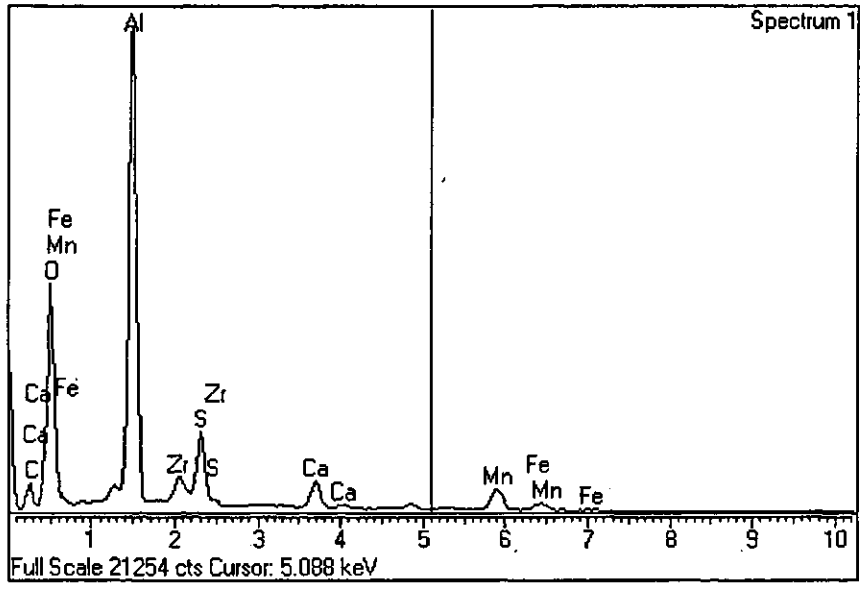

C	O	Al	S	Ca	Mn	Fe	Zr	Total
6.75	44.93	27.13	5.56	2.93	6.51	1.95	4.25	100.00

Figure 60: ASTM A193 Grade B16 barstock, as-received condition, a) SEM micrograph, b) Spectrum 1, Al-O particle.

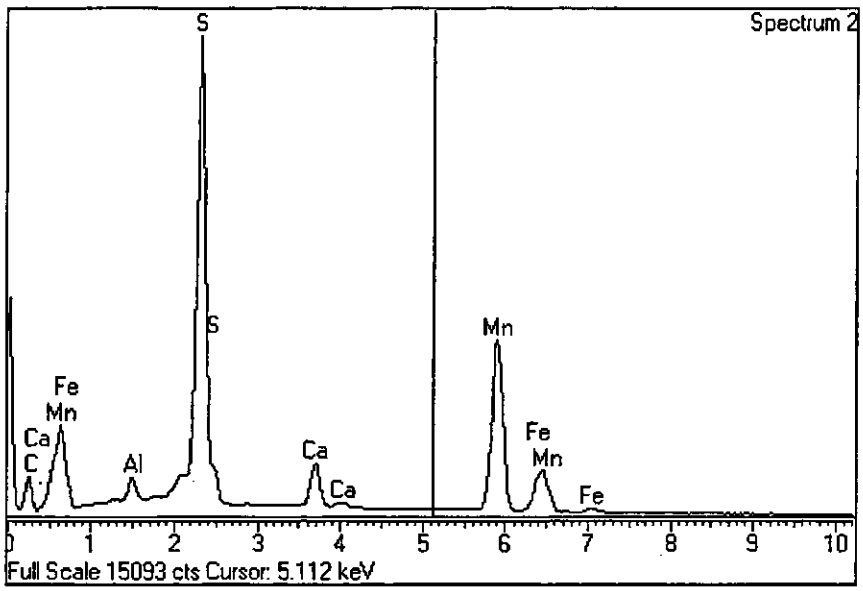

C	Al	S	Ca	Mn	Fe	Total
18.82	1.23	25.84	4.07	41.52	8.52	100.00

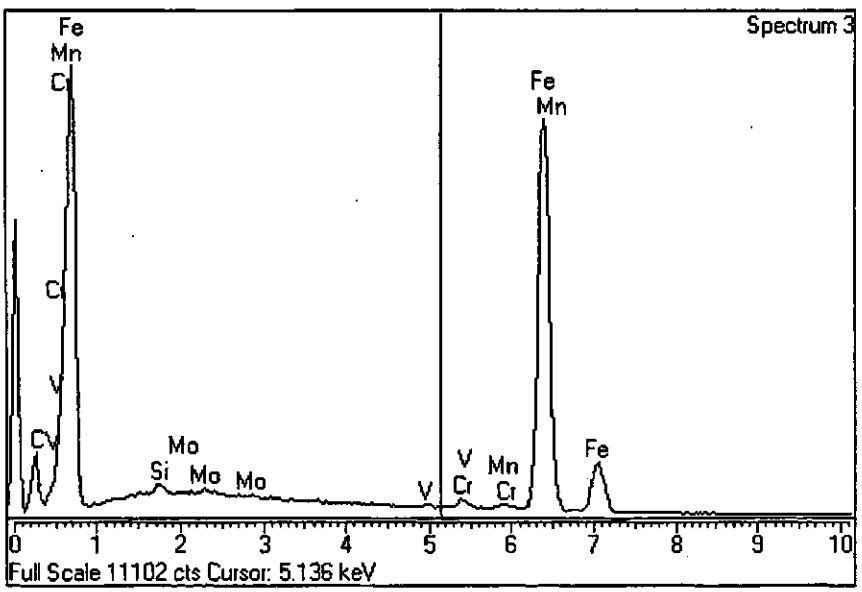

C	Si	V	Cr	Mn	Fe	Mo	Total
12.61	0.45	0.17	0.96	0.69	84.66	0.47	100.00

Figure 60: ASTM A193 Grade B16 barstock, as-received condition, c) Spectrum 2, S-Mn particle and d) Spectrum 3, matrix.

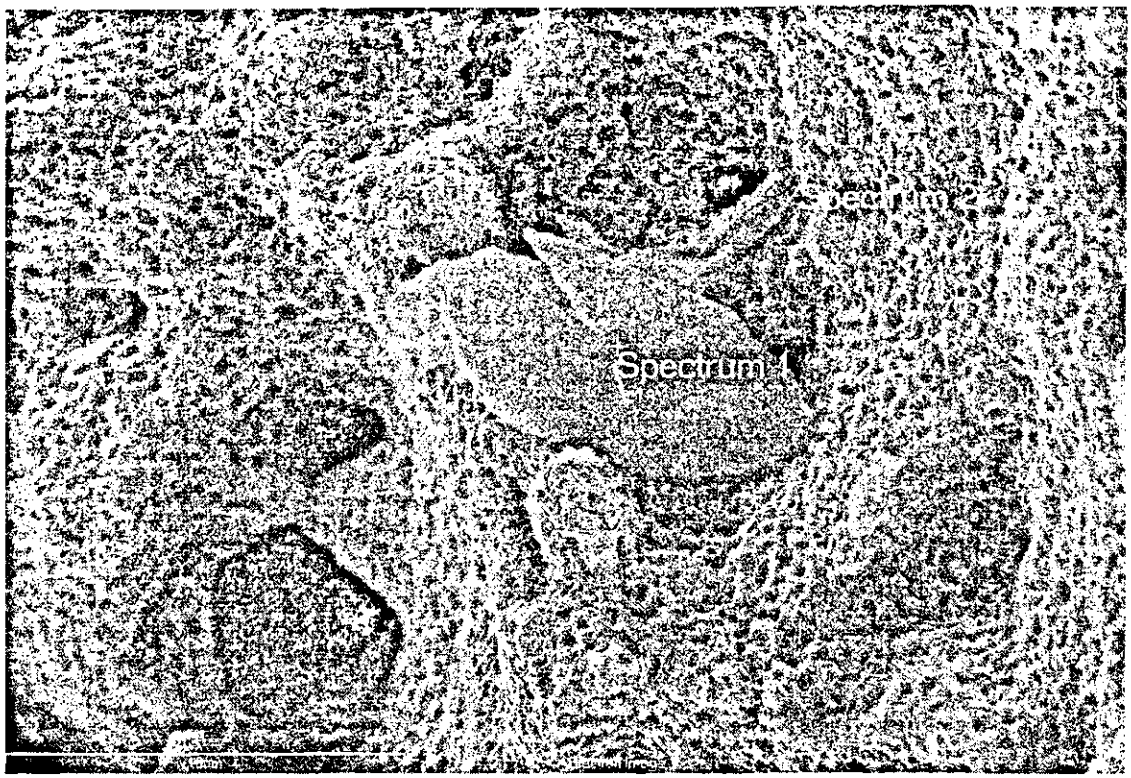

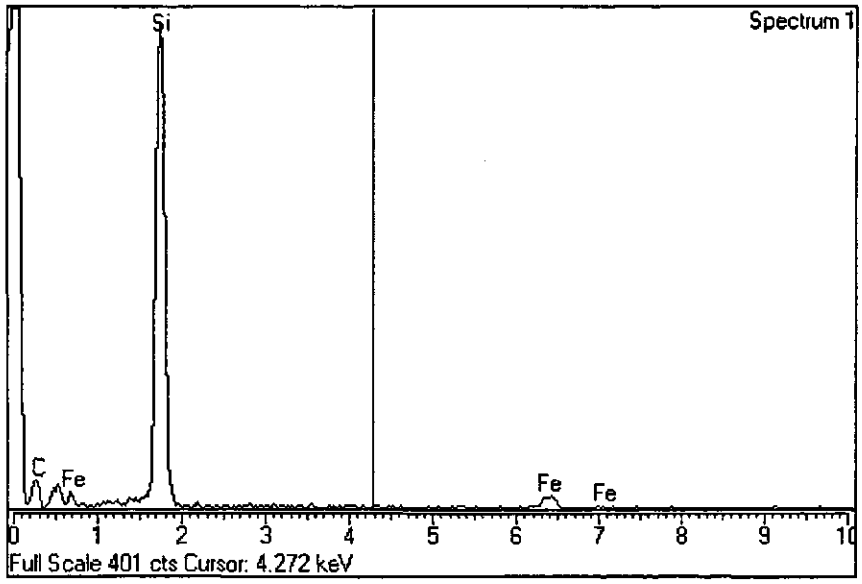

C	Si	Fe	Total
43.22	51.15	5.64	100.00

Figure 61: Fracture surface of Specimen 3B, 649°C, 53 hours, a) SEM micrograph, and b) Spectrum 1, Si-C particle.

4.3.2.2. ASTM A355 Class A

A polished slice of the barstock of A355 in the as-received condition was examined and, much like A193, large particles were observed as shown in Figure 62(a). EDX analysis revealed that these particles were inclusions of S-Mn, Si-C, and Al-N, as can be seen in Figure 62(c) and (d). Aluminum nitride particles were common throughout the microstructure and are no doubt a by-product of the significant aluminum content of this steel, as revealed in the EDX analysis of the matrix shown in Figure 62(b). It is interesting to note the absence of the small white particles seen in the A193 steel. The areas that are of a lighter shade were also examined and no difference in their composition was found compared to that of the darker areas.

Slices were also cut from ruptured specimens of A355 in both the longitudinal and transverse planes and examined. Again, inclusions of S-Mn were visible but very few Al-N particles were found.

4.3.2.3. ASTM A437 Grade B4B

The barstock of A437 in the as-received condition appeared very similar to that of A193. Large particles of Al-O and Si-C were found and the small white particles, which may be small chromium carbides, were also prominent. These features can be seen in Figure 63(a), which contains a particle which EDX analysis indicated contained mostly silicon and carbon.

The spectrum obtained from the matrix is displayed in Figure 63(b), and the chromium content should be noted. The weight percent of chromium was found to be around twelve, which is within the range required by the ASTM standard for this steel. EDX analysis performed at numerous locations returned similar results. It would appear that the EDX analysis confirms the result of the spectrochemical analysis.

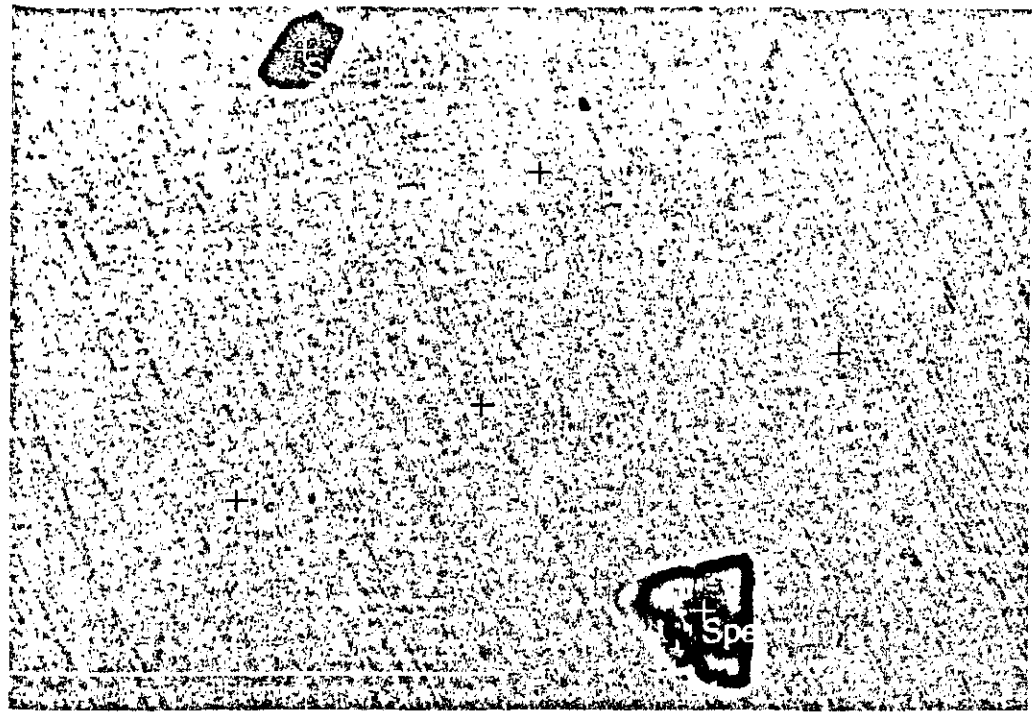

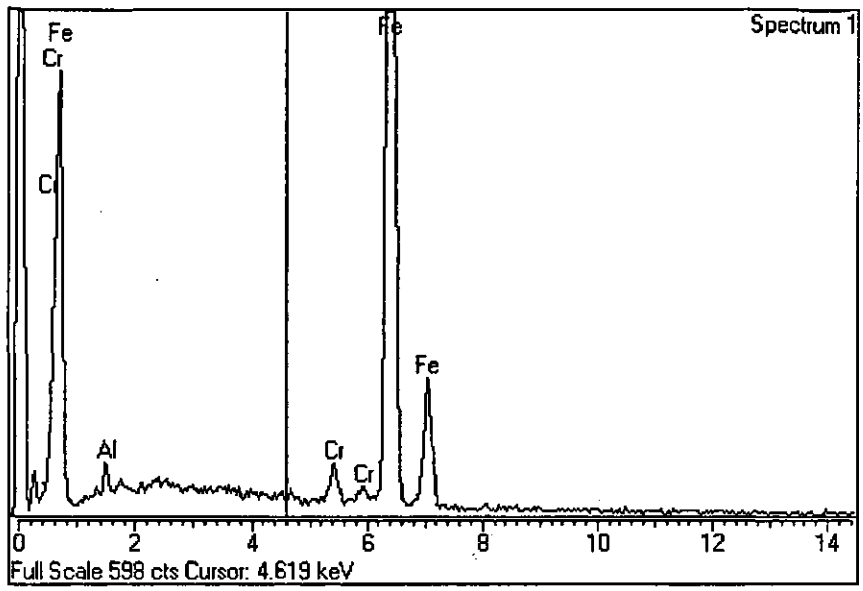

Al	Cr	Fe	Total
1.29	2.14	96.56	100.00

Figure 62: ASTM A355 Class A barstock, as-received condition, a) SEM micrograph, and b) Spectrum 1, matrix.

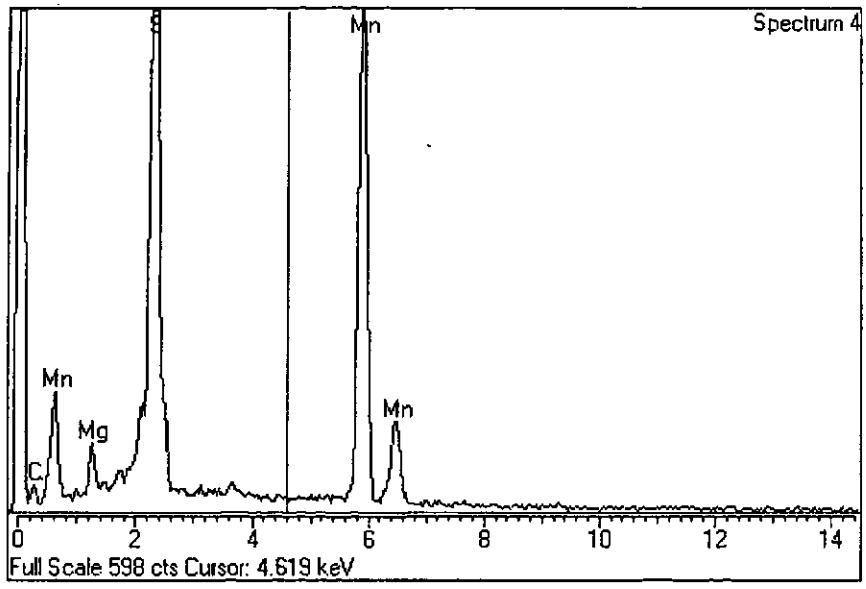

Mg	S	Mn	Total
2.40	36.48	61.12	100.00

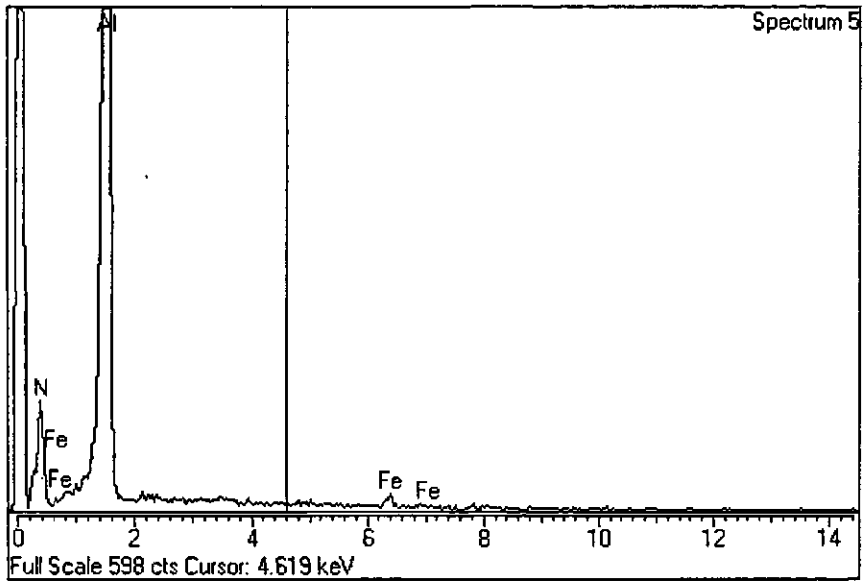

N	Al	Fe	Total
33.51	65.25	1.24	100.00

Figure 62: ASTM A355 Class A barstock, as-received condition, c) Spectrum 4, S-Mn particle, and d) Spectrum 5, Al-N particle.

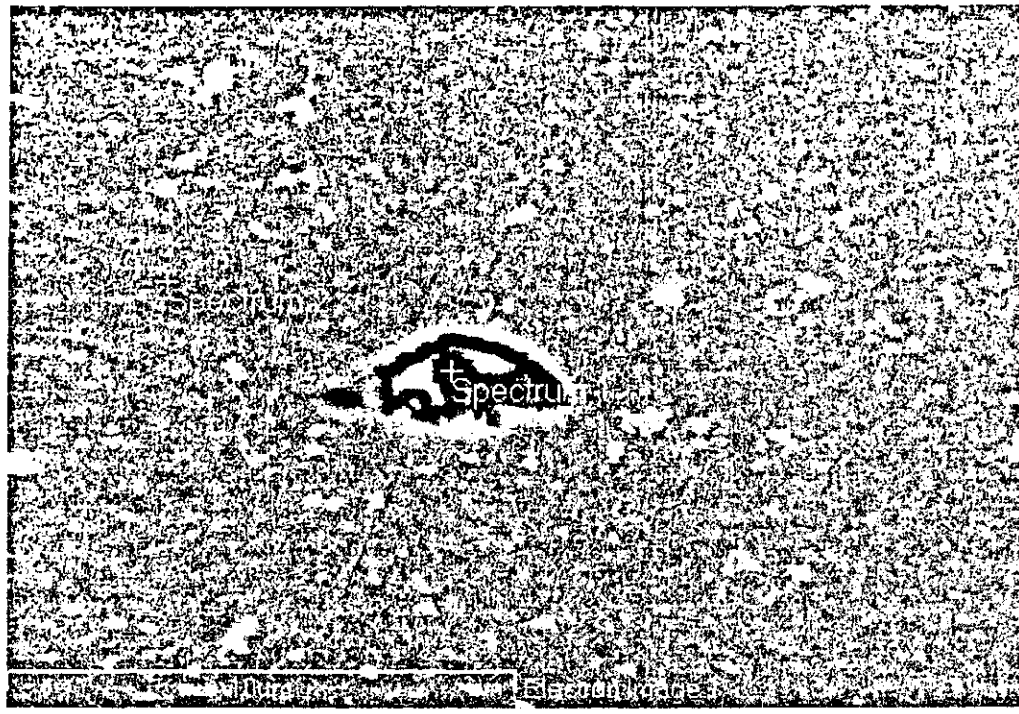

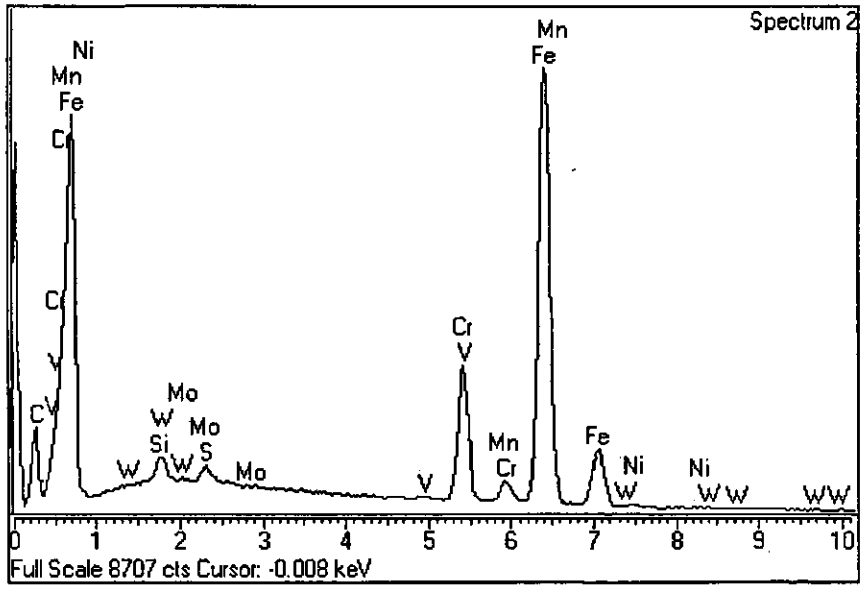

C	Si	V	Cr	Mn	Fe	Ni	W	Total
12.63	0.43	0.21	12.64	0.59	71.36	0.59	1.55	100.00

Figure 63: ASTM A437 Grade B4B barstock, as-received condition, a) SEM micrograph, Si-C particle, b) Spectrum 1, matrix.

Polished slices cut from ruptured specimens were prepared and examined as well. The large particles mentioned earlier were again visible. However, the smaller particles, which appeared bright white in the as-received material, were difficult to see in the ruptured specimens. The particles still appeared to be present but they were a much darker color and blended in with the matrix to the point that they were barely visible as can be seen in Figure 64. The large particle present appeared to be an Al-O particle when EDX analysis was performed.

A number of particles were observed on the fracture surfaces of ruptured A437 creep specimens as mentioned in the previous section. EDX analysis was used to try and identify the chemical composition of these particles.

Nodular type particles such as the one shown in Figure 65, many of which seem to be inside worm holes, were also observed and attempts were made to identify them. However, no substantial difference in their composition from the nominal composition of A437 could be discerned. It is difficult to obtain accurate compositions using EDX on rough surfaces due to the scatter of the electron beam. This is especially true for particles within holes.

The flake-type particles observed on several specimens were examined and found to contain large amounts of chromium and carbon. The particle found on Specimen 4J was representative of other similar particles and its spectrum is shown in Figure 66.

4.3.3. TEM Metallography

The use of a transmission electron microscope to examine the microstructure of ruptured creep specimens yielded some interesting results. However, the difficulty in obtaining good thin foil specimens somewhat limited the number of ruptured creep specimens that could be examined. The goal of performing transmission electron microscopy was to search for evidence which would denote the type of mechanism controlling the creep of these steels, and to examine the presence and composition of precipitate particles which are too fine for detection by a scanning electron microscope.

4.3.3.1. ASTM A193 Grade B16

Several good thin foil specimens were prepared from A193. The first thin foil specimen that had a reasonably sized thin area was created from Specimen 3F.

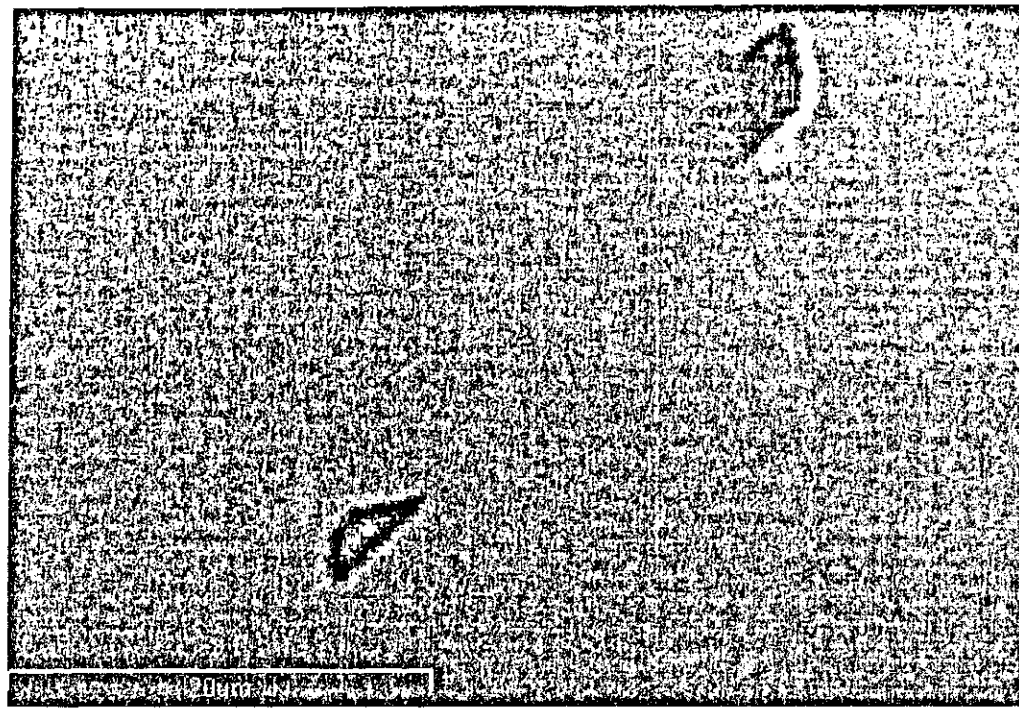

Figure 64: SEM micrograph of longitudinal section, Specimen 4J, 649°C, 156 hours.

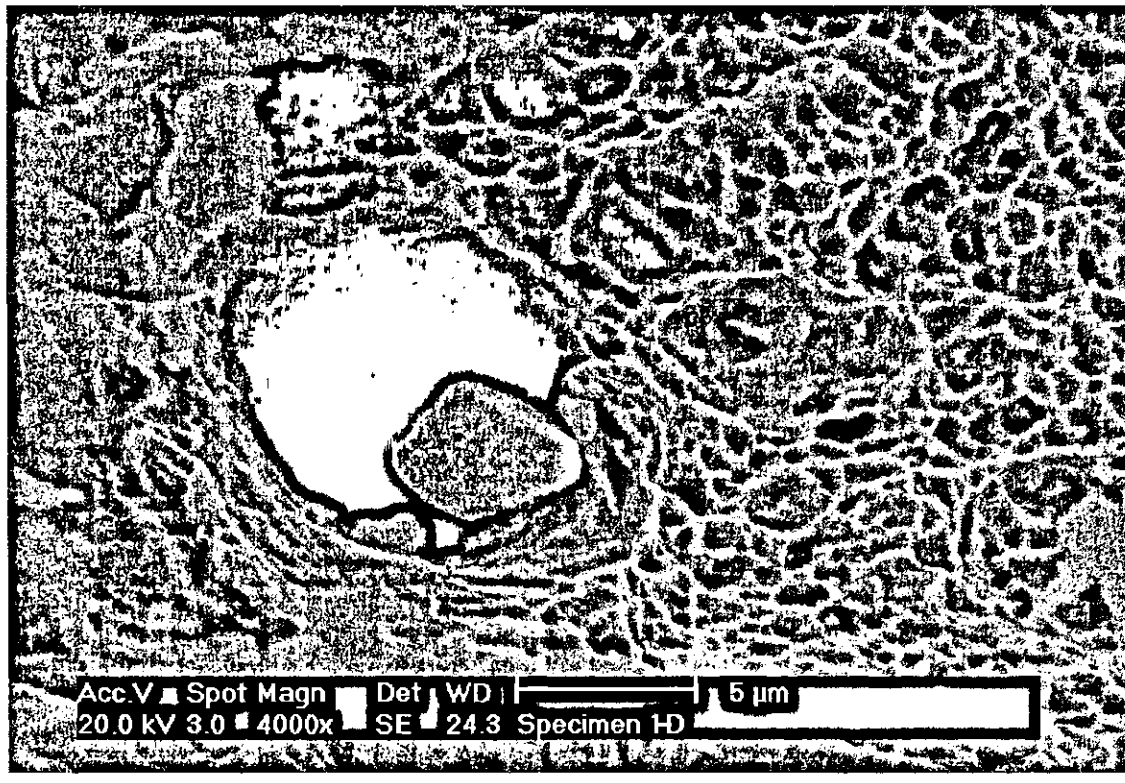

Figure 65: Particle on fracture surface of Specimen 4D, 538°C, 798 hours.

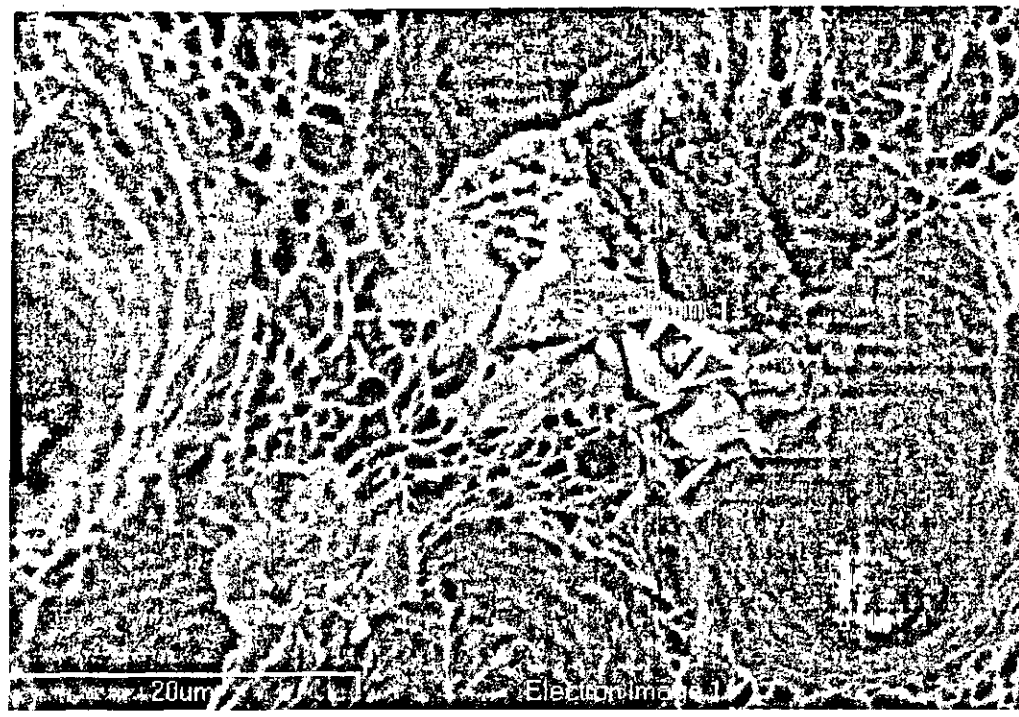

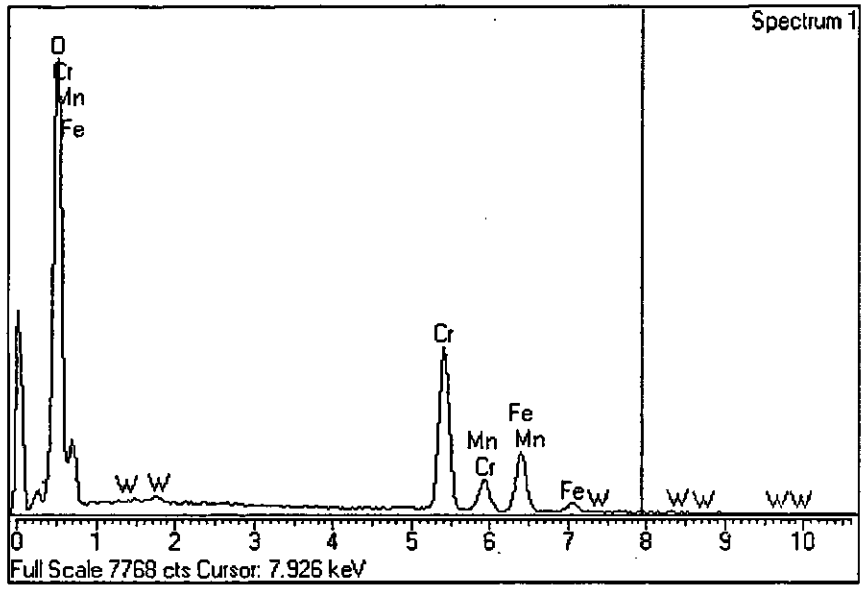

O	Cr	Mn	Fe	W	Total
39.04	36.54	3.44	20.05	0.92	100.00

Figure 66: Fracture surface of Specimen 4J, a) flake-type particle, and b) Spectrum 1.

The lighter colored region apparent near the center of Figure 67(a) was thought to be a void located at a triple point, where three grain boundaries meet. This type of feature is often evidence of grain boundary sliding, as a void must be created if one of the grain boundaries leading from the triple point is sliding. However, examining the developed photograph, the light area appears more likely to be another grain.

No other evidence of grain boundary sliding was observed in any of the specimens examined. Grain boundary sliding tends to be the controlling mechanism of creep at lower stresses. It is unlikely that grain boundary sliding would be a dominant factor at the relatively high stresses of the tests performed in this study.

The micrograph shown in Figure 67(b) displays a number of small dark particles with diameters on the order of 100 nm. These particles are possibly $M_{23}C_6$ particles of chromium and molybdenum.

An excellent thin foil specimen was also obtained from Specimen 3M. Examining this specimen at high magnification also revealed the presence of many small particles with diameters on the order of 100 nm as shown in Figure 68(a). EDX analysis was performed on the largest of these particles and the elements detected are listed in Table 12. Although the amount of iron detected is still very high, the chromium content is over 4% which is considerably greater than that present in the nominal composition of this steel. The only detector available was not able to measure the presence of carbon, so the fact that it is not listed does not mean that there is none present.

Table 12: EDX results for Specimen 3M.

Element	Fe	Mn	Si	Ni	Cr	V	Mo
	(wt%)	(wt%)	(wt%)	(wt%)	(wt%)	(wt%)	(wt%)
Spectrum 1	91.16	2.31	0.21	0.04	4.57	0.77	0.93
Spectrum 2	86.40	3.52	0.19	0.05	8.00	0.69	1.15

Figure 68(b), which is another micrograph taken from this specimen, displays a couple of larger particles. EDX analysis of the one in the bottom left corner revealed even greater chromium composition as shown in Table 12. The EDX detector is likely picking up iron from the area surrounding the particles but it appears that the particles contain significant amounts of chromium.

Figure 67: TEM micrographs of Specimen 3F, 538°C, 321 hours, a) grain boundary triple point, and b) small precipitate particles.

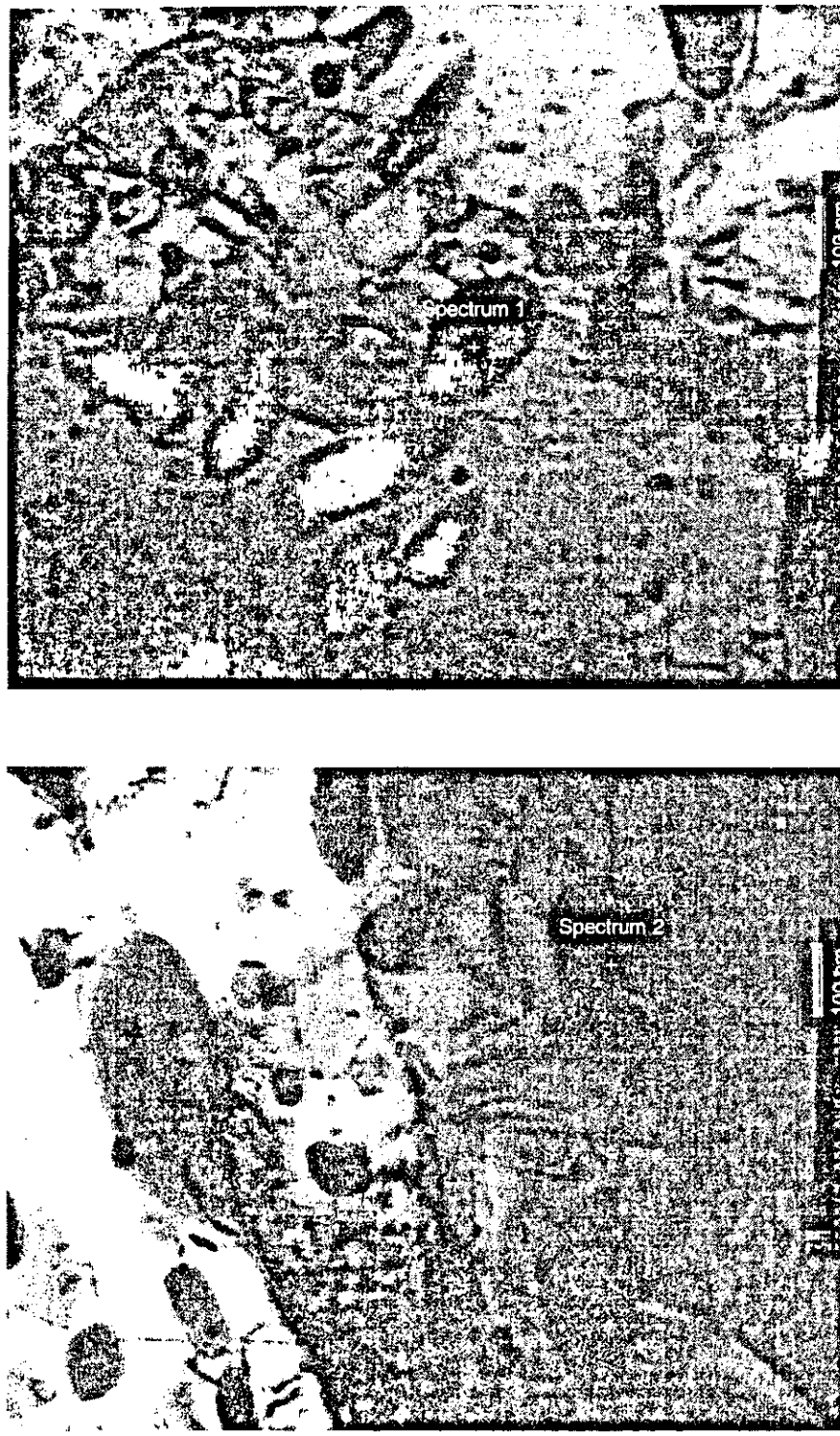

Figure 68: TEM micrographs of Specimen 3M, 538°C, 1726 hours, a) Spectrum 1, and b) Spectrum 2.

Even smaller particles, which are lighter in color and have diameters on the order of 25 nm, can be seen in the micrographs for both Specimen 3F and Specimen 3M. Although too small to be analysed using EDX, it is possible that they are MX type particles, most likely vanadium nitride.

4.3.3.2. ASTM A355 Class A

Only one thin foil specimen was obtained for A355 that contained a good thin area for TEM examination. The micrographs obtained from Specimen 1J reveal particles considerably larger than those observed for A193 with diameters in the order of 500 nm. EDX analysis was performed on the large particles in the center of the two micrographs shown in Figure 69. The results for two particles are listed in Table 13. For both particles, a significant amount of chromium and molybdenum was detected suggesting that these are $M_{23}C_6$ particles.

Table 13: EDX Results for Specimen 1J.

Element	Fe	Mn	Si	Cr	V	Mo
	(wt%)	(wt%)	(wt%)	(wt%)	(wt%)	(wt%)
Spectrum 1	87.63	2.63	0.00	7.11	1.06	1.57
Spectrum 2	86.00	3.08	0.01	9.02	0.77	1.13

The micrograph shown in Figure 69(a) is not particularly clear but what appear to be dislocations can be seen spreading out from the edges of the particle. The controlling mechanism of creep in the stress-temperature regime in which these tests are located is most likely dislocation creep. These dislocations are pinned by the precipitate particles that have been observed, which provides a strengthening effect. However, the size of these particles increases during creep and if they become overly large, they are not as effective at blocking dislocations.

The particles observed in Specimen 1J were considerably larger than those seen in the specimens of A193. However, Specimen 1J was tested at 649°C while Specimen 3F and 3M were only tested at 538°C and temperature has a large effect on the rate of grain growth.

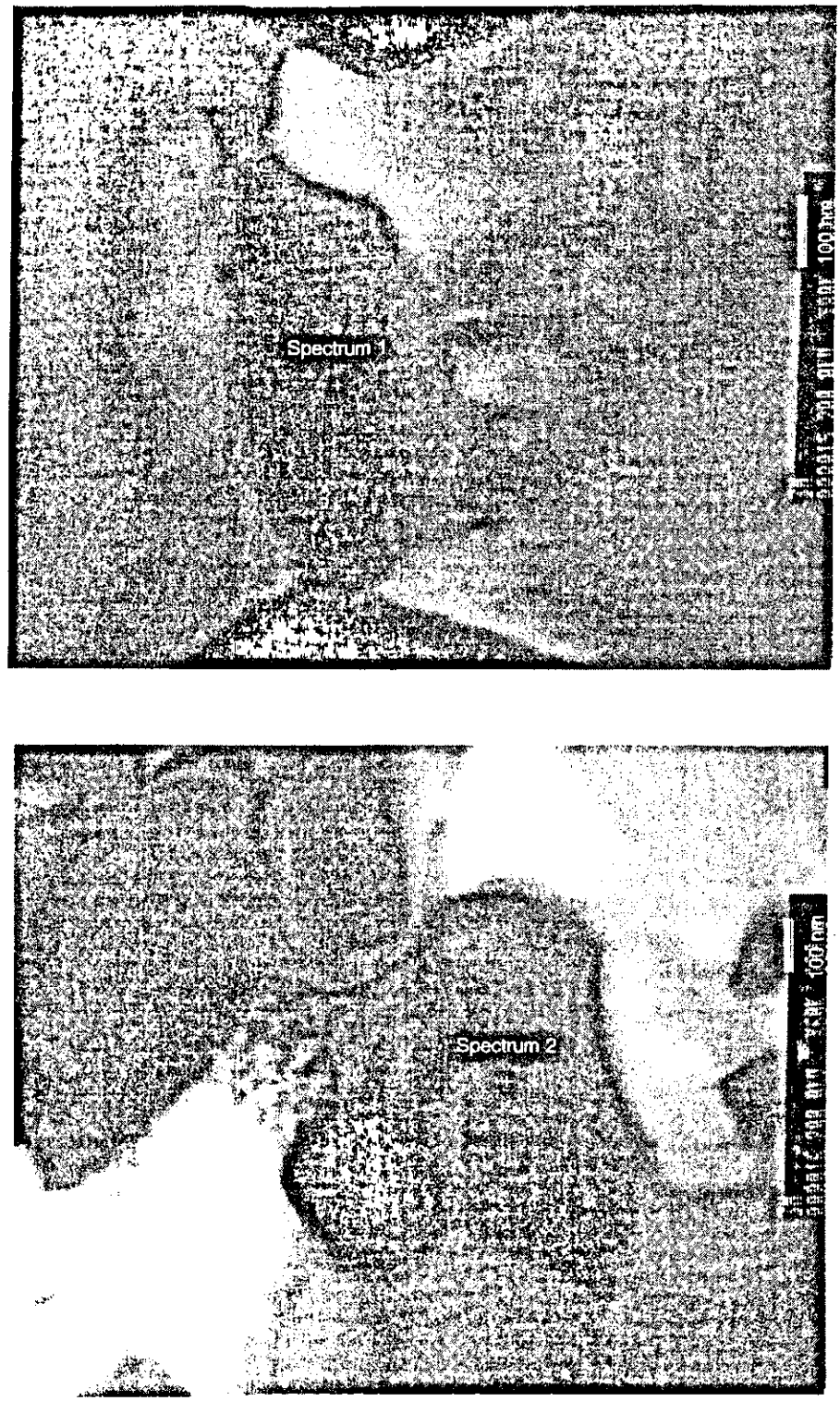

Figure 69: TEM micrographs of Specimen 1J, 649°C, 681 hours, a) Spectrum 1, and b) Spectrum 2.

4.3.3.3. ASTM A437 Grade B4B

The only A437 specimen from which a good thin foil specimen was obtained was Specimen 5F, which had a relatively long time to rupture of over 2000 hours at 649°C. Understandably then, this specimen should show considerably more ageing effects than the other specimens observed earlier.

As can be seen in Figure 70, however, the particles observed are of approximately the same size as those observed in Specimen 1J. EDX analysis was performed on the particles in Figure 70(a) and the results are listed in Table 14. It is difficult to be sure of the exact identity of the particles but again the amount of chromium detected was significantly more than that of the nominal composition of this steel.

The microstructure of this steel should be more resistant to ageing than that of A355 due to the precipitation of finer and more stable vanadium nitride particles. This thin foil specimen did not provide good enough results to be able to see if smaller particles were present.

Table 14: EDX results for Specimen 5F.

Element	Fe	Mn	Si	Ni	Cr	V	Mo	W
	(wt%)	(wt%)	(wt%)	(wt%)	(wt%)	(wt%)	(wt%)	(wt%)
Spectrum 1	72.37	1.13	0.79	0.79	21.25	0.24	1.71	1.42

A large number of dislocations can be seen spreading out from the large particle in Figure 70(b). Again, this particle is likely pinning these dislocations and thereby blocking their movement through the grain, thus improving the resistance of the steel to creep.

4.4. Application to Bolting

The purpose for testing these steels is to obtain a better understanding of their creep behaviour in order to determine whether they are suitable for use in steam turbine applications. ASTM Standards A193 and A437 are written as guidelines for steels used for bolting purposes, and that is the application in which the steels tested will be used. A discussion of the test results as they apply to bolting will thus be put forward in the following section.

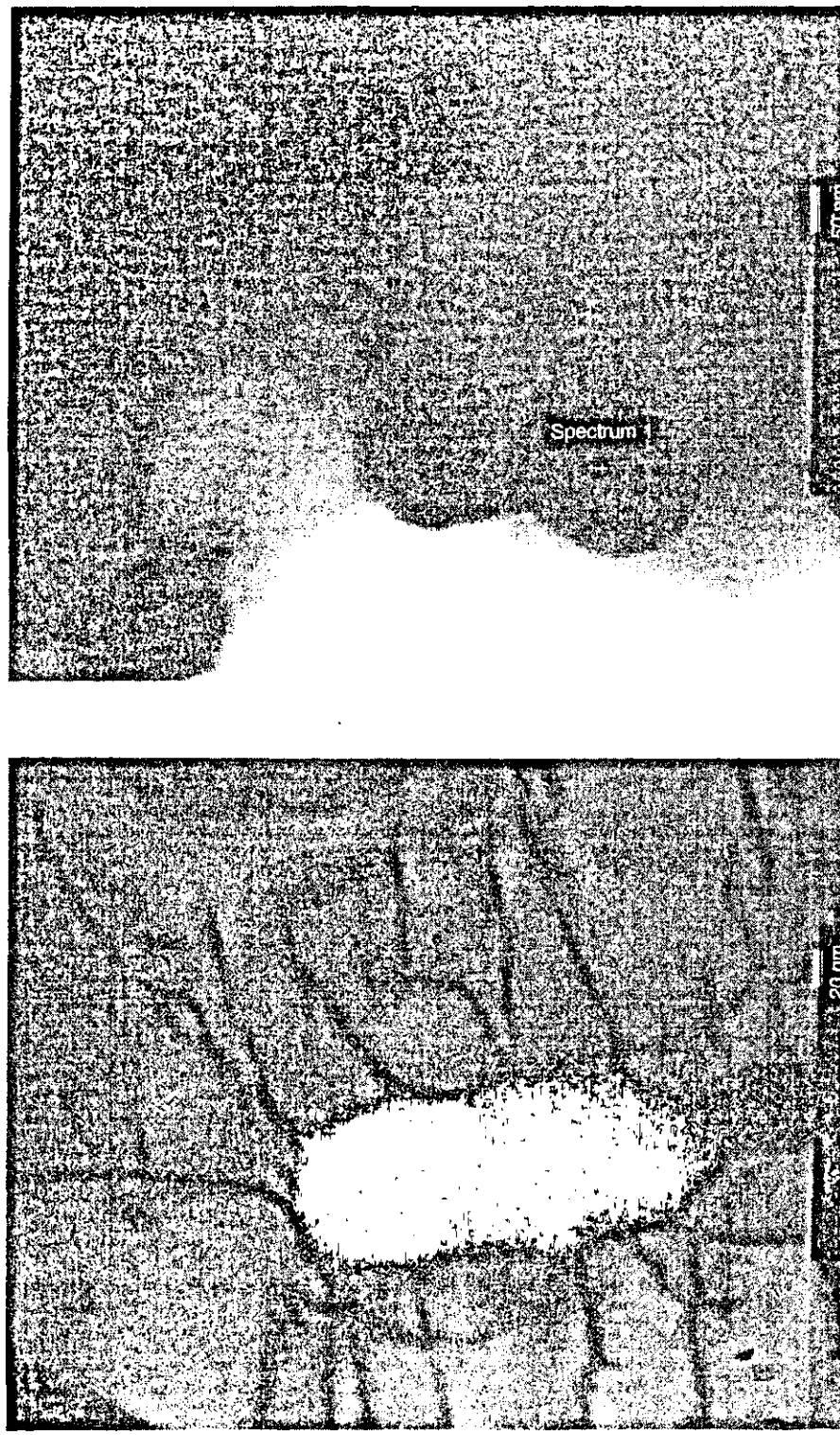

Figure 70: TEM micrographs of Specimen 5F, 649°C, 2128 hours, a) Spectrum 1, and b) large particle pinning dislocations.

4.4.1. Stress in Service

Bolting steels are utilized in many locations throughout a steam turbine to hold various casings and piping together and thus their performance is of utmost importance. Many parts of these steam turbines are subjected to both high pressures and high temperatures. The bolting must withstand these forces through many years of service.

Supersaturated steam at high pressure passes through these turbines increasing the forces on the bolting. If a leak were to occur it could create a serious safety hazard as supersaturated steam is not visible. As well, the main steam temperature of these turbines is around 538°C. Since there is no thermal insulating barrier between the casing and the bolts, it is reasonable to assume that the bolts are very close to the main steam temperature during service. At these high temperatures, the effects of creep are very important.

Knowing the actual stress in bolts under service conditions in a steam turbine would be extremely useful for comparison with creep test stresses. Bolts are tightened initially to a prescribed torque so that there is an initial tension in the bolts. When the steam turbine is in operation, the high-pressure steam creates additional stress.

The stress present in bolts used to clamp the head on a valve in a steam turbine was estimated to provide a typical bolt stress under operating conditions. The steel used in this application is a martensitic stainless steel equivalent to ASTM A437 Grade B4B.

The stresses were estimated as follows:

Initial stress after tightening	153 MPa
Operating stress	161 MPa

A complete description of the calculations performed can be found in Appendix C.

A stress of 161 MPa falls well below the applied stress of the A437 tests performed at 538°C. Using the Larson-Miller master curve created from the test data for this steel, a stress of 161 MPa should result in a rupture life of around 2.8 million hours if subjected to a temperature of 538°C. However, using the Larson-Miller master curve for Type 422 stainless steel predicts a rupture life of approximately 300 000 hours. These bolts are in service for well over 100 000 hours. It is likely that the actual rupture time of this material at a stress of 161 Mpa would lie between the two estimates.

4.4.2. Post-Rupture Hardness Test Results

As mentioned earlier, bolts used in steam turbine applications are tightened initially to a prescribed torque. The effect of creep at high temperatures does not result in elongation of the bolts but rather in stress relaxation. During service at high temperatures, the stress in the bolts will decrease gradually until they can no longer sustain enough force to stop steam leakage from occurring. As a result, the steam turbines are overhauled every 40 000 to 60 000 hours and the bolts are retightened.

The hardness of each bolt can be tested to give an estimation of its remaining creep strength. As stress relaxation of the bolting occurs, the hardness of the bolting material decreases. If the hardness of a bolt is below a certain value at the time of overhaul, the bolt will be replaced.

Hardness tests were performed on a number of ruptured creep specimens and the results are tabulated in Table 15. As much as possible specimens with approximately the same rupture times were chosen for comparison. In general, the hardness is greatest in the as-received condition and there is a continual decrease as the temperature is increased.

Table 15: Hardness of ruptured creep specimens.

Material	Specimen	Temperature (°C)	Rupture Time (hours)	Hardness	
				VHN	HB
A193	As Received			294	279
	3E	538	788	285	270
	3G	593	518	264	251
	3S	649	627	187	
A355	As Received			281	266
	1D	538	1554	254	242
	2H	593	1431	201	
	1J	649	681	202	
A437	As Received			314	298
	4K	538	1617	308	292
	4H	593	2316	286	271
	5C	649	2128	261	248

When performing overhauls on bolted casings using a martensitic stainless steel equivalent to A437, Hitachi Canadian Industries recommends replacement of any bolts that have a hardness value of less than 280 HB. As can be seen in Table 15, the

hardness of the ruptured A437 specimen tested at 538°C was still above this value even at rupture.

4.4.3. Creep Mechanisms

An understanding of the mechanisms that control the creep behaviour of these steels is of great importance in determining their suitability for any given application. However, this is perhaps the most difficult part of studying the creep characteristics of materials.

One of the biggest challenges is the estimation of long term creep properties from short term creep testing. Due to the very nature of these steels, this is extremely difficult for several reasons.

Firstly, as noted many times, the microstructure of these steels is continually evolving during creep. The greater creep resistance of these steels compared to a low carbon steel is a result of the addition of various elements such as chromium and vanadium. These elements provide both solid solution strengthening and precipitation strengthening. However, the contribution of these elements to creep strength changes over time as the microstructure changes. Different precipitate phases are formed at various stages during creep and all precipitate particles tend to grow larger under exposure to high temperatures. As different phases are formed, some elements which provide solid solution strengthening are dissolved in precipitates, thus reducing their effectiveness. Prediction of the long term creep life of these steels requires prediction of the precipitation and evolution of the many phases present in these steels.

In general, the more stable the precipitates, the greater the creep strength of these steels. Examining the shape of the creep curves of these three steels, the relative stability of the microstructure of these steels can be analysed. The creep curves of A193 and A355 have a very prominent tertiary stage with little or no steady state creep. This is likely due to the continual growth of grains and precipitate particles, whereby the creep strength of these steels is gradually diminished. The creep curves of A437 display a much more prominent steady state region, possibly indicating a more stable microstructure. The A437 steel has a martensitic microstructure which in itself is much more resistant to grain growth than a ferritic microstructure.

Another problem associated with estimating long term creep life is the possibility of a change in the controlling mechanism at low stresses. Creep at higher stresses tends to be dominated by dislocation creep, which is the movement of dislocations through the

material by a diffusion activated process. High temperatures make the movement of dislocations much easier. This is likely the controlling mechanism of creep in the stress-temperature regime into which the creep tests performed in this study fall. However, at lower stresses, creep is more often the result of grain boundary sliding and the mode of failure is more intergranular in nature. As a result, it is very possible that the mechanism controlling creep under the low stresses seen in service conditions is different from the mechanism controlling creep during high stress short time creep rupture tests. Many studies have observed a change in the controlling mechanism for these steels as the stress is decreased.

The steady state, or minimum, strain rate plotted as a function of stress often follows a power law relationship. A change in the value of the exponent of the power law often indicates a change in the controlling mechanism. No change was evident for A193 and A355. However, it appears that there may be a change indicated for A437 at a value of approximately 380 MPa. More data points need to be obtained to verify this trend.

The point is that it is very difficult to predict long term creep life without performing long term creep tests. Time-temperature parameters and other life prediction methods which are derived from short term test data are of little use for predicting long term behaviour if the controlling mechanism of creep has changed.

Another factor that has a great effect on creep life and is very complex in itself is oxidation. Oxidation is especially important for the low alloy steels, A193 and A355, and further complicates the extrapolation of short term creep data to actual service conditions.

5. CONCLUSIONS AND RECOMMENDATIONS

5.1. Conclusions

The creep behaviour of three alloy steels was examined in this study to determine their suitability for steam turbine applications. The high temperature creep characteristics of these three steels, as well as the mechanisms controlling their creep behaviour, were therefore of interest.

The evaluation of these steels was carried out using high temperature creep tests, hardness and tensile testing, and scanning and transmission electron microscopy. By examining the results discussed in the previous chapter, the following conclusions can be made.

1) The creep strength of the tempered martensitic stainless steel, A437, is considerably greater than that of the two low alloy steels, which is to be expected. Its tensile strength at room temperature is also greater than that of the other two steels.

2) The repeatability of the stress rupture tests appears to be relatively good. The variance in time to rupture for tests performed at the same temperature and applied stress was never more than 30% and was as low as 3%.

3) The shape of the creep curve for each steel is well established. The creep curves of the two low alloy steels, A193 and A355, are similar and contain a very prominent tertiary region and little or no steady state secondary region. On the other hand, the tempered martensitic stainless steel, A437, displays a more typical creep curve, with three well defined stages, including a prominent steady state phase. The general shape of the creep curve for each steel does not appear to be a function of stress or temperature.

4) The stress rupture data for the two low alloy steels does not fit well with the Larson-Miller time-temperature parameter. However, the data does meet the requirements necessary for using the Goldhoff-Sherby parameter. On the other

hand, the data for the A437 stainless steel did fit well with the Larson-Miller parameter.

5) The elongation at rupture appears to be a function of temperature for A193 and A355. The amount of elongation tends to increase as the temperature is increased. It was interesting to note that the increase is not uniform. The increase in elongation between specimens tested at 538°C and those tested at 593°C was fairly small. However, the elongation at rupture of those specimens tested at 649°C often showed a very large increase compared to those tested at 593°C. The dramatic increase in elongation was also accompanied by a corresponding increase in oxidation.

6) All three steels display large variations in rupture ductility as observed by examining the fracture surfaces of ruptured specimens. The rupture ductility appears to be a function of temperature. As the temperature was increased, the rupture ductility of the creep specimens almost invariably appeared to increase as measured by the overall reduction in area and the relative sizes of the ductile and brittle failure zones, observed on the fracture surface.

7) There were insufficient data to make any definite conclusions as to whether the rupture ductility of these steels is a function of applied stress.

8) Oxidation was a significant factor for the two low alloy steels, A193 and A355, at all three test temperatures. However, those tests performed at 649°C displayed significantly greater amounts of oxidation, which appeared to be accompanied by a significant increase in ductility as evidenced by elongation at rupture. As expected, the tempered martensitic stainless steel, A437, demonstrated significantly better oxidation resistance than the two low alloy steels.

9) Many particles were observable in the microstructure of these steels, which are most likely carbide and nitride particles. The largest of these particles were examined using EDX analysis and large amounts of chromium were found to be present, suggesting that they are likely chromium carbides. Many smaller particles were also observable which are likely vanadium nitrides, although they were too small for reliable EDX analysis.

10) No evidence of grain boundary sliding was observed, although the number of specimens examined was small. It is unlikely that grain boundary sliding would be a dominant mechanism of creep under the conditions of the tests performed.

11) Hardness decreases during creep. Hardness tests performed on ruptured creep specimens revealed a loss of strength relative to the test temperature. The A193 and A355 steels showed a significantly greater decrease in hardness than the A437 steel. This is further demonstration of the increased creep strength of this steel.

12) The creep behaviour of these steels under service conditions is not easily characterized using data obtained from short term creep tests performed at much higher stresses than would be seen in service.

5.2. Recommendations

A number of recommendations for areas of further study are as follows:

1) The creep testing program should continue with longer term tests. Stress rupture tests should be performed on the five machines not equipped with extensometers to continue to add data points to the master curves. Creep tensile tests should be performed on the five creep frames equipped with extensometers and allowed to run until they are into the secondary stage at which point they should be terminated.

2) Additional lots of each steel should be purchased and tested to assess material repeatibility.

3) A more detailed study of the microstructural evolution of these steels during creep should be undertaken using transmission electron microscopy. Examination of creep specimens at different stages of creep will yield useful information on the growth of grains and precipitate particles.

4) An attempt should be made to determine if and when changes occur in the controlling mechanism of creep as the amount of applied stress is decreased.

5) Etched surfaces of as-received and creep tested specimens should be examined using both optical and scanning electron microscopes to further understanding of the basic microstructure of these steels.

6) Many numerical models have been developed to describe the creep behaviour of materials. These numerical methods should be researched in greater depth to determine if any apply to these steels. Numerical modeling of the precipitation and growth of various phases could also be examined.

7) Many new steel alloys with improved creep resistance have been developed in the last two decades. More detailed research into the properties and creep behaviour of these new steels should be undertaken to assess their suitability for bolting applications.

There are many details of the creep behaviour of these steels that are yet unknown. Continuation of this project would add to the understanding of the complex phenomenon of creep and aid in the application of these steels in service.

6. REFERENCES

[1] P. Greenfield, *Creep of Metals at High Temperatures*, Mills & Boon Limited, London, 1972.

[2] M.G. Gemmill, The Technology and Properties of Ferrous Alloys for High Temperature Use, George Newnes Limited, London, 1966.

[3] N.D. Batsoulos, "Review mathematical description of the mechanical behaviour of metallic materials under creep conditions", *Journal of Material Science*, Volume 32: Number 10, 15 May 1997, p.2511.

[4] S. Ahila, P. Prasad, S. Ramakrishna Iyer, and V.M. Radhakrishnan, "Carbide precipitation in 2.25Cr-1Mo steel and its weldments during creep testing", *Materials Letters*, Volume 20, July 1994, p.107.

[5] S. Chaudhuri and R.N. Ghosh, "Some aspects of mechanisms and modelling of creep behaviour of 2.25Cr-1Mo steel", *ISIJ International*, Volume 38: Number 8, 1998, p.881.

[6] A. Jamieson, T.F. Gulvin, J.D. Baird, R.R. Barr, and R.R. Preston, "Effects of composition and structure on the creep strength of molydenum bearing ferritic steels", *Creep Strength in Steel and High-Temperature Alloys*, The Metals Society, London, 1974, p.196.

[7] J.D. Baird, A. Jamieson, R.R. Preston, and R.C. Cochrane, "Strengthening mechanisms in ferritic creep resistant steels", *Creep Strength in Steel and High-Temperature Alloys*, The Metals Society, London, 1974, p.207.

[8] G.L. Dunlop, D.V. Edmons, and R.W.K. Honeycombe, "Some effects of microstructure on the creep properties of low-alloy steels containing vanadium carbide", *Creep Strength in Steel and High-Temperature Alloys*, The Metals Society, London, 1974, p.222.

[9] M. Prager, "Long-term studies of strength and toughness of an advanced steel", *PVP Volume 380: Fitness-for-Service Evaluations in Petroleum and Fossil Power Plants*, American Society of Mechanical Engineers, New York, 1998, p.291.

[10] (R.A. Stevens and P.J. Flewitt, "Effect of phosphorous on the microstructure and creep properties of 2 1/4 %Cr 1%Mo steel", *Acta Metallurgica*, Volume 34: Number 5, May 1986, p.849.) *Referenced in 13.*

[11] (J. Pilling, N. Ridley, and D.J. Gooch, "Effect of phosphorous on creep in 2.25% Cr-1% Mo steels", *Acta Metallurgica*, Volume 30: Number 8, Aug 1982, p.1587.) *Referenced in 13.*

[12] (J. Yu and H.J. Grabke, *Metallurgical Science*, Volume 17, 1983, p.389.) *Referenced in 13.*

[13] Z. Larouk and R. Pilkington, "The effect of phosphorous on carbide composition in a CrMoV low alloy steel under creep conditions", *Materials Science & Engineering A*, Volume A251, 15 Aug 1998, p.77.

[14] R.W. Swindeman, "Isochronous stress versus strain curves for normalized-and-tempered 2 1/4Cr-1Mo steel", *PVP Volume 359: Fitness for Adverse Environments in Petroleum and Power Equipment*, American Society of Mechanical Engineers, New York, 1997, p.261.

[15] N. Gope, T. Mukherjee, and D.S. Sarma, "Influence of long term ageing and superimposed creep stress on the microstructure of 1 mass%Cr-0.5 mass%Mo steel", *Materials Transactions, JIM*, Volume 33: Number 2, Feb 1992, p.110.

[16] V. Sklenicka and V. Foldyna, "Some causes of variation in high temperature creep of a low alloy CrMoV steel after service", *Acta Technica CSAV*, Volume 35: Number 4, 1990, p.495.

[17] K. Maruyama, K. Sawada, J. Hoike, H. Sato, and K. Yagi, "Examination of deformation mechanism maps in 2.25Cr-1Mo steel by creep tests at strain rates of 10^{-11} to 10^{-6} s^{-1}", *Materials Science & Engineering A*, Volume A224, 31 Mar 1997, p.166.

[18] F.H. van Zyl, J.P. Strydom, P.P.J. Smit, and R. Emmerich, "The high-temperature ageing of a low-alloy steel in the presence and absence of strain", *International Journal of Pressure Vessels and Piping*, Volume 59, 1994, p.91.

[19] Z. Yang and T.B. Gibbons, "Improved steels for advanced power plant applications", *PVP Volume 374: Fatigue, Environmental Factors, and New Materials*, American Society of Mechanical Engineers, New York, 1998, p.371.

[20] R.B. Scarlin, "Development of advanced steels for steam turbine applications", *Processing and Design Issues in High Temperature Materials, Proceedings of the 1996 Engineering Foundation Conference*, The Minerals, Metals & Materials Society, Warrendale, PA, 1997, p.107.

[21] K. Sawada, M. Takeda, K. Maruyama, R. Ishii, M. Yamada, Y. Nagae, and R. Komine, "Effect of W on recovery of lath structure during creep of high chromium martensitic steels", *Materials Science and Engineering A*, Volume A267: Number 1, 1999, p.19.

[22] K. Iwanaga, T. Tsuchiyama, and S. Takaki, "Strengthening mechanisms in heat-resistant martensitic 9Cr steels", *Key Engineering Materials*, Volume 171-174, 2000, p.477.

[23] Y. Tsuda, M. Yamada, R. Ishii, Y. Tanaka, T. Azuma, and Y. Ikeda, "Development of high strength 12% Cr ferritic steel for turbine rotor operating above 600°C", *ASTM Special Technical Publication 1259: Proceedings of the 1996 2nd Symposium on Steel Forgings*, American Society for Testing and Materials, West Conshoken, PA, 1997, p.267.

[24] F. Abe, "Evolution of microstructure and acceleration of creep rate in tempered martensitic 9Cr-W steels", *Materials Science & Engineering A*, Volume A234-236, 30 Aug 1997, p.1045.

[25] R. Ishii, Y. Tsuda, and M. Yamada, "High strength 12% Cr heat resisting steel for high temperature steam turbine blade", *ASTM Special Technical Publication 1259: Proceedings of the 1996 2nd Symposium on Steel Forgings*, American Society for Testing and Materials, West Conshoken, PA, 1997, p.317.

[26] Y. Kadoya, N. Nishimura, B.F. Dyson, and M. Mclean, "Origins of tertiary creep in high chromium steels", *Proceedings of the 1997 7th International Conference on Creep and Fracture of Engineering Materials and Structures*, The Minerals, Metals & Materials Society, Warrendale, PA, 1997, p.343.

[27] T. Fujita, "Current progress in advanced high Cr ferritic for high-temperature applications", *ISIJ International*, Volume 32: Number 2, 1992, p.175.

[28] J. Hald, "Metallurgy and creep properties of new 9-12% Cr steels", *Steel Research*, Volume 67, Sept 9, 1996, p.369.

[29] H. Cerjak, P. Hofer, and B. Schaffernak, "The influence of microstructural aspects on the service behaviour of advanced power plant steels", *ISIJ International*, Volume 39: Number 9, 1999, p.874.

[30] F. Abe, T. Noda, and M. Okada, "Optimum alloy compositions in reduced-activation martensitic 9Cr steels for fusion reactor", *Journal of Nuclear Materials*, Volume 195, Oct 1992, p.51.

[31] L. Lundin and H.O. Andren, "Atom-probe investigation of a creep resistant 12% chromium steel", *Surface Science*, Volume 266, April 15, 1992, p.397.

[32] T.A. Marrison and A. Hogg, "Influence of nickel content on the structure and high-temperature properties of a 12% Cr-Mo-V-Nb steel", *Creep Strength in Steel and High Temperature Alloys*, The Metals Society, London, 1974, p.242.

[33] M. Snykers and J.J. Huet, "Dispersion-strengthened ferritic alloys for high-temperature application", *Creep Strength in Steel and High Temperature Alloys*, The Metals Society, London, 1974, p.237.

[34] R. Wu, R. Sansdstrom, and J. Storesund, "Creep strain behaviour in a 12%CrMoV steel", *Materials at High Temperatures*, Volume 12: Number 4, 1994, p.277.

[35] A. Orlova, J. Bursik, K. Kucharova, and V. Sklenicka, "Microstructural development during high temperature creep of 9% Cr steel", *Materials Science & Engineering A*, Volume A245: Number 1, 30 April 1998, p.39.

[36] F. Abe and S. Nakazawa, "The effect of tungsten on creep behaviour of tempered martensitic 9Cr steels", *Metallurgical Transactions A*, Volume 23A, November 1992, p.3025.

[37] A. Strang and V. Vodarek, "The effects of microstructural stability on the creep properties of high temperature martensitic 12Cr steels", *Proceedings of the 1997 7th*

International Conference on Creep and Fracture of Engineering Materials and Structures, The Minerals, Metals & Materials Society, Warrendale, PA, 1997, p.415.

[38] V. Foldyna, J. Purmensky, and Z. Kubon, "Development of advanced 9-12% Cr creep resistant steels with respect to structural stability", *Proceedings of the 1997 7th International Conference on Creep and Fracture of Engineering Materials and Structures*, The Minerals, Metals & Materials Society, Warrendale, PA, 1997, p.587.

[39] E. Cerri, E. Evangelista, S. Spigarelli, and P. Bianchi, "Evolution of microstructure in a modified 9Cr-1Mo steel during short term creep", *Materials Science & Engineering A*, Volume A245: Number 2, 1 May 1998, p.285.

[40] W. Blum and S. Straub, "Subgrain growth during creep of a tempered martensitic 12% Cr steel", *Steel Reseach*, Volume 62: Number 2, 1991, p.72.

[41] R. Wu and R. Sandstrom, "Carbide coarsening during creep in 12 percent CrMoV steel", *Journal of Engineering Materials and Technology*, Volume 118: Number 4, Oct 1996, p.485.

[42] P.J. Ennis, A. Zielinska-Lipiec, O. Wachter, and A. Czyrska-Filemonowicz, "Microstructural stability and creep rupture strength of the martensitic steel P92 for advanced power plant", *Acta Materiala*, Volume 45: Number 12, Dec 1997, p.4901.

[43] H. Nickel, P.J. Ennis, W.J. Quadakkers, "The creep rupture properties of 9% chromium steels and the influence of oxidation on strength", *PVP Volume 374: Fatigue, Environmental Factors, and New Materials*, American Society of Mechanical Engineers, New York, 1998, p.299.

[44] F. Larson and J. Miller, "A time-temperature relationship for rupture and creep stresses", *Transactions of the ASME*, July 1952, p.765.

[45] "Assessment and Use of Creep Rupture Data", *Metals Handbook Ninth Edition, Volume 8: Mechanical Testing*, American Society for Metals, 1985.

[46] M. Schirra and K. Anderko, "Anomalies in creep-curves of martensitic 9-14% chromium steels under long-term loading", *Steel Research*, Volume 61: Number 6, 1990, p.242.

[47] K. Kimura, H. Kushima, F. Abe, and K. Yagi, "Inherent creep strength and long term creep strength properties of ferritic steels", *Materials Science & Engineering*, Volume A234-236, 30 Aug 1997, p.1079.

[48] W. Bendick and M. Ring, "Creep rupture strength of tungsten-alloyed 9-12% Cr steels for piping in power plants", *Steel Research*, Volume 67: Number 9, 1996, p.382.

[49] S. Oh, H. Chang, M. Chung, and S. Lee, "Development of long-time creep safety life prediction of steam turbine rotor steel and AE evaluation", *Proceedings of the 1997 7th International Offshore and Polar Engineering Conference*, International Society of Offshore and Polar Engineers, 1997, p.589.

[50] R.C. Hurst, J.H. Rantala, and F. Bregani, "Application of creep models for lifetime prediction of ferritic power plant steels", *PVP Volume 362: Severe Accidents and Topics in the NESC Project*, American Society of Mechanical Engineers, New York, 1998, p.99.

[51] A.T. Yokobori Jr. et al, "The master curve and the constitutive equation for creep deformation and fracture for Cr-Mo-V steel throughout smooth, notched and precracked specimens", *Journal of Material Science*, Volume 31: Number 18, 15 September 1996, p.4767.

[52] "Standard Specification for Alloy-Steel and Stainless Steel Bolting Materials for High-Temperature Service", *A 193/A 193M – 97a, 1998 Annual Book of ASTM Standards*, American Society for Testing and Materials, West Conshoken, PA, 1998.

[53] K. Yagi and F. Abe, "Long-term creep and rupture properties and microstructural changes of heat resisting steels", *Proceedings of the 1997 7th International Conference on Creep and Fracture of Engineering Materials and Structures*, The Minerals, Metals & Materials Society, Warrendale, PA, 1997, p.427.

[54] www.nrim.go.jp:8080/public/index.html, *National Research Institute for Metals.*

[55] "Report on The Elevated-Temperature Properties of Chromium-Molybdenum Steels", *Special Technical Publication No.151*, American Society of Testing and Materials, Philadelphia, 1953.

[56] "Standard Specification for Alloy-Steel Turbine-Type Bolting Material Specially Heat Treated for High-Temperature Service", *A 437/ A437M – 97, 1998 Annual Book of*

ASTM Standards, American Society for Testing and Materials, West Conshoken, PA, 1998.

[57] G.V. Smith, "Evaluations of the Elevated Temperature Tensile and Creep Rupture Properties of 12 to 27 Percent Chromium Steels", *ASTM DS 59*, American Society for Testing and Materials, Philadelphia, 1980.

[58] "Heat-Resisting Steel Bars", *JIS G 4311*, Japanese Industrial Standards, 1987.

[59] "Standard Specification for Steel Bars, Alloys, for Nitriding", *A355 – 89, 1998 Annual Book of ASTM Standards*, American Society for Testing and Materials, West Conshoken, PA, 1998.

[60] C. Berger, S.M. Beech, K.H. Mayer, M. Staubli, and D.V. Thornton, "European achievements in the development of materials for advanced power plants", *PWR Volume 21, The Steam Turbine Generator Today: Materials, Flow Path Design, Repair and Refurbishment*, American Society of Mechanical Engineers, New York, 1993, p.63.

[61] R.F. Buck and W.M. Garrison, Jr., "Creep-resistant martensitic steel", *Advanced Materials & Processes*, Aug 1996, p.27.

[62] M. Igarashi, S. Muneki, and F. Abe, "Creep properties of advanced heat-resistant martensitic steels strengthened by $L1_0$ type ordered intermetallic phase", *Key Engineering Materials*, Volume 171-174, 2000, p.505.

7. BIBLIOGRAPHY

1. R.A. Flinn and P.K. Trojan, *Engineering Materials and Their Applications*, John Wiley & Sons, Toronto, 1995.
2. Frank Garofalo, *Fundamentals of Creep and Creep-Rupture in Metals*, The Macmillan Company, New York, 1965.
3. Harry Kraus, *Creep Analysis*, John Wiley & Sons, Toronto, 1980.
4. D.B. Williams and C.B. Carter, *Transmission Electron Microscopy*, Plenum Press, New York, 1996.
5. G.W. Krutz, J.K. Schueller, and P.W. Claar II, *Machine Design for Mobile and Industrial Applications*, Society of Automotive Engineers, Warrendale, PA, 1994.
6. R.C. Juvinall and K.M. Marshek, *Fundamentals of Machine Component Design*, John Wiley & Sons, Toronto, 1991.

APPENDIX A: MATERIAL TEST SHEETS

BH-110

CSC

4000 MAHONING AVE. N.W.
WARREN, OHIO 44483-1068

TEST REPORT

PAGE: 1 of 1

NO.

CUSTOMER PURCHASE ORDER NUMBER & DESCRIPTION	ORIG. T.R. DATE	REV. T.R. DATE	SALES ORDER
10-31413	01/22/1999		64923

SOLD TO: HY-ALLOY STEELS CO.
5100 WEST 73RD STREET
CHICAGO IL 60638

SHIP TO: A. M. CASTLE & CO.
26800 MILES ROAD
BEDFORD HEIGHTS OH 44146

DESCRIPTION OF MATERIAL ORDERED

FEET:	PIECES	WEIGHT	SIZE	SHAPE:	LENGTH:
		8,000	1"	RD	24'/20'

PRODUCT DESCRIPTION:
HR Q & T MACH STR STRESS REL

PART NUMBER: IAC-23399

GRADE: E CR-MO-V DH

SPECIFICATION
CSC010103
ASTM A29-93A
G19300-01 REV 11 DTD 7/10/98
PD-10305 DU REV PGBU-01WESTINGHOUSE
ASTM A193-96A GR B16 SUPP S2 & S6
ASTM A322-91

Heat No.	C	Mn	P	S	Si	Ni	Cr	Mo	Al	V	Cu
99349	.42	.53	.017	.016	.22	.16	.93	.52	.003	.280	.16

Jominy	1	2	3	4	5	6	7	8	9	10	11	12	13	14	15	16	18	20	24	28	32	Gr Size
- 1 -	57	57	56	55	55	54	54	53		52		50		48		45		43	41	39	37	6-8
- 2 -																						

Material Stamped with Heat Code: WV

Charge Number	Off Set	Yield PSI	Tensile PSI	Elong %	RA %
	.02	135,000	142,900	18.9	62.5
	.2	137,380			
	.02	135,640	142,890	19.6	64.1
	.2	139,900			

Hardness HB
SURFACE 302
MID RAD. 302
SURFACE 285
MID RAD. 285

QUENCH: 1700F 3 HOURS
MEDIA : OIL
TEMPER: 1260F 3 HOURS
STRESS: 1160F 3 HOURS

CHARPY Impacts

Impacts (Ft-Lb): 74/74/75 at +70F

Micro test satisfactory.

Macroetch meet S3, R3, C3.

Country of origin USA - qualifies NAFTA harmonized tariff classification 7228.30 (hot rolled) and 7228.50 (cold finished) preference criterion B.

CASTLE METALS – CLV
DATE REC'D 1-29-99
RD# 4634
APPROVED BY: Bma

We hereby certify that the above data are correct as contained in the records of CSC.

Veryl D. Kiser

Veryl D. Kiser,
Laboratory Services Superintendent

CSC MATERIAL IS NOT SUBJECTED TO MERCURY DURING PROCESSING OR TESTING. NO WELDING PERFORMED ON MATERIAL

MATERIAL PRODUCED AND CERTIFIED TO SPECIFICATIONS SHOWN ABOVE. NO ADDITIONAL CERTIFICATION IS IMPLIED OR WARRANTED.

CASTLE METALS - TOR

DATE REC'D: 2/12/99
REC'D. FROM: HY SAL IAC 23399
APPROVED BY:

ID# B-0212

Crucible Service Centers
A Divison of Crucible Materials Corporation

5639 W. Genesee St.
Camillus, NY
13031-0977

QUALITY ASSURANCE CERTIFICATE OF TEST

SOLD TO	SHIP TO	CRUCIBLE ORDER NUMBER
HITACHI CANADIAN INDUSTRIES LTD 826 58TH STREET EAST SASKATOON SK CANADA	HITACHI CANADIAN INDUSTRIES LTD 826 58TH STREET EAST SASKATOON SK CANADA	44-2257
		DATE 05/03/9

CUSTOMER ORDER # & DATE	CUSTOMER REQ. #	DISTRICT	SHIPPED FROM
3251 04/28/99		WINDSOR	WINDSOR

DESCRIPTION OF MATERIAL

1 NIT 135G MOD

MECHANICAL PROPERTIES

ITEM NO.	SIZE	QUANTITY	HEAT NO.	LOT	YIELD PSI	TENSILE PSI	%ELONG IN.	%RED AREA	HARD-NESS	IMPACT
1	1.25"DIA X 12FT	50	85862	32-1	105,250	130,780	21.20	50.40	SURFACE BHN 269	

CHEMICAL PROPERTIES

HEAT NO.	LOT	C	MN	P	S	SI	NI	CR	V	W	MO	CU	CO	AL
862	32-1	0.3800	0.6700	0.0090	0.0140	0.2700	0.1800	1.7500			0.350	0.170		1.160

SEE REVERSE SIDE FOR ADDITIONAL TECHNICAL INFORMATION

ID# B-0214

THE ABOVE MATERIAL WAS MANUFACTURED AND TESTED IN ACCORDANCE WITH THE ABOVE SPECIFICATIONS AND IS IN CONFORMANCE WITH THOSE SPECIFICATION REQUIREMENTS.

CRUCIBLE MATERIALS CORPORATION
ACTING BY AND THRCUGH ITS SERVICE CENTERS DIVISION

CERTIFIED BY: _____

Richard Ross
QUALITY ASSURANCE REPRESENTATIVE

Notes on Item 1

OFF SET	YIELD	TENSILE	ELONGATION	RED/AREA	HARDNESS
.02	99,950	130,780	21.2%	60.4%	
.2	102,980	128,380	21.1%	60.3%	SURFACE BHN 255
.02	97,920	128,380	21.1%	60.3%	FREQ/SEV .00/.00

DECARB: 006 QUENCH: 1700 F 2 HRS MEDIA: OIL TEMPER: 1250 F 3 HRS STRESS: 1150 F 3 HRS FERRITE LESS THAN 5% MACROETCH EQUAL TO OR BETTER THAN S2, R1, C2, IN ACCORDANCE WITH ASTM E381-94 NO INTENTIONAL LADLE ADDITION OF ELEMENTS EXCEPT SULFUR TO ENHANCE MACHINING WERE MADE. CSC010201 AMS 2301H ASTM E381-94 AMS 6470J EX BHN & MK MIL-S-6709A AM2 COND F1 EX PROP PD 10305 HD REV Y WESTINGHOUSE AMS 6472C EXC MK G.E. B5E1A-S21

JOMINY

GRAIN	1	2	3	4	5	6	7	8	10	12	14	16	20	24	28	32
7-8	55	55	55	55	55	55	54	54	53	52	51	48	45	43	42	41

1.0214

ID# B-0214

CERTIFICATE OF TESTS | ABNAHMEPRUEFZEUGNIS | CERTIFICAT DE CONTROLE

CERT-SERIAL#-000133281

CARPENTER

Carpenter Technology Corporation
P.O. Box 14662, Reading, PA 19612-4662

- THE RECORDING OF FALSE, FICTICIOUS OR FRAUDULENT STATEMENTS OR ENTRIES ON THIS DOCUMENT MAY BE PUNISHED AS A FELONY UNDER FEDERAL STATUTES INCLUDING FEDERAL LAW, TITLE 18, CHAPTER 47.
- THE VALUES AND OTHER TECHNICAL DATA REPRESENT THE RESULTS OF ANALYSES AND TESTS MADE ON SAMPLES COLLECTED FROM THE TOTAL LOT. ORIGINAL DATA RECORDS CAN BE TRACED BY REFERENCE TO THE CARPENTER ORDER NUMBER.
- MATERIAL IS MANUFACTURED FREE FROM MERCURY, RADIUM AND ALPHA SOURCE CONTAMINATION.
- THIS DOCUMENT SHALL NOT BE REPRODUCED, EXCEPT IN FULL, WITHOUT THE WRITTEN CONSENT OF CARPENTER TECHNOLOGY CORPORATION.

05/13/99

CUSTOMER / BESTELLER / CLIENT	SELLER / VERKÄUFER / VENDEUR
HITACHI CANADIAN IND. LTD., 826 58TH STREET EAST SASKATOON, SASK. S7K 5Z4 ,CANADA	CARPENTER TECHNOLOGY (CANADA) LTD., 6114 EDWARDS BLVD., MISSISSAUGA, ONTARIO L5T 2V7 ,CANADA

CUSTOMER ORDER NO./BESTELL-NR./N° DE COMMANDE	CARPENTER NO./WERKS-NR./N° DE REFERENCE INTERNE	DATE/DATUM/DATE	WEIGHT/GEWICHT/POIDS
33224	TOR878201 L38776	05/13/99	48.000

HEAT NUMBER / SCHMELZE-NR. / N° DE COULEE : 717854

PRODUCT DESCRIPTION: 636 (AISI 616) HOT FINISH TREATED STRESS RELIEVED PICKLED
POWER GEN HARDNESS MIN 277.0 / MAX 331.0 HB

SPECIFICATION: WESTINGHOUSE 10705BU REV H (09/20/88) EXCPT LTR (02/19/90)

SIZE 1.125000 IN.(28.57 MM) RD BAR

PRIMARY HEAT CHEMISTRY:

C	MN	SI	P	S	CR
0.21	0.73	0.33	0.014	0.001	11.82
NI	**MO**	**W**	**V**		
0.85	1.09	1.03	0.22		

I HEREBY CERTIFY THAT ALL INSPECTIONS AND TESTS REQUESTED BY THE SPECIFICATION HAVE BEEN COMPLETED WITH RESULTS CONSISTENT WITH THE SPECIFICATION REQUIREMENTS.

DISCS MACROETCHED AND APPROVED

INCLUSION RATING - ASTM E45 METHOD A

A		B		C		D	
THIN	HEAVY	THIN	HEAVY	THIN	HEAVY	THIN	HEAVY
0.0	0.0	0.0	0.0	0.0	0.0	1.0	0.0
0.0	0.0	0.0	0.0	0.0	0.0	1.0	0.0
0.0	0.0	0.0	0.0	0.0	0.0	1.0	0.0
0.0	0.0	0.0	0.0	0.0	0.0	1.0	0.0
0.0	0.0	0.0	0.0	0.0	0.0	1.0	0.0
0.0	0.0	0.0	0.0	0.0	0.0	1.0	0.0

(T)RANSVERSE (L)ONGITUDINAL	L	L
YIELD STRENGTH, (0.20 %) KSI(MPA)	121.0(834)	121.0(834)
TENSILE STRENGTH, KSI(MPA)	146.0(1007)	145.0(1000)
ELONGATION IN 2.00", %	18.0	18.0
REDUCTION OF AREA, %	57.0	53.0

MICROSTRUCTURE - FERRITE - NONE

ID# B-0215

CONTINUED ON NEXT PAGE

CERTIFICATE OF TESTS ABNAHMEPRUEFZEUGNIS CERTIFICAT DE CONTROLE

CERT SERIAL# 000133281

CARPENTER

Carpenter Technology Corporation
P.O. Box 14662, Reading, PA 19612-4662

05/13/99

CUSTOMER / BESTELLER / CLIENT

SELLER / VERKÄUFER / VENDEUR

HITACHI CANADIAN IND. LTD.,
826 58TH STREET EAST
SASKATOON, SASK.
S7K 5Z4 ,CANADA

CARPENTER TECHNOLOGY
(CANADA) LTD.,
6114 EDWARDS BLVD.,
MISSISSAUGA, ONTARIO
L5T 2V7 ,CANADA

CUSTOMER ORDER NO./BESTELL-NR./N° DE COMMANDE	CARPENTER NO./WERKS-NR./N° DE REFERENCE INTERNE	DATE/DATUM/DATE	WEIGHT/GEWICHT/POIDS
33224	TOR878201 L38776	05/13/99	48.000

HEAT NUMBER / SCHMELZE-NR. / N° DE COULEE : 717854

HB HARDNESS AS SHIPPED

BAR #	END
5	321
11	321
17	321
29	321
22	321

ARPENTER'S QUALITY MANAGEMENT SYSTEM WAS REGISTERED AS OF DECEMBER 21, 1993
O THE REQUIREMENTS OF ISO 9002 BY LLOYD'S REGISTER QUALITY ASSURANCE LTD.
I CERTIFY THE ABOVE INFORMATION TO BE A TRUE AND CORRECT RESTATEMENT OF
PORTIONS OF THE APPLICABLE TEST AND ORDER DATA.

SHARON L. RITCHIE
CERTIFICATION/AMQR ANALYST I
CARPENTER TECHNOLOGY CORPORATION

B-0215

ID# B-0215

APPENDIX B: CREEP TEST RESULTS

This appendix summarizes some of the experimental data. The experimental data for each creep tensile test performed are contained on the enclosed compact disc due to space constraint.

B.1 ASTM A193 Grade B16

Temperature **Estimated Time to Rupture (hr)**

(°C)	(°F)	180	320	560	1800	3200	5600	
538	1000	3F	3A	3E	3M	3R	3V	Specimen
		2/3/00	1/23/00	2/2/00	3/9/00	4/2/00	5/30/00	Start Date
		261.4	246.3	226.6	190.8	173.9	161.1	Stress (Mpa)
		320.67	391.58	787.94	1725.81			Time to Rupture (hrs)
593	1100	3D	3C	3I	3G	3J *	3U	
		1/28/00	1/28/00	2/16/00	2/4/00	2/18/00	5/12/00	
		157.8	142.7	129.1	101.4	92.5	83.6	
		113.91	170.24	440.46	518.36	719.54	983.1	
649	1200		3B	3K	3H	3P *	3S	
			1/26/00	3/3/00	2/4/00	3/16/00	4/30/00	
			76.1	65.6	48.1	40.3	35.8	
			52.78	61.8	278.93	424.22	626.93	

(°C)	(°F)	560	560	3200
538	1000	3N	3O	
		3/10/00	3/15/00	
		226.8	226.5	
		579.29	730.68	
593	1100			3T
				5/12/00
				92.8
				661.7
649	1200	3L	3Q	
		3/6/00	4/1/00	
		65.6	65.5	
		83.33	76.88	

* overtemped

B.2 ASTM A355 Class A

Temperature **Estimated Time to Rupture (hr)**

(°C)	(°F)	32	56	180	320	560	1800	3200
538	1000	2E	2C	1E	1D	1C	2N	
		4/5/00	3/10/00	11/2/99	10/24/99	10/30/99	6/7/00	
		252.8	238.2	206.8	190.7	179.7	152.1	
			500.56	1220.55	1554.31	2246.18		
593	1100		2K	1A	1B	2B	1H	2H
			5/4/00	10/23/99	10/23/99	2/11/00	11/18/99	4/6/00
			155.3	127.2	114.8	106.7	86.1	76.9
			103.28	255.88	325.53	521.99	1156.41	1430.79
649	1200			1F	1G	1I	1J *	
				11/6/99	11/11/99	11/23/99	12/2/99	
				71.3	61.9	53.3	38.5	
				71.24	120.54	163.61	681.35	

(°C)	(°F)	56	56
538	1000	2F	2J
		4/5/00	4/15/00
		237.9	238.5
		550.65	619.85

* overtemped

(°C)	(°F)	560	560	
593	1100	2I	2L	Specimen
		4/7/00	4/28/00	Start Date
		106.5	106.7	Stress (Mpa)
		506.99	519.07	Time to Rupture (hrs)

B.3 ASTM A437 Grade B4B

Temperature **Estimated Time to Rupture (hrs)**

(°C)	(°F)	180	320	560	1800	3200	5600	
538	1000	4B	4C	5D	4K	5B	4L	4D
		9/22/99	9/24/00	1/22/00	10/7/99	10/13/99	5/28/00	9/28/00
		426.6	400.0	394.3	348.7	330.8	308.7	370.6
		18.37	111.05	185.36	1616.84	3931.91		797.76
593	1100	4E	4F	4I	4G	4H		
		9/29/00	10/1/99	10/6/99	10/3/99	10/3/99		
		305.8	276.7	260.3	220.8	197.6		
		134.14	299.42	524.85	1277.00	2316.29		
649	1200	5I	5A	4J	5C	5F	4M	Specimen
		3/5/00	10/9/99	10/6/99	10/13/99	1/26/00	6/8/00	Start Date
		181.7	159.6	139.7	93.5	80.3	50.2	Stress (Mpa)
		35.98	76.33	155.56	2081.99	2127.9		Time to Rupture (hrs)

(°C)	(°F)	560	560
538	1000	5H	5J
		2/18/00	3/14/00
		394.6	394.2
		234.49	214.97
649	1200	5E	5G
		1/23/00	2/6/00
		139.9	139.9
		173.95	

APPENDIX C: CALCULATION OF BOLT STRESS

An outline of the analysis performed to estimate the stress in a bolt under typical service conditions is given in this appendix. First, the general case of a bolted connection subjected to an external joint separating force will be considered.[1,2] Then, the procedure will be applied to the more specific case of a bolt in the head of a main stop valve.

C.1 General Case

Bolts are typically used to hold parts together in opposition to forces tending to pull them apart. In this type of situation, the stress in the bolt is the result of two forces: an initial force, F_i, due to the tightening of the bolt at installation, or bolt preload, and the external joint seperating force, F_e.

A free body diagram of a typical bolted joint holding two plates together is shown in Figure 1, where F_b is the bolt axial load, and F_c is the clamping force between the plates.

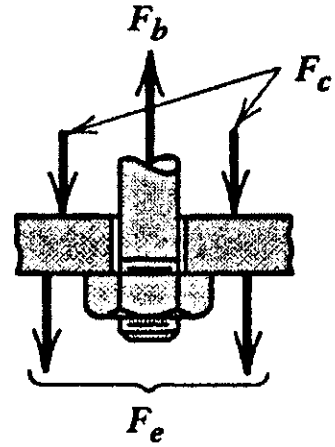

Figure 1: Free body diagram of bolted joint.[1]

On initial tightening, $F_b = F_c = F_i$. However, with the application of F_e, equilibrium requires an increase in F_b and a decrease in F_c. The bolt and the clamped members elongate the same amount, δ, and the relative magnitude of the changes in F_b and F_c are dependent on the relative stiffness of the bolt and clamped member.

From Figure 1, the external force must be equal to the sum of the increased bolt force plus the decreased clamping force, or

$$F_e = \Delta F_b + \Delta F_c \tag{1}$$

ΔF_b and ΔF_c are defined as

$$\Delta F_b = k_b \delta \quad \text{and} \quad \Delta F_c = k_c \delta \tag{2}$$

where k_b and k_c are the spring constants for the bolt and clamped members, respectively. Combining equations (1) and (2), the following expression for ΔF_b can be derived

$$\Delta F_b = \frac{k_b}{k_b + k_c} F_e \tag{3}$$

The force on the bolt, F_b, is equal to the sum of the bolt preload and the change in the force on the bolt due to the addition of the external load, or

$$F_b = F_i + \Delta F_b \tag{4}$$

$$F_b = F_i + \frac{k_b}{k_b + k_c} F_e \tag{5}$$

From the basic equations for axial deflection and for spring rate,

$$k_b = \frac{A_b E_b}{g} \quad \text{and} \quad k_c = \frac{A_c E_c}{g} \tag{6}$$

where A = the effective cross-sectional area, E = the modulus of elasticity, and the grip g represents the approximate effective length of the bolt and clamped members.

The effective cross-sectional area of the clamped members is difficult to determine. An empirical procedure that approximates A_c is illustrated in Figure 2.

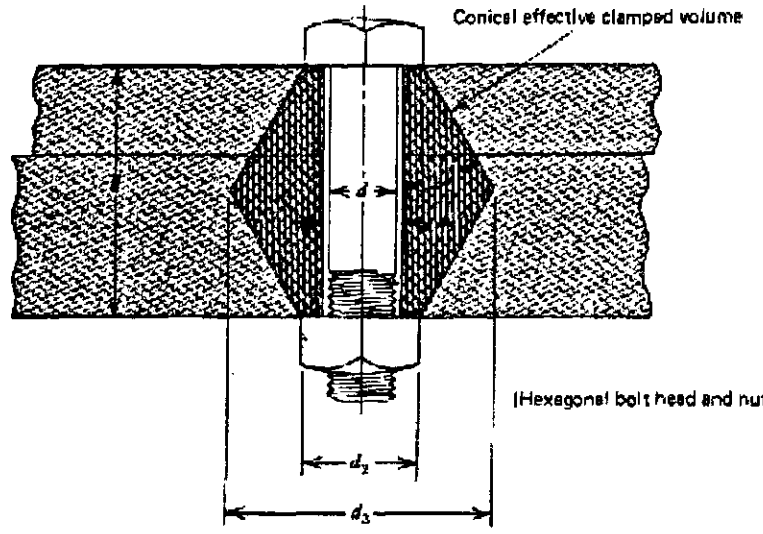

Figure 2: Effective cross-sectional area of clamped members.

$$A_c = \frac{\pi}{4}\left[\left(\frac{d_3 + d_2}{2}\right)^2 - d_1^2\right] \tag{7}$$

where d_1 is the bolt hole diameter, d_2 is the nut diameter, and

$$d_3 = d_2 + g \tan 30^\circ \tag{8}$$

The initial force on the bolt, F_i, can be determined if the amount of bolt elongation that occurred during tightening, δ_i, is known, using the following expression

$$F_i = k_b \delta_i \tag{9}$$

The bolt is assumed to be in uniaxial tension. Neglecting stress concentrations at and near the threads, the stress on the bolt σ_b is,

$$\sigma_b = F_b / A_b \tag{10}$$

where A_b is the cross-sectional area of the bolt.

C.2 Bolt in Main Stop Valve

Sixteen bolts are used to fasten the cover plate of the valve to the body and the stress in these bolts was analysed using the procedure detailed above. The bolts are of a tempered martensitic stainless steel similar to ASTM A437 Grade B4B.

The stress in each bolt during service is a result of two forces: an initial force, F_i, due to the initial tightening of the bolt at installation, and an external force, F_e, due to the effect of the high pressure steam contained inside the valve which exerts a force attempting to separate the cover plate from the valve body. The external force was calculated using the following expression

$$F_e = p\left[\frac{\pi\left(D_{cp}\right)^2}{4(\#bolts)}\right] \tag{11}$$

where p is static pressure, and D_{cp} is the diameter of the cover plate.

The dimensions of the bolt and clamped members are listed below:

Diameter of Bolt, d = 76.2 mm

Diameter of bolt hole, d_1 = 80 mm

Nut Diameter, d_2 = 117 mm

Effective length of bolt, g = 225 mm

Diameter of cover plate, D_{cp} = 576 mm

Other important values needed are:

Initial Bolt Elongation, δ_i = 0.18 – 0.23 mm

Pressure, p = 127.5 kg/cm^2 gage

Temperature = 538°C

The modulus of elasticity for most ferritic and martensitic stainless steels is approximately 200 MPa at room temperature. However, the value of the modulus varies significantly with temperature. One source showed the modulus of elasticity of pure iron to vary from 200 MPa at room temperature to a value of approximately 150 MPa at 538°C.[3] This was assumed to be a reasonable value for the martensitic stainless steel in question.

The results of the stress analysis are shown in Table 1. The analysis shows that the majority of the stress is a result of the preload, F_i. Higher stress, due to over tightening, shortens bolt life, thus preload is very important.

Table 1: Results of stress calculation for bolts.

δ_i (mm)	F_i (kN)	ΔF_b (kN)	F_b (kN)	σ_b (MPa)
0.18	547	36.4	584	128
0.23	699	36.4	736	161

Several assumptions were made to simplify this calculation. Thermal effects due to differential expansion were assumed to be negligible since the bolt and the clamped members have the same coefficient of thermal expansion. Dimensional effects due to stress concentrations in the bolt threads or the presence of a gasket were also considered to be negligible.

---

[1] R.C. Juvinall and K.M. Marshek, *Fundamentals of Machine Component Design*, John Wiley & Sons, Toronto, 1991.

[2] G.W. Krutz, J.K. Schueller, and P.W. Claar II, *Machine Design for Mobile and Industrial Applications*, Society of Automotive Engineers, Warrendale, PA, 1994.

[3] L.H. Van Vlack, *Elements of Materials Science and Engineering*, 6th edition, Addison-Wesley, New York, 1989.